Validation, calibration and evaluation of a Delft3D-FLOW model with ferry measurements

Arjen Luijendijk

September 2001

Validation, calibration and evaluation of Delft3D-FLOW model with ferry measurements

M.Sc. Thesis

A.P. Luijendijk
C9535180
September 2001

Preface

This report describes the study, which has been carried out as a master thesis, as part of the study Civil Engineering at Delft University of Technology. The study in this report concerns the validation, calibration and evaluation of a numerical model with ferry measurements.

In a co-operation between NIOZ (Netherlands Institute for Sea Research) and the ferry company TESO (Texels Eigen Stoomboot Onderneming) continuous observations from the ferry 'Schulpengat' are carried out in the Texel inlet between the North Sea and Dutch Wadden Sea. Since all data obtained are collected by NIOZ, this study took place at NIOZ on Texel. I would make a special thanks to my supervisor here at NIOZ, Herman Ridderinkhof. His experience in numerical modelling and willingness to share his knowledge were a big support during this study. The running aground of his sailing boat provided a nice practical experience of the tidal motions in an outer delta.

When I arrived at NIOZ for my Masters, I had no working experience with UNIX and Matlab. Furthermore several questions were raised during the interpretation of the data processing of the ADCP measurements. I would therefore like to thank especially Frans Eijgenraam for giving explanations and answering these questions.

I would like to thank my supervisors from the University of Delft and WL | Delft Hydraulics, prof.dr.ir. G.S. Stelling, prof.dr.ir. M.J.F. Stive and dr.ir. J.A. Roelvink for sharing their knowledge and support during this study. Special thanks goes out to postdoc Hans Bonekamp for the regular exchange of experiences, results and post-processing routines during this model study.

Last words of thanks go out to the Ph.D. students of the department and to other graduate students 'In den Potvis', for making my stay on Texel very pleasant.

Arjen Luijendijk,
't Horntje-Texel,
4 September 2001

Summary

Measurements of the bottom topography indicate that the Marsdiep basin (southernmost basin of the Wadden Sea) has still not reached a morphological equilibrium after the closure of the Afsluitdijk in 1933. In the last decades large amounts of sediment (2 - 4 million m^3 per year) have been imported into the Marsdiep basin. The understanding of the mechanisms that cause this transport of sand and silt is rather limited. To improve this understanding, it is essential to get a better insight in the variability of the tidal currents through the Texel inlet. Since late 1997 continuous measurements have been carried out with an ADCP mounted on the ferry between Den Helder and Texel. These consist of measurements of currents and discharges through the inlet. Also water levels measured at several locations are available. These three types of measurements are used in this study for the validation and calibration of a detailed numerical flow model.
The detailed model contains the area around the Texel inlet, which forms the connection between the Marsdiep basin and the adjacent North Sea. The boundary conditions for the detailed model are extracted from the Wadden Sea model, which simulates the tidal movement in the western Wadden Sea. The Wadden Sea is, in turn, nested in the ZUNO model, which simulates the astronomic tidal movement in the southern North Sea.
To compare the model results with the measurements, a harmonic analysis is applied. The approach in this study yields the required amplitudes and phases of eight harmonic tidal components. These tidal components also include higher harmonics. Higher harmonics are generally the consequence of distortion of the primary tidal components, due to nonlinear mechanisms that influence the tidal wave propagation in shallow seas. Due to the presence of these higher harmonics the currents in the Marsdiep basin exhibit asymmetry between flood and ebb currents, which can cause net sediment transport. Generally for the M_2 tide, the second harmonic M_4 is the most important cause of tidal asymmetry. The relative phase difference between M_4 and M_2 plays a large role in the tidal asymmetry.

Validation of the models with the water levels shows that the modelled amplitudes and phases correspond with the measurements around the Texel inlet. The Wadden Sea model produces better amplitudes and phases in the Marsdiep basin than the ZUNO model. At most water level stations the modelled M_4 phase has a rather large deviation of about 20 minutes with the observed M_4 phase. The modelled discharge through the inlet shows similar amplitudes and phases to the measured discharge. The exception is the modelled M_4 phase, which deviates 50 minutes from the measured M_4 phase.
The local bathymetry in the model is adjusted to the depths in the ferry measurements. After this adjustment, the modelled currents across the Texel inlet correspond closely with the measured currents.

The knowledge acquired during sensitivity studies is used to adjust the existing detailed model. This new ‘model’ contains the most recent bathymetry and the grid is extended to the watershed between the Marsdiep basin and the Vlie basin. During calibration the boundary conditions are adjusted in order to minimise the difference in the M_4 phase between the modelled and the measured discharge. Comparisons of the model results with the measured water levels and discharge show that the model is capable of reproducing similar amplitudes and phases for almost all analysed components in the measurements. The modelled residual currents across the inlet show some deviations with the measured residual currents. To get a first idea of the bed load transport (simplified by u^3), cubic tidal currents are time averaged. The main influence on the magnitude of these residual cubic currents is the throughflow from the Vlie basin. Integrating the residual cubic currents across the inlet gives an export for the measurements and also for the run with the new boundary conditions. However, runs with the default boundary conditions give an import of bed load transport into the Marsdiep basin, caused by a larger influence of the tidal asymmetry.
On the basis of the analyses in this model study no distinct explanation can be given for the large-scale import into the Marsdiep basin. Suggestions for further studies are the addition of wind and wave processes and salinity gradients caused by fresh water discharge at the sluices.

Contents

Appendices

1 Introduction

The northern coast of the Netherlands consists of a chain of barrier islands separated from the mainland by the Wadden Sea. The Dutch part of the Wadden Sea consists of ten more or less separated tidal basins drained by inlets between the islands (see figure 1.1). The Wadden Sea basins are tidally dominated areas crossed by one or two meandering main channels with depths of about 5-10 meters. These tidal basins contain large areas with tidal flats, which significantly influence the tidal propagation. The surface area of the tidal flats is about 50-70% of the total basin area. Some of the basins have a regular supply of fresh water from the continent. One basin is in fact an estuary having a continuous supply of fresh water from the river Eems. The transport of water and sediment through the inlets is of importance for the functioning of the ecosystem in the Wadden Sea and for the morphological developments in the Wadden Sea and the adjacent coastal zone.
Typically, a single tidal basin is characterised by an inlet with a length and width of a few kilometres. The inlet is bounded by two barrier islands and connects the open sea with the inner embayment. On the seaward side of the inlet a relatively shallow outer delta (also known as ebb-tidal delta) occurs with depths between 1 and 5 m and with a sandy bed. Outer deltas are complex, highly dynamic morphological structures of channels and shoals, which play an important role in the exchange of water and sediment between the tidal basin and the coastal zone.

The southernmost tidal inlet of the Wadden Sea is the Texel inlet (or Marsdiep), which forms the connection between the largest basin of the Wadden Sea and the adjacent North Sea. The inner embayment is called the Marsdiep basin. This basin has two deep channels of 10-30 meters and a small tidal flat area (about 15% of the total basin area). An overview of the Marsdiep basin can be seen in figure 1.2. The basin contains two sets of sluices, near Kornwerderzand and near Den Oever, which discharge fresh water from the IJsselmeer into the Wadden Sea.

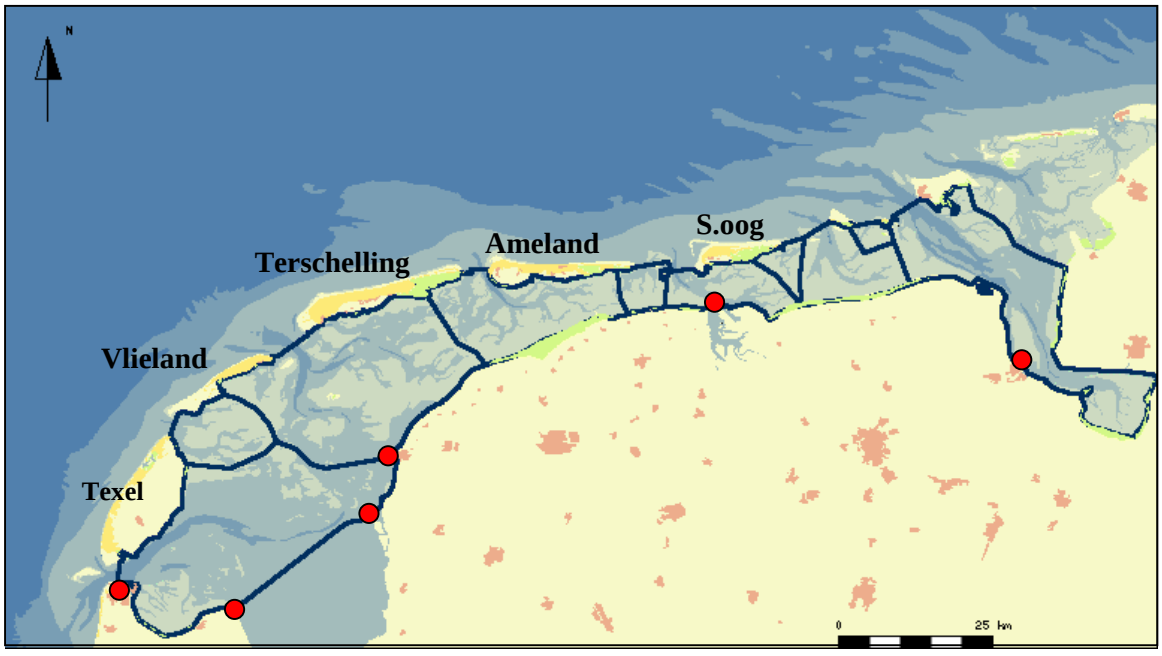

Fig. 1.1 The tidal basins of the Dutch Wadden Sea. The black lines represent the watersheds between the basins. The red dots represent the sluices, which regularly supply fresh water into the Wadden Sea.

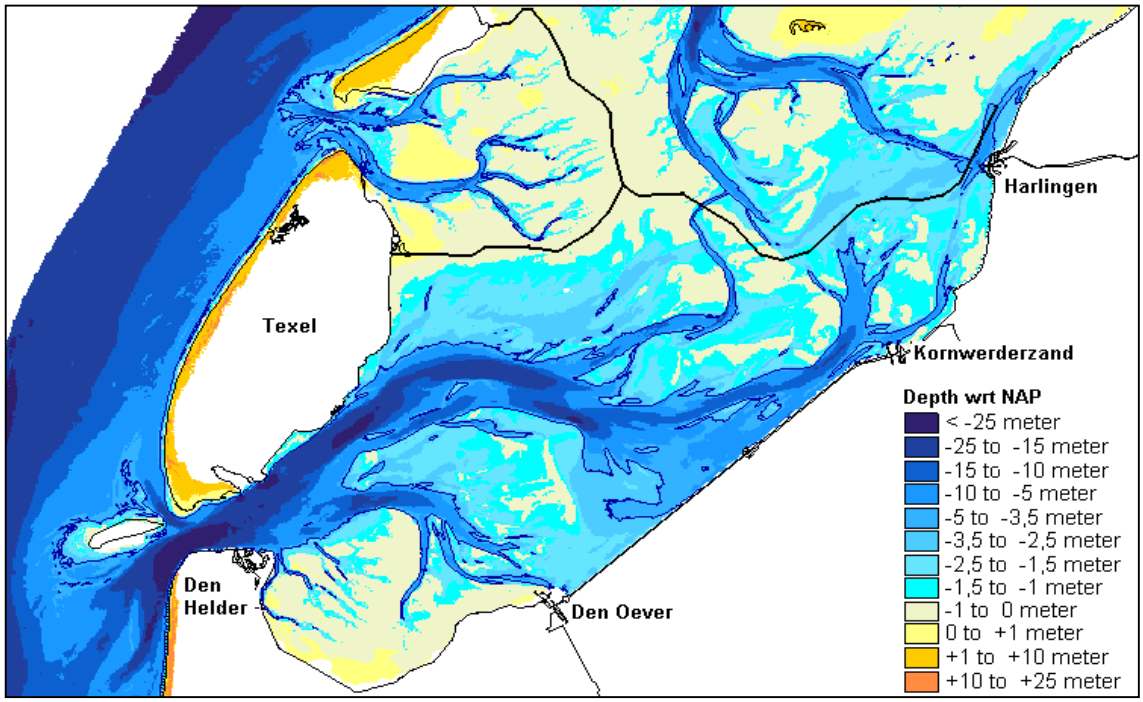

Fig. 1.2 The Marsdiep basin. The black solid lines represent the watersheds separating the basins.

The Texel inlet is 2.6 km wide at its minimum. Typical current velocities through the inlet are of order 1 m/s. The water motion in the tidal inlet system is driven merely by tides and waves, but also wind and density driven motions play a role. During a mean tidal period the tidal prism is $1 \cdot 10^9$ m^3 (Postma, 1982). The Texel inlet with its outer delta is shown in appendix A.

An important event for the tidal movement in the Marsdiep basin was the closure of the Zuiderzee in 1933, by the Afsluitdijk. Measurements of the bottom topography strongly indicate that the Marsdiep basin has still not reached a morphological equilibrium after the closure. In the last decades large amounts of sediment (~ 4 million m^3 per year) have been imported into the Marsdiep basin (Louters & Gerritsen, 1994). The understanding of the processes that cause this sediment transport is rather limited.

To improve this understanding, it is essential to get a better insight in the variability of the tidal currents through the Texel inlet. Since late 1997 continuous current measurements with an ADCP mounted on the ferry between Den Helder and Texel have been carried out. The ferry measurements are unique because of the frequency and duration of the observations. This allows studies on the magnitude and variations in the tidal currents through the Texel inlet. The coherent data set that is obtained forms an excellent set for validation and calibration of numerical models for the area. Besides the ferry measurements, also time series of water level elevations in several tidal gauges are available.

The aim of this study is to validate, calibrate and evaluate a hydrodynamic Delft3D-FLOW model with these observations, which is reliable and useful for further model studies on the exchange processes in an inlet. The exchange processes in the inlet result in sediment transport. To get a first idea of the bed load transport, the mean cubic currents in the inlet are evaluated.

Validation is a continuous process during the entire course of a modelling project. It involves the verification of model results with measured data, explanation of the differences and conclusions on the model performances. Validation also includes sensitivity analysis, which consists of systematic variation of model parameters and comparison of the results of the computations. During calibration the comparisons between measurements and model results are used to improve the computations for optimal results.

In chapter 2 the tides in shallow seas are described together with the method, which is used to analyse the tides. In chapter 3 observations that are used for validating the models, are discussed and a first analysis of the measurements is given. An overview of the Delft3D model system and the set up of three models are given in chapter 4. The validation of the models with the observations is presented in chapter 5. Chapter 6 describes a sensitivity analysis of a detailed model, which simulates the tidal movement in and around the Texel inlet. The final run is analysed in chapter 7 including an evaluation of the concerning run. Conclusions and recommendations for further study are given in chapter 8.

2 Tides in shallow seas

In this chapter the tides and the method, which is used for analysing the model results and observations, are discussed. In the first three paragraphs the propagation of the tidal wave from the ocean to the Marsdiep basin is described. In paragraph 2.4 the nonlinear mechanisms that influence the tidal wave propagation are discussed. In the last paragraph the harmonic analysis and its requirements are described, together with a description of tidal asymmetry.

2.1 Tide generating forces

Tides are the result of gravitational attraction between stellar bodies, mainly the Earth, moon and sun. The gravitational force varies with distance from the attracting body; it is larger at points on the earth's surface closer to the sun (or moon) and smaller at points on the opposite side. Tides are the result of the balance between the gravitational force and the centrifugal force, which is determined by the angular velocity of the earth's movement. The two forces balance each other exactly at the earth's centre and when integrated over the mass of the earth. On the earth's surface the balance is not exact, and the remaining force varies in strength and direction. It is directed outward, acting in the opposite direction to gravity (i.e. in the vertical) at the point directly under the sun (or moon) and at the point directly opposite. This produces a minuscule variation of gravity, not enough to be noticeable without extremely sensitive instruments and certainly not enough to produce oceanic tides of the observed magnitude. More importantly, over most of the earth's surface the remaining force acts horizontally. It is this horizontal component which is responsible for tides in the ocean and is therefore known as the tide-generating force. This paragraph is partially adapted from Tomczak (1996).
The tide-generating force is periodic around the earth and produces a series of convergences and divergences. The sequence of divergences and convergences of the tide-generating force sweeps around the earth once every day. As a result, water is moved and accumulates in one region and is drained away in another region. In other words, oceanic tides are waves of very long wavelength driven by currents, which are produced by the horizontally acting tide-generating force.

2.2 Tides in the North Sea

Marginal seas or estuaries cannot produce a response to astronomical tidal forcing. If there is tidal movement in these regions, it is forced by the tidal currents of the deep ocean, which enter and leave the region periodically at the connection to the ocean. Tides generated in this way are known as co-oscillation tides. Marginal seas have their own resonance frequencies, determined by their dimensions. As a consequence, the amplitudes and phases of co-oscillation tides depend on the closeness of a resonance frequency to one of the tidal frequencies and on the amplitude of the tidal currents in the deep ocean at the connecting line with the marginal sea.

The North Sea can be schematised as a tank or bowl with a small opening in the south-west (the Channel) and a large opening in the north-west (Atlantic Ocean). The tide in the North Sea is influenced by the tide in the Atlantic Ocean via these two openings. The North Sea is a relative shallow shelf sea, which largely distorts the tidal wave. Besides this distortion (mainly caused by the geometry) also the Coriolis force is of importance. The Coriolis force is an apparent force, which is caused by the rotation of the earth. This force deflects the tidal movement to the right in the northern hemisphere, which causes a counterclockwise rotation. In the southern hemisphere this deflection is to the left. However, this effect is very small in e.g. tidal basins. When the Coriolis terms are of the same magnitude as the gravitational terms, a geostrophical equilibrium is

reached and the result is a Kelvin wave. The amplitude of the Kelvin wave is the highest along the coasts on the right hand side relative to the direction of propagation (de Swart, 1996). The tidal wave in the North Sea has the character of such a wave. Because the tidal wave is continuously turned off to the right (seen from the propagating direction) a wave is generated, that travels round in the North Sea. This results in large differences in phase between the western and eastern coasts. High water at the coast of England can occur simultaneously with low water at the coast of Denmark. The central point around which the wave propagates is called an amphidromic point (see figure 2.1). In this point the vertical amplitude of the tide is (almost) zero. However, there is a horizontal tide in this point.

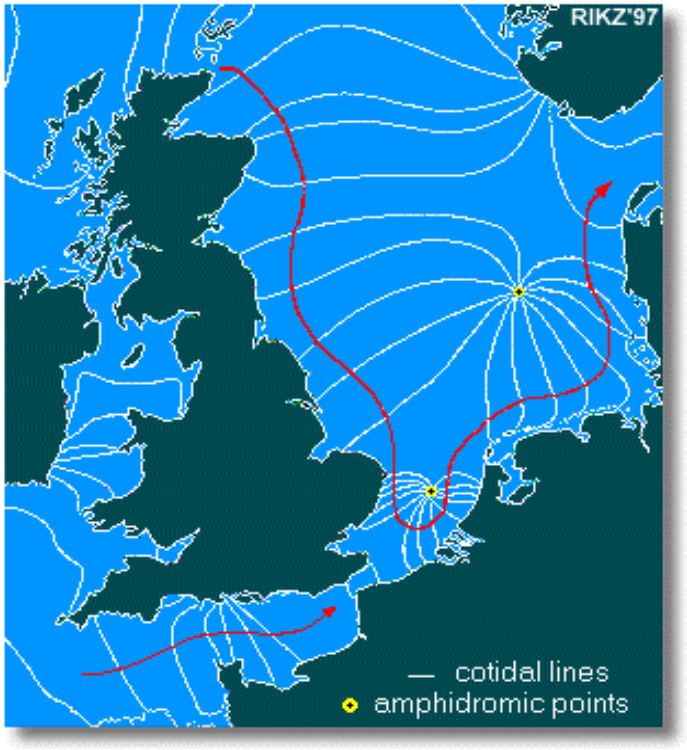

Fig. 2.1 Cotidal chart of the North Sea and its amphidromic points

Another important effect is the 'closed' boundary in the south, due to the relatively small opening of the Channel. When the tidal wave from the north reaches this boundary, reflection takes place and the tidal wave is enlarged. However, frictional effects attenuate this enlargement of the tidal wave.

The tidal wave propagates along the Dutch North Sea coast in north-east direction, while the amplitude of the tidal wave rapidly diminishes from about 4 m near Vlissingen to a minimum value of 1.4 m in Den Helder. The tidal range then gradually increases north-eastward along the Frisian Islands coast to about 3 m.

In figure 2.2 the water level time series at three locations along the Dutch coast are plotted, calculated with the tide generator. The differences in the phases confirm that the tidal wave is

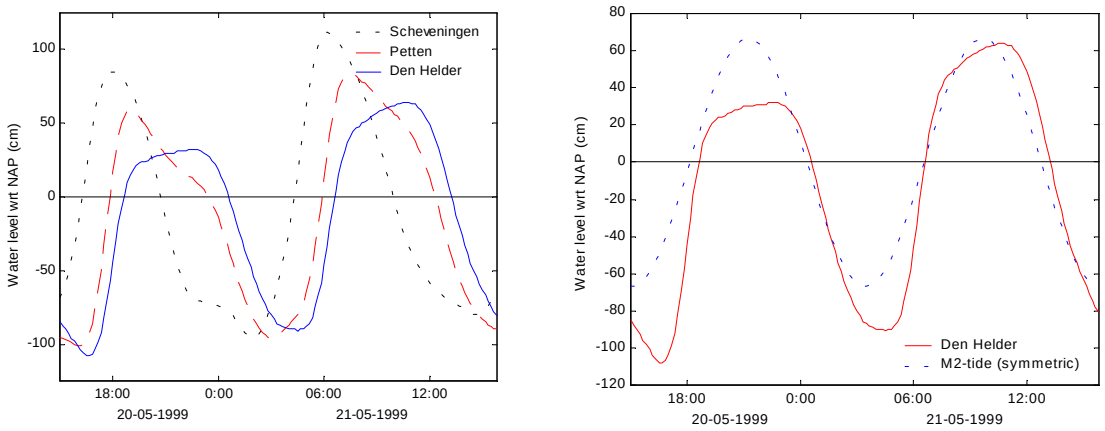

Fig. 2.2 Water level series along the Dutch coast (a) and asymmetry at Den Helder (b)

propagating from the south to the north. The amplitudes differ due to fact that the northern tidal gauges are situated closer to the amphidromic point between the Netherlands and Great Britain. In the second plot the water level curve in Den Helder is plotted together with the symmetric M_2 tide, which has equal rise- and fall periods. The water level curve shows that the rise period is shorter than in the case of the symmetric M_2 tide and the fall period has about the same length.
After the tidal wave has entered the Texel inlet, it propagates along the coast towards the next tidal inlet, the Eierlandse Gat.

2.3 Tides in the Marsdiep basin

Within the Marsdiep tidal basin the tidal wave propagates from the entrance towards the end of the basin. The amplitude and phase of the tidal wave within the basin are determined by the large-scale geometry of the basin. For an overview of the Marsdiep basin see figure 1.2. The most important aspects are the overall length and depth of the basin and the relative area of the tidal flats. The depth of the basin is important in that it determines the travel speed of the tidal wave and, thereby, its length. So, the overall length and depth in the main channel determine whether or not the basin is close to resonance. Due to the construction of the Afsluitdijk in 1932, the length of the basin decreased. The length of the main channel from Den Helder to Harlingen became about 60 km. This length is close to a quarter of the tidal wave length and therefore closer to tidal resonance.
The depth of a basin is also important in that it determines the relative influence of bottom friction. Bottom friction dissipates the energy of the wave and can reduce its amplitude. In the Marsdiep basin the interaction of the incoming and the reflected tidal wave can increase the tidal amplitude drastically from the entrance toward the land ward end of a basin.

In figure 2.3 the oscillation of the tidal wave in the Marsdiep basin is illustrated. Inward of the basin, the tidal amplitude becomes larger. The period between the tidal wave top in Den Helder and Harlingen is about 3 hours, but this period varies as can be seen in the figure, due to the asymmetry in the tidal wave. The tidal wave in Den Helder shows the highest asymmetry.

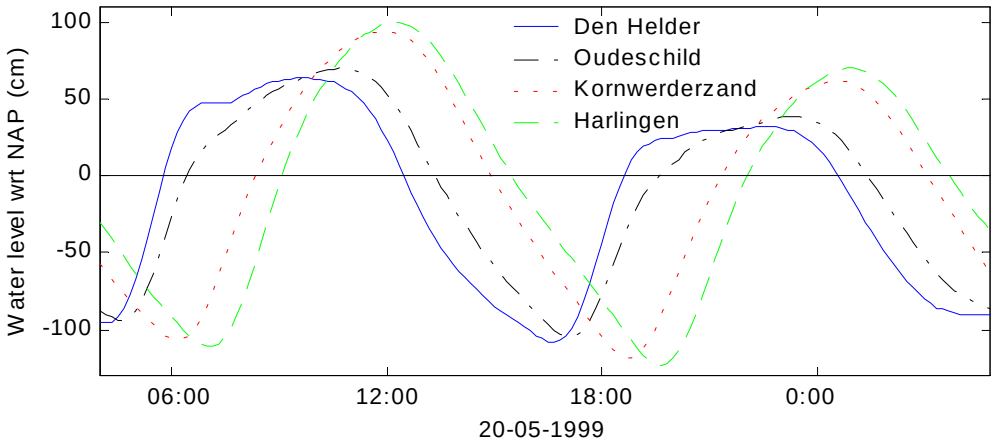

Fig. 2.3 The oscillation of water levels in the Marsdiep basin

The tidal wave in the Texel inlet has a propagating character. The amplitude of the reflected wave is negligible compared with the amplitude of the incoming wave. Bottom friction has dissipated the energy of the reflected wave before it reaches the inlet. Since the tidal propagation is of such nonlinear nature it is not a pure wave-like motion. Further into the basin, the amplitude of the reflected wave enlarges and the tidal wave becomes more of a standing character towards Harlingen. In the case of a standing wave, a faster tidal rise (or –fall) than the tidal fall (or –rise) results in higher flood currents than ebb currents.

2.4 Mechanisms generating higher harmonics

The description of the (nonlinear) mechanisms in this paragraph is partially adapted from Parker (1991). The wave propagation velocity for long waves without friction ($c_0=(gh)^{1/2}$) is approximately constant over a tidal cycle only if the tidal amplitude (η) is much smaller than the depth (h), so if $\eta/h << 1$. For a progressive long wave in shallow water, where η/h is not negligibly small and where η therefore significantly affects the total depth, the wave crest travels faster than the trough. The resulting wave profile is distorted from a perfect sinusoid, showing a faster rise to high water and a slower fall to low water. High water occurs earlier and low water occurs later. Subtracting the original sinusoid (e.g. the semi-diurnal constituent M_2) from this distorted profile, energy is found in the second harmonic (M_4) and in other even harmonics.

The first-order effects of friction are to decrease the wave propagation velocity and the attenuate the wave amplitude. This linear effect does not distort the wave profile; both high and low waters are delayed and decreased in amplitude. However, the two nonlinear aspects of the frictional momentum loss will lead to distortion. The effect is that the frictional loss of momentum per unit volume of fluid is smaller for greater depths and greater for smaller depths, so the crest will travel faster than the trough. This asymmetric effect can thus generate M_4 and other even harmonics.

Second harmonics, including M_4, are generated by the above mechanisms because the maximum wave propagation velocity and minimum attenuation occur at the crest and the opposite occurs at the trough.

Quadratic friction causes maximum attenuation and minimum wave propagation velocity at both maximum flood and maximum ebb with the opposite occurring at slack waters. The result of this symmetric effect is a third harmonic, M_6.

In general the influence of these nonlinear interactions on tidal distortion is relatively small on the shelf as compared to their influence in relatively shallow tidal basins with large intertidal areas.

The effects of a mean flow on the tide can also be explained in terms of changes in waves propagation velocity and frictional attenuation. A mean flow makes ebb current speeds larger and flood current speeds smaller. Due to the quadratic nature of the frictional momentum loss, the increased loss during the ebb phase is greater than the decreased loss during the flood phase. The result is a greater loss than if the mean flow were not present and thus greater damping of the tidal wave and a reduced tide range. Quadratic friction effects, being greater during ebb than during flood and thus asymmetric, also lead to generation of M_4; low waters are delayed and high waters are accelerated. Frictional generation of M_6 also takes place. The M_6 constituent is both generated and dissipated by bottom friction.

2.5 Analysis of tides

In this section the method of harmonic analysis is described, which is used for comparing the measurements with the model results. It also includes a description of tidal asymmetry.

2.5.1 Harmonic analysis

Harmonic analysis is a form of signal demodulation, in which the user specifies the frequencies to be examined. The harmonic analysis makes use of least-squares techniques, which is based on the minimisation of the squared error. The use of this technique for tides appears to have originated with Lord Kelvin (1824-1907) around 1867.
The harmonic analysis method has a variety of attractive features. It permits resolution of several hundred tidal constituents of which 45 are typically astronomical in origin and identified with a specific frequency in the tidal potential. Each of these 45 constituents corresponds with one of the relative astronomical motions between earth, sun and moon. The remaining constituents include shallow water constituents associated with bottom frictional effects and non-linear terms in the equations of motion as well as radiational constituents originating with atmospheric effects. These remaining constituents are compound or higher harmonic constituents. The familiar hierarchy of 'harmonic' tidal constituents is dominated by diurnal and semidiurnal motions, followed by motions with fortnightly, monthly, semi-annual and annual variability.

The harmonic analysis approach yields the required amplitudes and phase lags of the harmonic tidal components or any other constituents that the user wishes to specify. Each of the components has an amplitude and phase, which is unique to a given location. In this context, phase means the fraction of the tidal cycle that has been completed at a given reference time.
Once these coefficients have been determined, we can use them to reconstruct the original time series. The original time series is reconstructed with the following formula:

$$Q(t) = A_0 + \sum_{i=1}^{n} A_i \cos(\omega_i t - \alpha_i)$$

in which Q(t) is the time series, A_0 the mean value of the record and where A_i, ω_i and α_i are respectively the amplitude, frequency and phase of the *i*-th constituent that is specified.
In the case of tidal motions, subtraction of the reconstructed tidal signal from the original record yields a time series of the non-tidal component of the time series. This component plays an important role in the sediment transport in tidal inlets.

Based on the amplitudes and phases derived by means of a tidal harmonic analysis, relative accurate comparisons can be made between observations and model results. Deviations in amplitude and phase can be precisely quantified.

Nyquist criterion

When using a harmonic analysis the Nyquist criterion determines the highest distinguishable frequency, the so called Nyquist frequency, f_n :

$$f_n = \frac{1}{2 \cdot \Delta t}$$

In the time series of the discharge through the Texel inlet, only one value is found every crossing. The time difference Δt between two discharge values is 30 minutes, which results in a f_n of 1

cycle/hour or 24 cycles/day. In this study only constituents with frequencies up to 6 cycles per day are taken into account. So this is not a restriction in the analyses.
For the lowest separable frequency, it is necessary that the time series contains at least one period of the chosen component (Godin, 1972). Thus records must have minimum length of 13 h in order to incorporate at least one cycle of the M_2 tidal frequency (period of 12.42 h). The mean component A_0 is also included. As the length of the record is increased, additional constituents can be added to the analysis. For example, the K_1 constituent (period of 23.93 h) can be adequately determined once the record length exceeds 24 h, although less reliable estimates can be made for shorter record lengths.

The aim of least-squares analysis is to estimate the tidal harmonic constituent amplitudes and phases, which can then be used for long-term tidal predictions. The least-squares method can be applied to any combination of tidal frequencies. However, the rational approach is to select the allowable frequencies on the basis of two factors:

- their relative contribution to the tide-generating potential. The constituent should be one that makes a significant contribution to the tide-generating force. Due to noise limitations, the amplitudes of many constituents are too small to be adequately resolved by most oceanic data sets.
- their resolvability in relation to a neighbouring principal tidal constituent. The record should be of sufficient duration to permit accurate separation of neighbouring frequencies.

Criteria for the second factor, indicating which frequencies can be resolved in a time series, are only applicable to equidistant time series. As is already stated, the time series obtained with the ADCP attached to the ferry are non-equidistant. However, an indication of the lowest and highest frequency, and the smallest frequency difference that can be distinguished is desirable. The highest frequency used in the harmonic analysis in this study has a value of 6 cycles per day. The difference with the calculated 24 cycles per day is sufficient, so the Nyquist criterion is not a restriction.

Rayleigh criterion

To distinguish two components that have frequencies, which are relatively close to one another, a requirement is made for the minimum length of the time series. This criterion is known as the Rayleigh criterion and is given as follows:

$$|f_2 - f_1| = \frac{1}{T}$$

where f_2 and f_1 are the frequency components and T is the record length of the data set. This criterion requires that only constituents, separated by at least one complete period from their neighbouring constituents over the length of data record, be included in the harmonic analysis of a given time series (Godin, 1972)

Important for the harmonic analysis of the ferry observations is that the method allows gaps in the time series. So times for which there are no data can be ignored.

	O_1	P_1	K_1	mu_2	N_2	nu_2	M_2	λ_2	L_2	S_2	K_2	M_4	MS_4	M_6
O_1		14.8	13.7	1.1	1	1	1	1	1	0.9	0.9	0.3	0.3	0.2
P_1			183	1.1	1.1	1.1	1.1	1	1	1	1	0.3	0.3	0.2
K_1				1.2	1.1	1.1	1.1	1	1	1	1	0.3	0.3	0.2
mu_2					31.8	27.6	14.8	10.1	9.6	7.4	7.1	0.5	0.5	0.3
N_2						206	27.6	14.8	13.8	9.6	9.1	0.5	0.5	0.3
nu_2							31.8	15.9	14.8	10.1	9.6	0.5	0.5	0.3
M_2								31.8	27.6	14.8	13.7	0.5	0.5	0.3
$\lambda 2$									206	27.6	23.9	0.5	0.5	0.3
L_2										31.7	27.1	0.5	0.5	0.3
S_2											183	0.5	0.5	0.3
K_2												0.5	0.5	0.3
M_4													14.8	0.5
MS_4														0.5
M_6														

Table 2.1 Periods in days needed to distinguish two constituents

Table 2.1 shows for some important diurnal and semidiurnal constituents, how long at least the observation period or record length must be to distinguish them in an analysis. The period that is at least needed to distinguish the M_2 and S_2 constituent is 15 days. A very common period for an analysis is 29 days, since the distinction of most of the important constituents requires a period shorter than 29 days.
Since the measured data is analysed for rather long periods (varying from 3 months to two years) to filter the meteorological and the irregular sluice discharges effects, often all the constituents are being distinguished from their neighbouring constituents.
Although the L_2 and nu_2 are not taken into account in the analyses of the models, it is chosen to take at least a period of 32 days, in order to distinguish M_2 from nu_2 and $labda_2$ and S_2 from L_2. In this way, the models and measurements can be reasonably compared.

In table 2.1 also a compound tide can be found. Compound tides are merely a convenient way to describe the modulations of the primary tidal components. For example, when the M_2- and S_2-tidal waves are in phase, the total depth under the crest of the combined wave will be greater than when they are out of phase. Thus, the generation of M_4 due to greater depth at the crest than at the trough ($\sqrt{(gh)}$) will be modulated by the M_2-S_2-cycle, causing a new constituent, MS_4. Similar processes play a role for the other compound tides.

Relative phases

The calculation and graphical display of the amplitude and phase for tidal constituents can help understanding the tide induced dynamic processes in coastal seas. This is a nice instrument in the verification process of a numerical model for a specific area. Besides this, an additional graphical display can be made, in which the phases are presented relatively to each other. Hereby the relative phase difference is determined between two constituents. This phase difference can be calculated from the harmonic analysis by writing the M_2 constituent as follows:

$$u_{M_2} = a \cdot \cos(\omega t) + b \cdot \sin(\omega t)$$

$$= \sqrt{(a^2 + b^2)} \cdot \cos(\omega t - \varphi_{M_2})$$

In which a and b are the amplitudes which are determined with the harmonic analysis, ω is the angle velocity and φ_{M_2} the phase of the M_2 constituent. This phase is calculated by:

$$\varphi_{M_2} = \arctan(\frac{b}{a})$$

in which the angle φ_{M_2} must be in the same quadrant as the vector (a,b). The M_4 constituent has an angle velocity 2 times the angle velocity of the M_2 constituent and can be written, in the M_2 angle velocity, as follows:

$$u_{M_4} = c \cdot \cos(2\omega t) + d \cdot \sin(2\omega t)$$

C and d are the amplitudes of M_4, ω is the angle velocity of the M_2 constituent. For the M_4 phase the phase equation for the M_2 phase can be used, where a and b must be replaced by c and d. The phase difference between M_4 and M_2, is calculated relative to the time of maximum positive amplitude of the M_2 constituent:

$$\max(\sqrt{(a^2 + b^2)} \cdot \cos(\omega t - \varphi_{M_2})) \Rightarrow t = \frac{\varphi_{M_2}}{\omega}$$

Filling this value into the equation of the M_4 constituent gives:

$$u_{M_4} = \sqrt{(c^2 + d^2)} \cdot \cos(2\omega \cdot \frac{\varphi_{M_2}}{\omega} - \varphi_{M_4})$$

$$= \sqrt{(c^2 + d^2)} \cdot \cos(2 \cdot \varphi_{M_2} - \varphi_{M_4})$$

Thus the phase difference between M_4 and M_2 is defined as:

$$\Delta\varphi_{M_2-M_4} = 2 \cdot \varphi_{M_2} - \varphi_{M_4}$$

A similar calculation can be made for any combination of tidal constituents. In the further analysis relative phase differences of the constituents are all relatively to the M_2 constituent.

2.5.2 Tidal asymmetry

The nonlinear mechanisms influence a tidal wave propagating in shallow waters. A consequence of this is the appearance of distortions of the primary tidal constituents, generally represented by overtides. Due to the presence of these overtides the elevations and currents within an estuary are not perfect sine waves, but exhibit asymmetry between flood and ebb elevations and currents. Generally for the M_2 tide, the first overtide M_4 (at twice the M_2 frequency) is the most important cause of tidal asymmetry.

Asymmetry in tidal currents implies that the flood part of the velocity-time curve has a shape different from the part representing the ebb. When considering a single fundamental harmonic, e.g. M_2, and its first overtide M_4, and assuming a rectilinear current, the current can be expressed as:

$$u(t) = \hat{u}_{M_2} \cos \omega t + \hat{u}_{M_4} \cos(2\omega t - \beta)$$

in which $\hat{u}_{M2}$ is the amplitude of the M_2 tidal current, $\hat{u}_{M4}$ is the amplitude of the M_4 tidal current ω is the angular frequency of the M_2 tide and β is the phase of M_4 relative to M_2. The definition of β is already discussed.

In figure 2.4 current curves u(t) are plotted for four different values of the phase difference of M_4 with M_2, β, for 15 hours. The amplitude of the M_2 tidal current is defined as 1 m/s and the amplitude of the M_4 tidal current is defined as 0.20 m/s.

When defining a symmetry axis at the time of slack water, the curve u(t) is symmetric only for $\beta=90^o$ and $\beta=270^o$. For all other values, the current curves are asymmetric. For $-90^o < \beta < 90^o$ flood velocities (defined as positive) are larger and the flood duration is shorter than for the ebb. The reverse holds for $90^o < \beta < 270^o$ (Van de Kreeke, 1993).

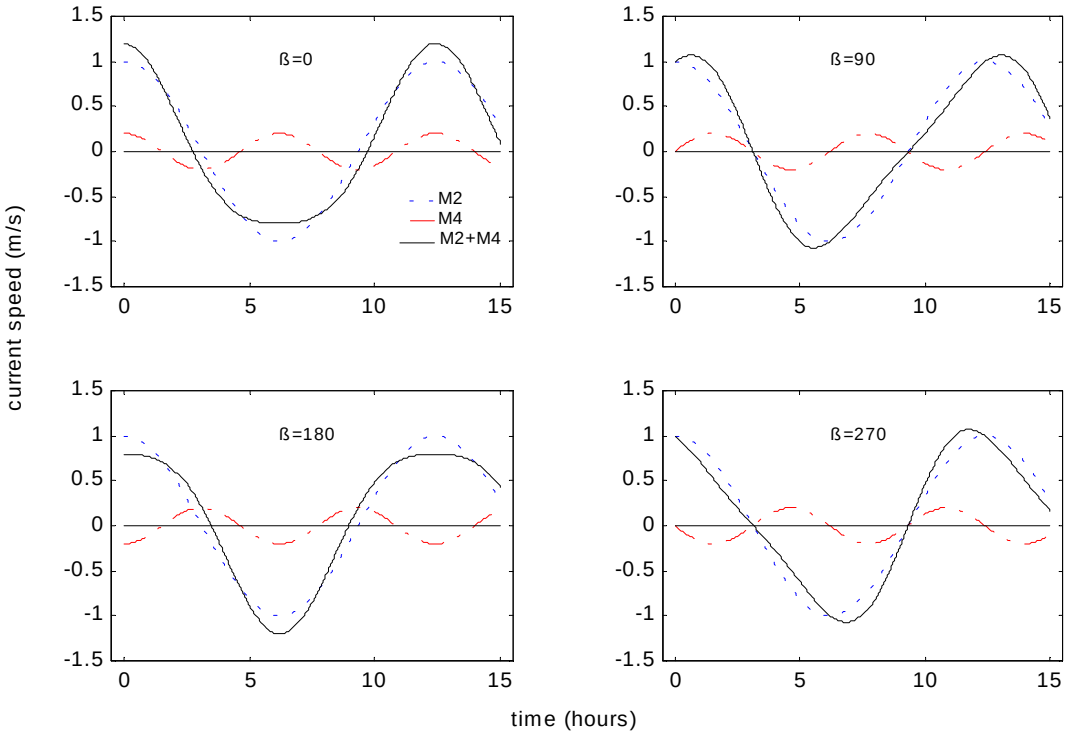

Fig. 2.4 The M_2 and M_4 tidal current constituents for different values of β

The asymmetry in tidal currents is mostly quantified by the ratio between the M_2 and M_4 tidal current amplitude and the phase difference between both. In combination, these determine the direction and magnitude of the net transport of sediments due to tidal asymmetries.
Thus tidal asymmetries are very important for the net tidally averaged transport of sediments. These asymmetries can cause a net transport of sediments even if there is no net transport of water. In the Texel inlet the net transport of water is directed outwards, which influences the net transport of sediments. Two types of tidal asymmetries can be distinguished:

- the average magnitude of the flood currents differs from the average magnitude of the ebb currents, accompanied by a difference in the duration of the flood and the ebb periods (Friedrichs and Aubrey, 1988).
- there is a difference in the rate at which current and direction of the current change near high-water slack as compared to low-water slack (Dronkers, 1986).

The first type is most important for bed load transport (coarse-grained material), whereas the second type is important for suspended matter transport (fine-grained material).

3 Observations

To validate models, model results are compared with measured data in that area. Besides the water levels and the discharge, also currents will be used to validate the models. The possibility of validating a model with a time series of discharge and currents across an inlet is rather unique. This data set is generated from measurements of an ADCP mounted on a ferry. This chapter gives a description of these three types of observations. First the water levels are discussed in paragraph 3.1. Paragraph 3.2 gives an explanation about the ferry observations. The measured currents are described in paragraph 3.3. A first analysis and verification of the measurements are presented in the last paragraph.

3.1 Water levels

The water level elevation is measured at several locations in Holland (see figure 3.1). Every measuring location is fitted with a digital instrument. The float of the instrument drifts in a tidal gauge, which is connected to the water outside. The water level is measured with respect to the NAP (Normaal Amsterdams Peil). The continuous measured water level is averaged every 10 seconds. These mean values are averaged to one value every 10 minutes. This mean value is being saved on a central system.
Since late 1997 NIOZ has collected the water level variation of four of these tidal gauges from the Dutch RWS Berichtencentrum. The four tidal gauges are Den Helder, Texel Noordzee, Den Oever and Harlingen. The collected water level variation includes the effect of storms, but with the use of a harmonic analysis most of these variations are filtered.

The water level elevation in the other stations is predicted with the tide generator of the Dutch RWS. The generated astronomical water levels will differ from the levels actually occurring. The predictions are valid for average meteorological conditions and average river discharges; deviations of these conditions affect the actual tides.

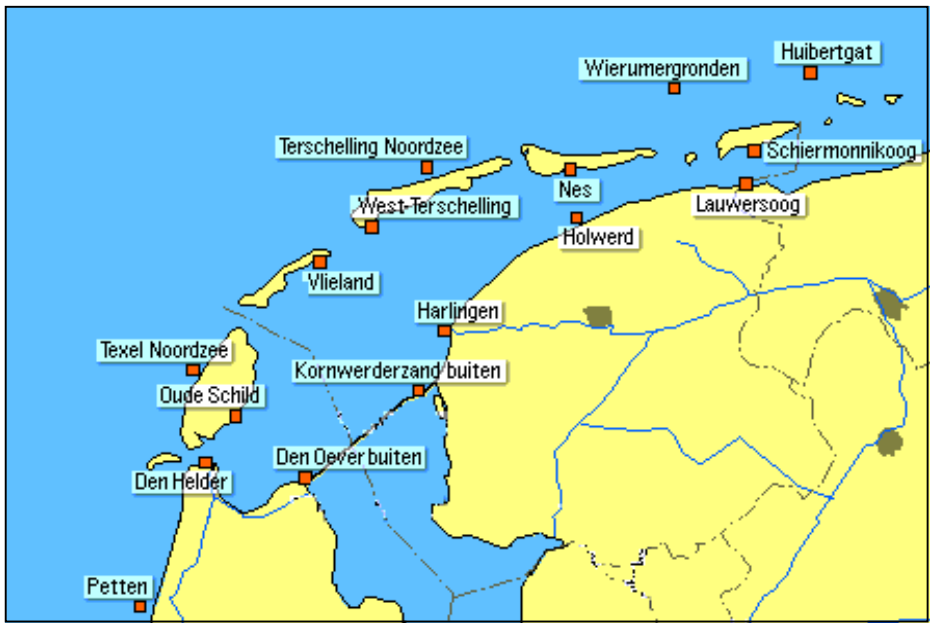

Figure 3.1 Tidal gauges used for validating the models

3.2 Ferry observations

In a co-operation between NIOZ (Netherlands Institute for Sea Research) and the ferry company TESO (Texels Eigen Stoomboot Onderneming) continuous observations from the ferry 'Schulpengat' are carried out in the Marsdiep tidal inlet between the North Sea and Dutch Wadden Sea. The measurements include surface temperature, salinity and fluorescence as obtained from a through-flow system as well as vertical profiles of velocity and echo-intensity, obtained with an Acoustic Doppler Current Profiler (Nortek-ADCP). During maintenance activities late 1997 the ADCP was placed below the hull of the ferry. In addition a temperature sensor (Seabird) was attached near the ADCP. The continuing observations started early 1998. Further description of the ferry observations is adapted from Ridderinkhof (2000).

Location of the ferry observations

The ferry observations are performed in the Marsdiep tidal inlet, the southernmost tidal inlet of the Wadden Sea, see figure 3.2. The Marsdiep inlet forms the connection between the largest basin of the Wadden Sea and the adjacent North Sea.

The ferry crosses the inlet twice per hour, daily between 06.00 a.m. and 10.00 p.m. Each trip takes 12-15 minutes (the ferry speed is about 10-12 knots) so that more or less synoptic observations are obtained. The right side of figure 2.2 shows typical tracks of the ferry during one day. The tracks are marked with small dots. Navigational purposes cause some variation in the track of the ferry across the inlet. This variation depends strongly on the phase of the tide and also on the presence of other vessels in the area.

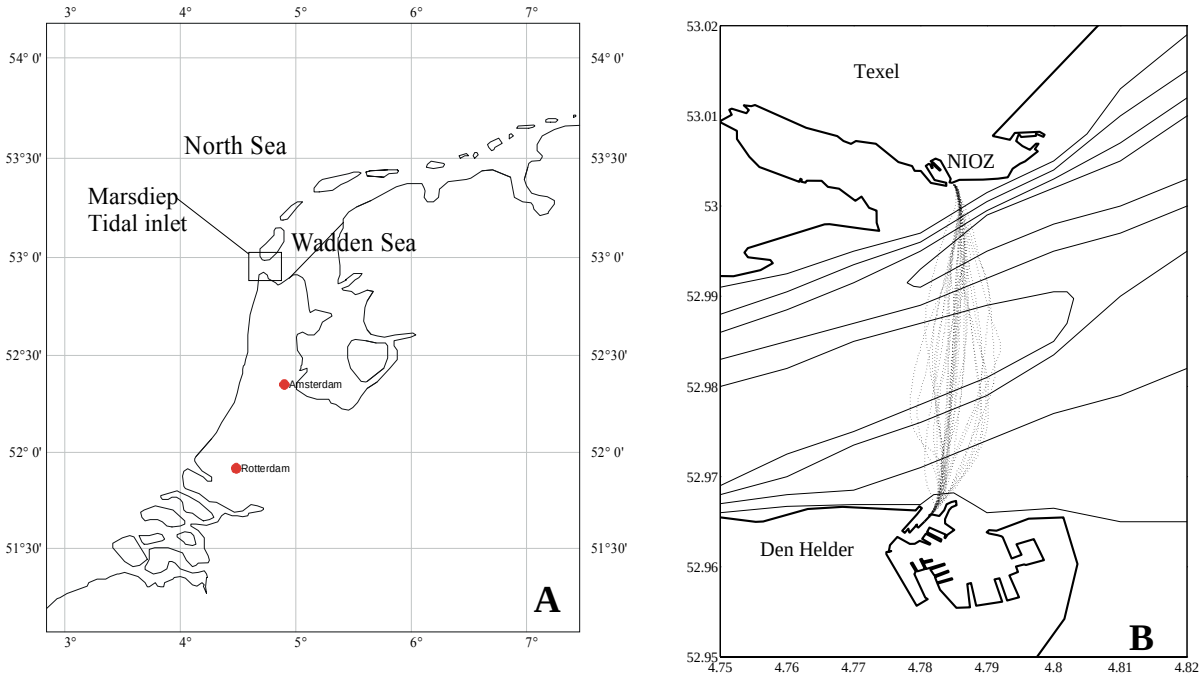

Figure 3.2. Map of the area where the ferry observations are carried out (a) and tracks of the ferry during one day (b)

The distance between the ferry harbours at both sides of the inlet is about 4.5 km. The water depth in the inlet varies between about 10 m just outside of the harbours and about 25 m in the deepest part.

Instrumentation

A 1.5 MHz ADCP (Nortek, 1998) is attached near the keel of the ferry in the middle of the vessel at 4.3 m below the sea surface. The instrument has been fastened to a plate below the ferry's hull leaving some 30 cm open space between the hull and the instrument. This device has been chosen to minimise the possibility of air bubbles, affecting the acoustic measurements, most presumably present in a thin layer below the hull of the ferry.

Fig. 3.3 Iron cage at the keel of the ferry

The instrument is electrically shielded from the ferry and well protected against corrosion. An iron cage protects the instrument against damage from collisions with floating debris. See figure 3.3 en 3.4. The ADCP records current speed and direction and intensity of the back-scattered signal in 0.5 m vertical bins between 4.8 m (the blanking distance is 0.5m, i.e.1 bin and the draught of the ferry is 4.3 m) below the surface and the bottom. The bottom is detected using the derivative of the intensity of the back-scattered signal, which increases significantly because of the strong reflection at the bottom. In the period March-July 1998 the ADCP recorded each 4.5 s, from August 1998 the interval between successive observations is 2.5 sec. Thus, each trip of the ferry across the inlet results in some 300 vertical profiles of each ADCP parameter. Next to the ADCP a temperature sensor (Seabird) records the water temperature every second. The functioning of the observational system is fully automated using data from the GYRO and DGPS system onboard the ferry. Recording of data starts automatically when the ferry is outside the harbour jetties.

Fig. 3.4 Attaching the ADCP in the iron cage

A dedicated computer onboard of the ferry combines and stores the data from the through-flow system, ADCP, DGPS and GYRO. By combining the last three instruments a correction for the ferry speed is made. The measured current is stored as currents in three directions: east-west, north-south and in the vertical. Each time when the ferry docks in the harbour of the island Texel, the collection of one hour of data is transmitted by telemetry to the computer system of the institute, located at about 300 m from the ferry harbour. The ADCP is checked visually each time when the ferry is in dock for maintenance (each winter). At night the ferry docks in the harbour of Texel.

To verify the measurements from the ferry, calibration measurements are regularly carried out in the inlet, which cover a 13 hour-span. Apart from current velocities and echo intensities, these measurements also include salinity, temperature and suspended matter. Instruments that are being used during these moorings are a CTD, a moored ADCP and a filtrate system for determining the amount of suspended matter. The latter is measured to verify and afterwards calibrate the echo intensity as being a measure for the suspended matter concentration.

Data processing

For each trip of the ferry the transport of water through the inlet, Q(t), is determined from:

$$Q(t) = \sum(\sum(ve_{(i,j)} \cdot binsize) + ves \cdot ds) \cdot \Delta y_{(j)}$$

in which $ve_{(i,j)}$ is the eastward component of the velocity at bin *i* for observation *j*, *binsize* is the cell size (0.5 m), *ves* is the surface velocity, *ds* is the vertical distance between the water surface and the first bin (4.8 m) and $\Delta y_{(j)}$ is the northward displacement (in m) of the ferry between two successive ADCP observations as obtained from the DGPS system. For the surface velocity, *ves*, the mean value of the eastward velocity for bin 1 and 2 is taken. The (inner) summation runs from *i=1* to *i=nd-1* in which *nd* is the cell where the bottom depth is found, and (outer) from *j=1* to *j=npings*, in which *npings* is the total number of ADCP observations during one trip of the ferry. The resulting value of Q is attributed to the mean value of t (in GMT) for the specific trip. This procedure results in 32 values per day, with an interval of about 30 minutes, between 6 a.m. and 10 p.m. The series is extended with additional values if the ferry makes extra trips outside of the regular service. This happens regularly (for ambulance service during night-time).

Outliers within this time series, e.g. due to malfunctioning of the DGPS or the connection between the ADCP and the computer network, are removed. A smoothed time series, by taking the average value of two successively observed values for Q, has been used for further analysis.

The resulting time series that is used runs from March 15, 1998 to December 31, 2000 and contains 23530 values. Figure 3.5 illustrates this time series as a function of time in which day 0 corresponds with January 1, 1998. The top shows the entire record and the bottom a sub-sample of a record for one week in April 2000.

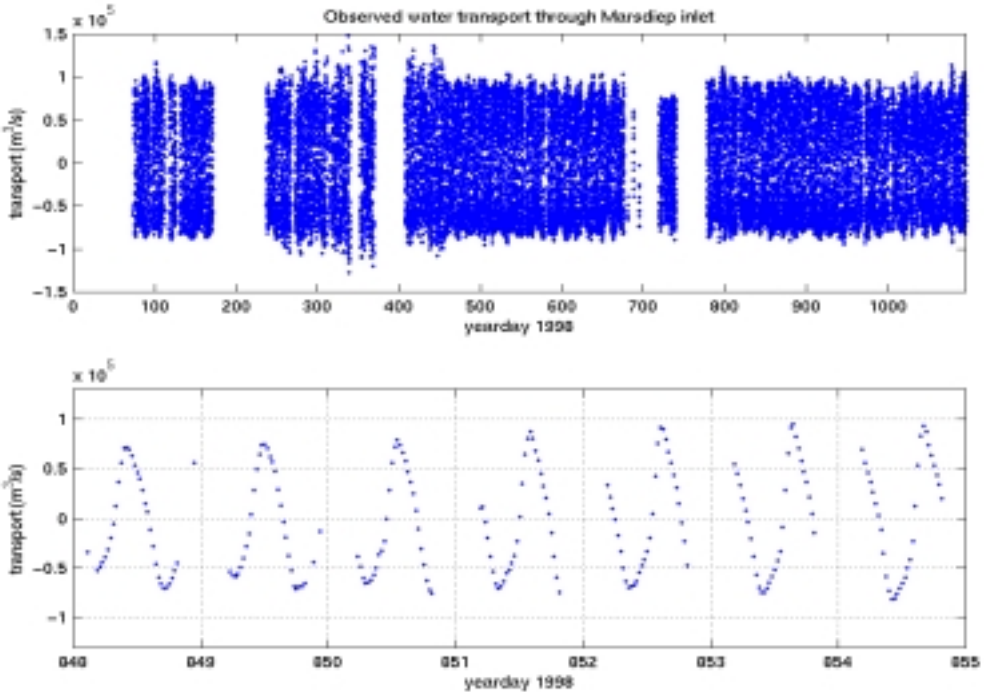

Fig. 3.5 Observed volume transport through the Texel inlet

Relatively long gaps in the record (roughly one month, see top of figure 3.5) occur each winter when the ferry is out of service for maintenance. In 1998, in the period around day 200, there is a relatively long period without observations due to technical problems in the cable connection. After solving this technical problem no major problems were encountered during the entire period between summer 1998 and winter 2001. The data series for one week (bottom figure 3.5) clearly illustrates the presence of a spring-neap cycle (and one extra value due to ambulance service on day 848).

3.3 Currents

To analyse the tidal movement through the inlet, 17 evenly spread locations are selected across the inlet. The locations are numbered from north (point 1) to south (point 17), as can be seen in figure 3.6. For every crossing of the ferry the measurement that is closest to each of these separate points is taken as a data point. In this way, time series for each of the 17 locations are generated, with time steps between 10 and 50 minutes, depending on the place of the chosen point. Near the harbours time steps are 10 and 50 minutes successively, in the middle of the inlet the time steps are in the order of 30 minutes.

The obtained time series include velocities in east-west and north-south direction. The vertical velocities are rather small and will not be taken into account in the analyses. These three velocity time series of every depth-cell in the vertical are treated independently. When combining the currents in the east-west and north-south direction, a main axis can be determined, along which the difference between flood and ebb current is maximal.

The axes are rotated in the direction of the main axes of the depth-mean current, so that the (depth-mean) main current coincides with the main axes. The signal of the secondary current, perpendicular to the main current, showed a large noise to signal ratio. Since the currents are measured every 0.5 m in the water column, vertical current profiles can be determined across the tidal inlet. This work was done in a previous study by R. de Leeuw.

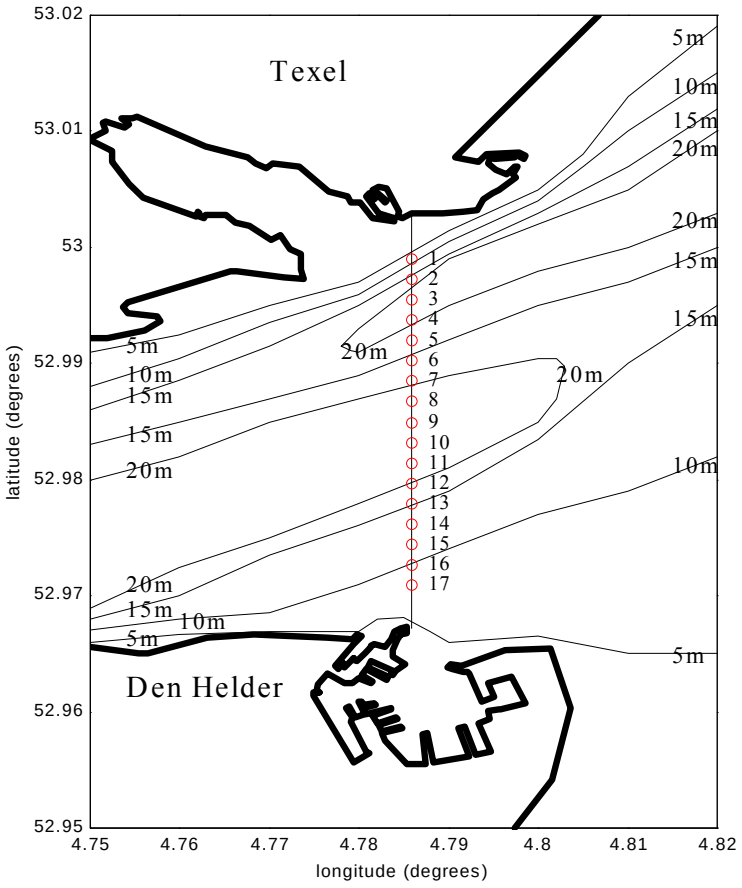

Fig. 3.6 The locations of the 17 data points

3.4 First analysis of measurements

Vertical water movements, associated with the rise and fall of the tide, are accompanied by horizontal water motions called tidal currents. Harmonic analysis was carried out on the time series of the measured currents in the main, east-west and north-south direction. In these two directions the time series through every depth-cell in the vertical are treated independently, so mutual influence through the harmonic analysis is excluded. Parts of this paragraph are adapted from a preliminary abstract by Ridderinkhof (2000).

Due to the long data set of current velocities and water levels, it was possible to distinguish a large amount of components. In the first analysis of the currents 65 components were taken into account. The interpretation of the results of a harmonic analysis with such a large amount of tidal components is not unambiguous, since some primary tidal components are accompanied by compound tides with exactly the same frequency. These compound tides are the result of wave-wave interactions which are characteristic for the non-linear tidal motion in shallow waters.

The percentage of the signal that was declared with the harmonic analysis of 65 constituents for the currents in the main direction was on average 90%, varying between 85% (close to ferry and bottom: high noise-to-signal ratio) and 95% ('undisturbed' part of water column).

The overall error Δ in the estimated harmonic amplitudes (Godin, 1972) can be approximated by:

$$\Delta = \frac{\sigma}{\sqrt{N}}$$

in which σ is the standard deviation of the residue (= observed value – fitted value) and N the number of data points. This error was in the order of $2\text{-}3*10^{-3}$ m/s for the ferry observations. Obviously, the meaning of this very small error is doubtful because even with a large standard deviation, the error can still be small as a result of the long data set (N ~ 18.000).
Moreover, the percentage explained variance has the same drawbacks since expanding the number of tidal constituents generally leads to an increase of this variance and a decrease in the overall error of the estimated harmonic amplitude, even if non-tidal frequencies are included in the harmonic analysis. This is a well-known problem in the case of non-equidistant time series, for which merely questionable criteria exist regarding the goodness-of-fit.

Due to the fact that the model simulation period covers only 32 days not all constituents are taken into account. To compare the model results with the measured data, a harmonic analysis including the eight most important constituents is chosen. These eight constituents are the largest components in the discharges and water levels. In table 3.1 these eight constituents are presented with their origin and period. Besides the constituents with diurnal and semidiurnal variability, which are typically astronomical in origin, one compound and two higher constituents are taken into account.

Tidal constituent	*Description*	*Period (hours)*
O_1	Lunar diurnal constituent	25,891
K_1	Lunisolar diurnal constituent (declination)	23,934
N_2	Lunar elliptic semi-diurnal constituent	12,658
M_2	Principal lunar semi-diurnal constituent	12,421
S_2	Principal solar semi-diurnal constituent	12,000
M_4	M_2-derived higher harmonic constituent	6,211
MS_4	M_2-S_2-derived higher harmonic constituent	6,105
M_6	M_2-derived higher harmonic constituent	4,140

Table 3.1 Tidal constituents used in the harmonic analysis

Verification of the ferry data

The general character of the tide in an area can be expressed by the first few diurnal and semidiurnal constituents. The factor F, defined by

$$F = \frac{K_1 + O_1}{M_2 + S_2}$$

Where K_1, O_1, M_2 and S_2 are the amplitudes of the corresponding constituents, may be used as an indicator of the type of tide as follows:

F = 0.00 - 0.25 : semidiurnal tides
F = 0.25 - 1.50 : mixed, mainly semidiurnal tides
F = 1.50 - 3.00 : mixed, mainly diurnal tides
F > 3.00 : diurnal tides

F is 0.17 in the case of the water level in Den Helder. The ratio in the area is always less than 0.25 and, in consequence, the tide can be classified as semi-diurnal. So, in this area the semidiurnal tides predominate, the ratio of mean spring range to mean neap range is given by $(M_2+S_2)/(M_2-S_2)$, where M_2 and S_2 denote the amplitudes of the respective constituents. In this area the spring range is about twice the neap range.

The transport through the inlet is driven by tidal variations in the water level, ζ. Therefore it is interesting to compare the amplitudes of the tidal components for ζ with the amplitudes of the volume transport, Q. Moreover such a comparison can be used as a 'check' on the results for the volume transports. This verification is a result of previous studies by Ridderinkhof and De Leeuw. A harmonic analysis, using the same 65 tidal components, was applied also to the observed water level variations in Den Helder, a 'standard' water level station in south-western part of the tidal inlet.

In figure 3.7 the amplitudes for both ζ and Q are shown relative to the amplitude of M_2 by dividing the results by the amplitude of M_2. Only components with an amplitude larger than 3 % of the M_2 amplitude are shown.
The figure shows that the relative amplitude of both variables is very similar, especially for the semi-diurnal components. The relative amplitude of the diurnal components is for the water level roughly two times higher than for the volume transport which can be explained from the simplified continuity equation for relatively short basins: $Q \sim \partial\zeta/\partial t$.
The relative amplitude of e.g. the K_1 constituent with the M_2 constituent can be written as:

$$\frac{Q_{K1}}{Q_{M2}} = \frac{\partial \xi_{K1}}{\partial t_{K1}} \cdot \frac{\partial t_{M2}}{\partial \xi_{M2}}$$

This relation shows that the K_1 component for ζ relative to M_2 is expected to be 1.9 (= T_{K1} / T_{M2}) as large as the relative magnitude of the K_1 component for Q, which is indeed the case as can be seen in the figure.

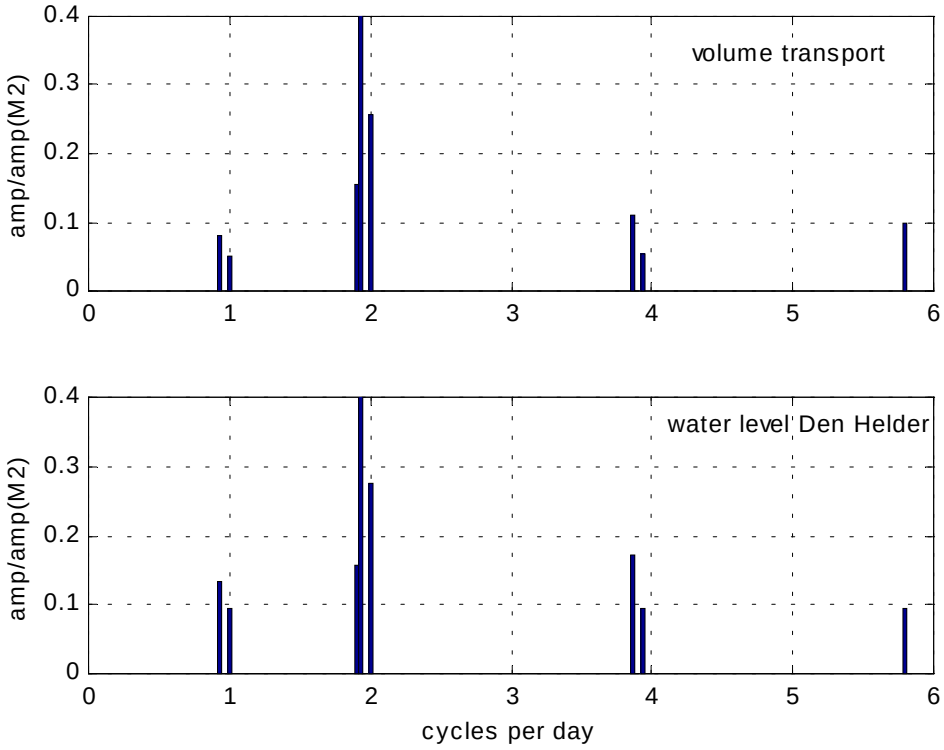

Fig. 3.7 The relative amplitude of volume transport and water level in Den Helder

4 The Delft3D model

In this chapter the Delft3D modelling system of WL | Delft Hydraulics is described. In this study only the flow module is used as the focus of this study is on hydrodynamics. Some additional programs are used for preparing files needed in the Delft3D-FLOW. These additional programs for creating grids and bathymetries are briefly described in appendix B. The post processing is done with self-developed Matlab routines, in order to make reasonable and relative accurate comparisons with the measurements.
In paragraph 4.1 the flow module of Delft3D is introduced. Paragraph 4.2 describes the set up of three models that are used in this study.

4.1 The flow module of Delft3D

Theoretical background
Delft3D-FLOW is the hydrodynamic program of Delft3D-MOR. It provides the hydrodynamic basis for morphological computations. Delft3D-FLOW calculates non-steady flow and transport phenomena resulting from tidal and meteorological forcing.
The main purpose is the two-dimensional (2D, depth averaged) and three-dimensional (3D) simulation of tidal and wind-driven flow by solving the unsteady shallow water equations in two (depth averaged) or three dimensions. In this approach the vertical momentum equation is reduced to the hydrostatic pressure relation. Vertical accelerations are assumed to be small compared to the gravitational acceleration and are not taken into account. The momentum equations in x- and y-direction are:

$$\frac{\partial u}{\partial t} + u\frac{\partial u}{\partial x} + v\frac{\partial u}{\partial y} + g\frac{\partial \eta}{\partial x} - fv + \frac{\tau_{bx}}{\rho_w(d+\eta)} - \frac{F_x}{\rho_w(d+\eta)} - \nu\left(\frac{\partial^2 u}{\partial x^2} + \frac{\partial^2 u}{\partial y^2}\right) = 0$$

$$\frac{\partial v}{\partial t} + u\frac{\partial v}{\partial x} + v\frac{\partial v}{\partial y} + g\frac{\partial \eta}{\partial x} + fu + \frac{\tau_{by}}{\rho_w(d+\eta)} - \frac{F_y}{\rho_w(d+\eta)} - \nu\left(\frac{\partial^2 v}{\partial x^2} + \frac{\partial^2 v}{\partial y^2}\right) = 0$$

(1) (2) (3) (4) (5) (6) (7) (8)

in which:

d	= water depth below plane of reference(m)
f	= Coriolis parameter (1/s)
$F_{x,y}$	= x- and y-component of external forces (N/m^2)
u,v	= depth averaged velocity (m/s)
U	= absolute magnitude of total velocity, $U=(u^2+v^2)^{1/2}$; (m/s)
ρ_w	= mass density of water (kg/m^3)
ν	= diffusion coefficient (eddy viscosity); (m^2/s)
η	= water level variation above plane of reference (m)
g	= gravity of acceleration (m/s^2)
$\tau_{bx,y}$	= x- and y-component of the bed shear stress (N/m^2)

The formulas consist of the following terms:

(1) velocity gradients
(2), (3) advective terms
(4) barotropic pressure gradients
(5) Coriolis force
(6) bottom stress
(7) external forces (wind)
(8) viscosity

The bottom roughness in the Delft3D-FLOW program can be defined in several ways. For a depth-averaged flow (2D) the shear stress on the bed in the x- and y-direction induced by a turbulent flow is given by a quadratic friction law:

$$\tau_{bx} = \rho_w g \left(\frac{|U| u}{C^2} \right)$$

$$\tau_{by} = \rho_w g \left(\frac{|U| v}{C^2} \right)$$

The 2D-Chézy coefficient C can be determined with the following formulations:

- Chézy formulation: C = Chézy coefficient [$m^{1/2}/s$]

- Manning formulation: $C = \frac{\sqrt[6]{h}}{n}$ h = total water depth [m]
  n = Manning coeff. [$m^{1/3}/s$]

- White Colebrook's formulation: $C = 18 \log_{10}(\frac{12h}{k_s})$ h = total water depth [m]
  k_s = Nikuradse roughness length [m]

For 3D computations the bed stress formulation is quite similar. In these computations the bed shear stress is related to the current in the first layer, using u_b (velocity at bed boundary layer) instead of U and C_{2D} instead of C_{3D}. The Chézy coefficients are generally used for calibration.

The depth-averaged continuity equation is given by:

$$\frac{\partial \eta}{\partial t} + \frac{\partial (d+\eta) u}{\partial x} + \frac{\partial (d+\eta) v}{\partial y} = 0$$

The set of partial differential equations in combination with an appropriate set of initial and boundary conditions for water levels and horizontal velocities is solved on a finite difference grid. The equations for the water levels are solved with an Alternating Direction Implicit (ADI) technique (Stelling, 1984). This means that the water levels and velocities in the x-direction are implicitly solved in the first half time step while in the second time step y becomes the implicit direction for both water level and velocity. For more details about this numerical method and the staggered grid, reference is made to the Delft-3D-FLOW user manual and Stelling (1984).

The main physical phenomena, which are accounted for in Delft3D-FLOW, are:

- Coriolis force.
- Turbulence model to account for the vertical turbulent viscosity and diffusivity based on the eddy viscosity concept. Four options: κ-epsilon, k-L, algebraic and constant model are provided.
- Shear stress exerted by the turbulent flow on the bottom based on a quadratic Chézy or Manning formula.
- Simulation of the thermal discharge, effluent discharge and the intake of cooling water at any location and any depth in the computational field (advective-diffusion module).
- Simulation of drying and flooding of inter-tidal flats (moving boundaries) for both 2D and 3D cases.

Besides this, Delft3D-FLOW has the facility to model wind stresses on the water surface by a quadratic friction law. However, wind effects are not taken into account in this study. For a complete review of physical phenomena and facilities, which are taken into account in their implementation, reference is made to the Delft3D-FLOW user manual.

Grid and bathymetry

In the horizontal plane a staggered grid is used (see figure 4.1). Each cell contains a water level point, a point for the bottom depth, a point for the velocity in x-direction (u-velocity) and a point for the velocity in y-direction (v-velocity). These points are not the same. The water level points are defined in the middle of each cell and the current components are defined on the cell boundaries.

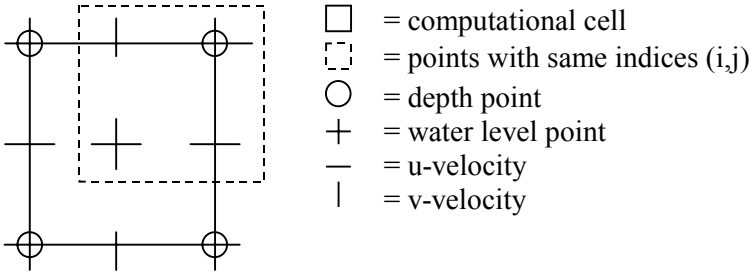

Figure 4.1 Staggered grid in Delft3D-FLOW

An additional program of Delft3D (RGFGRID; see appendix B) is used for creating orthogonal curvilinear grids. A curvilinear grid allows a high grid resolution near the area of interest and along the seacoast and a low grid resolution outside this area. Hereby the total number of cells is reduced and so the computational time. The grid allows to locate the boundaries of the grid well outside the area of interest, which reduces errors due to boundary effects. Depending on the available bottom data and the desired accuracy in the area of interest, a grid resolution can be chosen for the model.

For construction of the bathymetry another additional program of Delft3D (Quickin; see appendix B) is used. By using interpolation, the data of sample points is assigned to the grid cells. The bathymetry observations are generally obtained by:

- Digitising bathymetric charts (Admiralty Charts, Fair Sheets);
- Extracting the bottom schematisation of the area to be modelled from the bottom schematisation of an overall coarser hydrodynamic model
- Using available measurements (echo-soundings).

Initial and boundary conditions
A set of differential equations has no unique solution unless appropriate boundary conditions are specified. At the start of the simulation the currents and water levels are set to zero in the whole area. Boundary conditions are applied on the open boundaries, which are used to keep a limited computational area.

There are four basic types of open boundaries, each of which to be applied in different situations:

- Water level boundaries
- Velocity boundaries
- Flux boundaries
- Riemann boundaries (weakly reflective boundaries)

The Riemann boundary is a weakly reflective boundary. Both water level and currents have to be known. Usually these boundaries are used to obtain a limited computational area. Waves can cross these boundaries unhampered and without reflections.

The choice of the type of boundary condition depends on the phenomena to be studied. When modelling tidal flow in a large basin, forcing by prescribing only water levels is generally used. If these boundary conditions do not satisfy, combinations of water level and current boundaries can be imposed. The criteria to determine what conditions are satisfactory may be extracted from other models or from measurements.

When the dimensions of the model are relatively small, the use of only water level boundaries is not recommended. Water level is a global variable and behaves rather stiffly; i.e. there is a large correlation between water levels that are not far apart. This means that a small error in the prescription of water levels can only be compensated by a response of the internal forces in the model, i.e. high currents. On the other hand, when the differences in depth of the boundary of the detail model and the overall model are considerable, velocity boundaries can give inaccurate results. The boundaries are therefore located as far away as possible from the area of interest.

Boundary conditions can be obtained from measurements or by extracting the desired boundary conditions from a larger model, in which the detailed model is nested. This nesting is executed as follows:

- In the detail model the open boundaries of the grid are marked and the types of boundary are selected.
- Observation points are created in the overall model around the begin- and endpoint of each boundary section in the detailed model.
- By executing the overall model with these observations points the water levels and currents in these points are computed.
- Using a special option in the Delft3D-FLOW program (Nesting I & II) the observation points in the overall model are rewritten as boundaries for the detailed model;
- Time series for the boundary conditions are now generated. These time series can also be transformed into harmonic conditions.

For the detail model the boundaries can be chosen as time series. It is also possible to use harmonic components, which is based on the fact that tidal time series can be written as:

$$h_t, v_t = A_0 + \sum_{i=1}^{n} A_i \cos(w_i t - \varphi_i)$$

in which h_t, v_t are the water level and current at a specific time t, respectively. A_0 is an average value (A_0 component), A_i, ω_i and φ_i are the amplitude, the angular frequency and the phase angle of a harmonic component indexed by i.

The use of harmonics components has some advantages. It is a lot easier to model a long period of time, without having very large input files. Besides this, harmonic boundaries facilitate studies on the sensitivity of the open boundary conditions.

Numerical stability
In Delft3D-FLOW the Courant number is an indication for numerical stability and accuracy. The directives for the Courant number are based on experience. For places with large differences in bottom geometry or coastline, the Courant number should not exceed the value of 10. The Courant number for two-dimensional problems is defined as (Stelling, 1984):

$$C = 2\Delta t \sqrt{gh\left(\frac{1}{\Delta x^2} + \frac{1}{\Delta y^2}\right)}$$

in which:

C	= Courant number
Δt	= time step (s)
g	= acceleration due to gravity (m/s^2)
h	= local water depth (m)
Δx	= grid mesh size in x-direction (m)
Δy	= grid mesh size in y-direction (m)

The Courant number gives the relation between the propagation speed and time step. The magnitude of the time step determines the total computational time. To reduce the total computational time, it is necessary to choose the largest time step possible, without the loss of accuracy and stability. The following parameters are of importance for the time step:

- stability
- required accuracy
- size of the smallest grid cell
- depth
- available calculation time

Physical parameters
The salinity and temperature are assumed to be constant, as density gradients are not taken into account. This is also the case in the discharge water from the sluices. This choice is made since it is rather complicated to define the time dependent values for these parameters at the model boundaries. For the horizontal eddy viscosity a value of 1 m^2/s is taken, which is considered 'normal' for a true scale simulation.

4.2 Set up of the models

In this paragraph the schematisations of the three models, which are used in this study, are presented.

4.2.1 The ZUNO model

Along the west coast of Holland the tidal wave moves from the south to the north. This tidal movement is one of the main driving forces for the water flow at the Wadden Sea and has to be incorporated at the boundaries of the detail models. The hydrodynamics in the southern part of the North Sea is simulated by the ZUNO model. The validated ZUNO model (from WL | Delft Hydraulics) was made available for this study.

The ZUNO model has its boundaries in deep water between Scotland and Denmark and in the Channel between France and England. The ZUNO grid consists of more than 21.000 active grid cells. Towards the Dutch coast a refinement is made. Here the grid sizes are approximately 1 by 0.5 km. The ferry track in the Texel inlet however, is only schematised by six grid cells.
In figure 4.2 a detailed picture of the grid shown. The curvilinear grid is clearly visible.

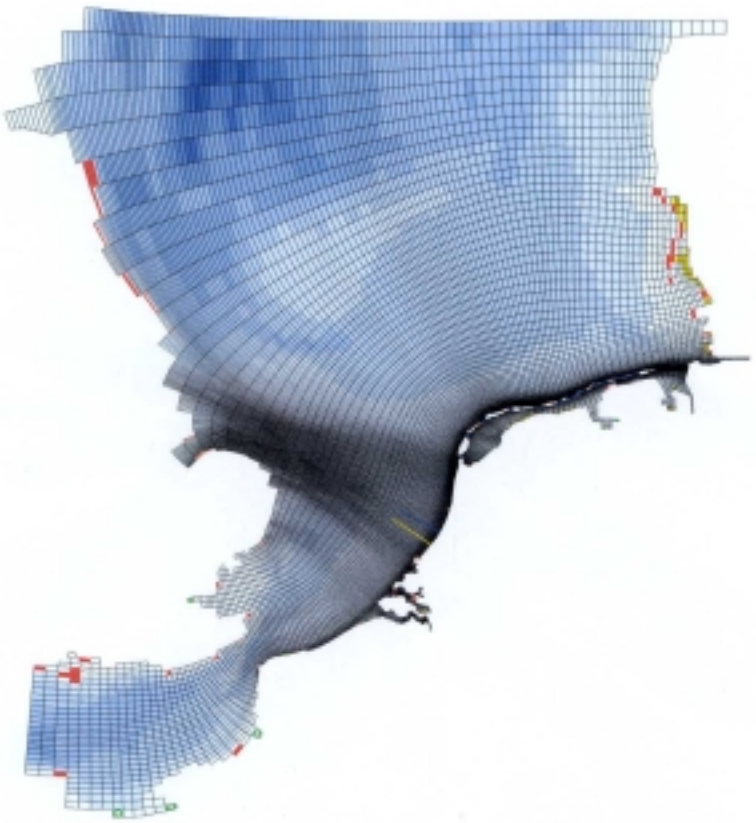

Fig. 4.2 The grid and bathymetry of the ZUNO model

The model is forced by fifty astronomical components. Hence, for normal conditions an arbitrary period can be taken easily. During calibration of the model corrections were applied. Corrections were made to the amplitude (multiplicative) and the phase (additive) of a few components, which was already done by WL | Delft Hydraulics.

In this model the Manning coefficient in the quadratic friction law is variable. For depths smaller than 30 metres a Manning coefficient of 0.024 is used and for depths larger than 30 metres a Manning coefficient of 0.028 is used. The time step used in the model is 2 minutes.

For validation of the model, by using water levels, about twenty observation points were added. These points correspond with locations of tidal gauges in and just seawards of the Wadden Sea. To validate currents through the Texel inlet, another six observation points were added on the ferry track. Along the gridline corresponding the ferry track, a cross-section was placed. The cross-section area along this gridline is 82.970 m^2.

4.2.2 The Wadden Sea model

Due to the fact that the Wadden Sea has a very low resolution in the ZUNO model, differences in depths along the boundary of the detail model and the overall model can be considerable. When using velocity boundaries this can give inaccurate results. If a grid cell has a larger depth in the detail model, this grid cell gets a too high current and therefore a larger discharge is forced. The low resolution also influences the tidal flow through the inlet and therefore the water movement in the Marsdiep basin. To smooth the rather large transition in the nesting procedure, another model is used. This is called the Wadden Sea model, which will be nested in the ZUNO model.

The Wadden Sea contains a part of the Wadden Sea and the area seawards of the Wadden Islands to about 60 km from the coastline. The model has about 21.500 active grid cells. Figure 4.3 shows a picture of the grid. The grid is locally refined in the tidal inlets. In the Texel inlet the grid sizes are approximately 0.4 by 0.3 km. The gridline corresponding the ferry track in this model contains of 19 grid cells.
The bathymetry data for the Wadden Sea model is obtained from the National Institute for Coastal and Marine Management (RIKZ), which regularly carries out measurements in parts of the Wadden Sea and outer deltas. In this way the bathymetry of the whole Wadden Sea is determined every 6 years. The measurements are carried out with echo sounders on board of measuring ships. In some areas with large changes, important for the shipping, the bathymetry is even measured a few times per year.

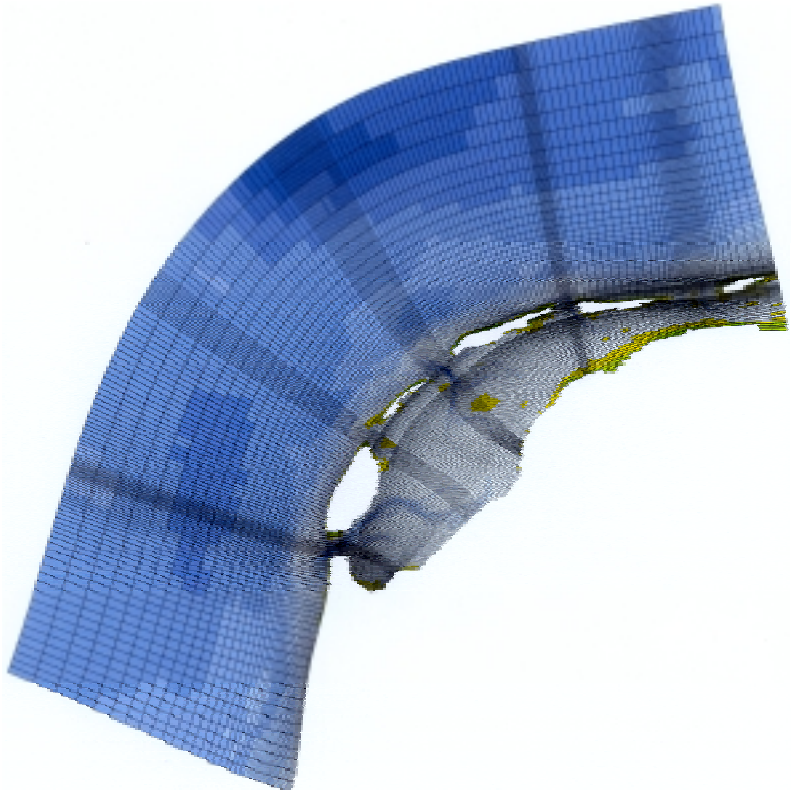

Fig. 4.3 The grid and bathymetry of the Wadden Sea model

The southern open boundary is situated at about 50 km south of Den Helder and the eastern boundary is placed along the watershed just eastwards of Schiermonnikoog. The model is forced by time series of water levels generated from the ZUNO model.

The bottom roughness is computed with a Chézy coefficient of 65 $m^{½}/s$. The time step in this model is one minute. Observation points are placed corresponding with the locations of the water level stations in this area. Also 19 points are placed on the gridline corresponding with the ferry track. Along this gridline also a cross-section is added, which has an area of 92.110 m^2. Cross-sections are also placed in the other tidal inlets.
The grid cells in the Wadden Sea are still fairly large with dimensions varying from 0.75 x 0.6 km to 3 x 1 km.

4.2.3 The Texel model

This model was created during previous studies (Steijn et al., 1998) on sediment transport along the coast of the south-western part of Texel. Therefore, this model was also already available and some calibration had already been performed.

The Texel model contains a part of the North Sea (to about 20 km from the coastline) and a large part of the Marsdiep basin. The part of the North Sea starts about 20 km south of Den Helder and ends about 20 km north of Den Helder.
The Texel model has a grid with grid dimensions decreasing with the distance to the area of interest: the tidal inlet including the ferry track. The grid is also refined along the coast. The model has approximately 21.700 active grid cells. See figure 4.4 for a picture of the grid. In the inlet the grid sizes are about 0.1 km by 0.2 km. The gridline corresponding with the ferry track contains of 55 grid cells.

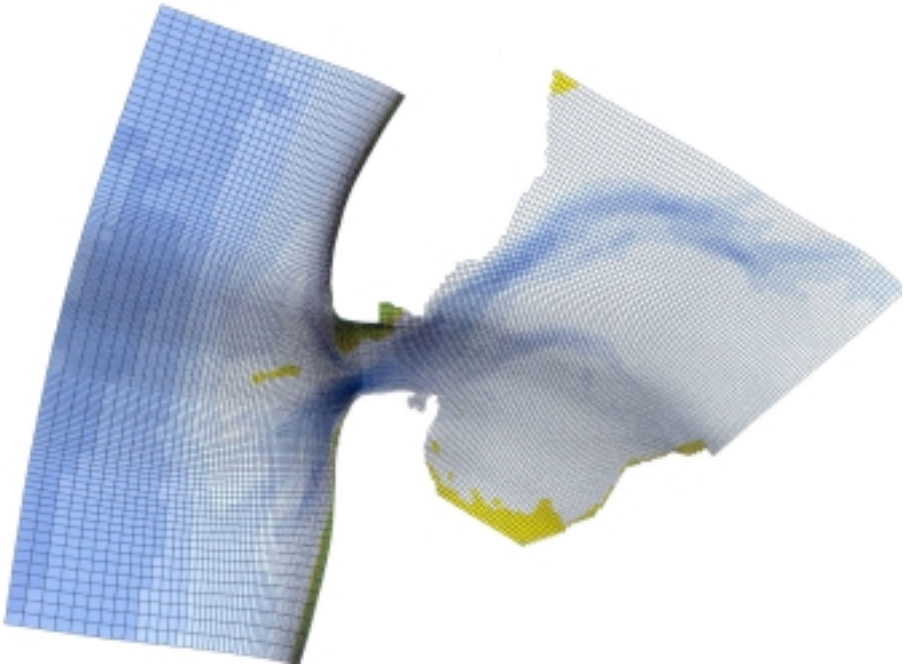

Fig. 4.4 The grid and bathymetry of the Texel model

Three open boundaries are situated in the North Sea and one open boundary is located in the Marsdiep basin. Since the model was originally created for investigating some measures to reduce the erosion in the south-western part of Texel, the model boundary in the Wadden Sea was placed in the Marsdiep basin. Apparently, insufficient attention was paid to place the boundary along a watershed. The eastern boundary starts at the north-east coast of Texel and ends at the middle of the Afsluitdijk. The model is forced with a combination of water level and current boundary conditions. These time series were generated in the ZUNO model, in which the Texel model was nested.

The bottom roughness is computed with a Manning coefficient of 0.026 $m^{1/3}/s$. The time step in this model is 1 minute. Four observation points were added to compare the water level elevations with the tidal gauges: Den Helder, Texel Noordzee, Oudeschild and Den Oever. These points are placed at grid cells which are closest to the geographical location of the water level stations. To validate the model with the ferry current observations 17 points were placed corresponding the locations of the 17 data points in the ferry data. The grid cells in the tidal inlet have a size of about 100 to 150 meters in the north-south direction and 150 to 300 metres in the east-west direction.
A cross-section was placed along the gridline with the highest resemblance to the mean ferry track. The cross-sectional area is 80.470 m^2.

5 Validation

In this chapter first the modelled water levels will be compared with the measured water level elevation and evaluated. Then the discharge through the Texel inlet will be analysed and compared with the measurements from the ADCP on the ferry. For a detail comparison, the modelled currents across the inlet will be compared with the measured currents and evaluated.

After a first validation of the models the differences in amplitudes of the modelled water levels with the measured water levels were a motivation to tune the ZUNO model again for the area near the Marsdiep basin. The M_2 amplitude of the modelled water level elevation in Den Helder, which is in the Texel inlet, differed 10-15 % with the measured water level.
The ZUNO model was tuned at WL | Delft Hydraulics. One of the tuning parameters was the bathymetry near the Texel inlet. In the outer delta the channel 'Nieuwe Schulpengat' (see figure 1.2 in the introduction) was deepened towards the south. The southwestern part of the Texel inlet was also deepened together with the channel Texelstroom in the Marsdiep basin. Besides this, the Mokbaai was schematised with a thin dam and shallower depth.
The modelled waterlevels were compared with analysis of the tidal gauges done by the National Institute for Coastal and Marine Management (RIKZ). Some differences still existed in a few locations inside the Wadden Sea. In Harlingen the M_2 amplitude was too high and the M_2 phase too low. The M_4 phase in Den Helder was 16 degrees higher in the model.

5.1 Water level

5.1.1 Observations

For a good validation of the ZUNO and Wadden Sea model on water levels, ten tidal gauges are used. For the tidal gauges in Petten, Den Helder, Texel Noordzee, Oudeschild, Den Oever, Kornwerderzand, Harlingen, Terschelling Noordzee, Wierumergronden and Huibertsgat the water level elevation is harmonically analysed. With these ten tidal gauges it is also possible to analyse the tidal wave propagation in and just outside the Wadden Sea. For validation of the Texel model, only four tidal gauges are used: Den Helder, Texel Noordzee, Oudeschild and Den Oever.
The time series of the measured water levels in Den Helder, Texel Noordzee, Den Oever and Harlingen are compared with the predicted results from the Tide Generator. The time series have a record length of almost 2 years and the results from the Tide Generator are calculated first for 2 months. The deviation in the amplitudes and the relative phases of the Tide Generator with the measurements are rather small (a few cm at most in the smaller constituents). Since the study includes the validation of the model results with measured data, the time series of the available measured water elevation at the four tidal gauges are used for further analysis. For the other tidal gauges, the water level elevation was calculated with the Tide Generator.

5.1.2 Models

Amplitude

In the harmonic analysis of the water levels eight constituents are taken into account as described in chapter 4: O_1, K_1, N_2, M_2, S_2, M_4, MS_4 and M_6. The simulation period of the models is 34 days. The first two days are not taken into account during the analyses. The measurements are also harmonic analysed over the same period of 32 days, beginning on April 21, 1999 until May 23, 1999. The M_2 tidal amplitude is by far the greatest constituent in the model results. Every other constituent is less than 30 % of the M_2 tidal amplitude.

Figure 5.1 shows a comparison of the Wadden Sea model and measured elevation data for the amplitude of the M_2 tidal constituent. If agreement were perfect all the points (representing different locations) would lie on a line inclined at 45 degrees to the vertical. The 0.04 m lines are marked on the amplitude plot, corresponding to 5 % of the largest amplitude. The deviations of M_2 amplitudes of the model with the measurements are smaller than 5 % at most of the tidal gauges. In Den Helder the difference in amplitudes is even smaller than 0.5 %. Only in Den Oever and Kornwerderzand the M_2 amplitude is more than 6 % higher in the model.

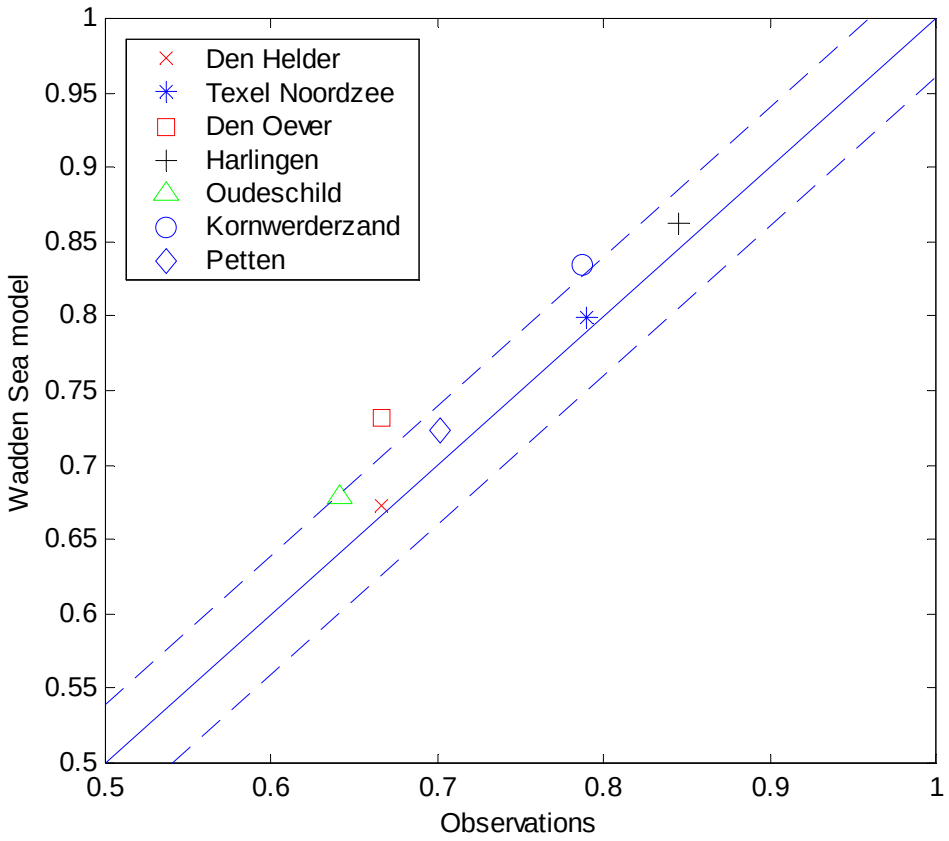

Fig. 5.1 M_2 amplitude of the water levels in several locations

To compare the water levels in the three models with the measured data, the results for each location are harmonic analysed. The results are presented for two water level stations, namely Den Helder and Texel Noordzee. Figure 5.2 shows the amplitudes of eight constituents and the mean water level in Den Helder.
The maximum deviation in the M_2 amplitude of the models and the measured water level in Den Helder is rather small: 1 %.

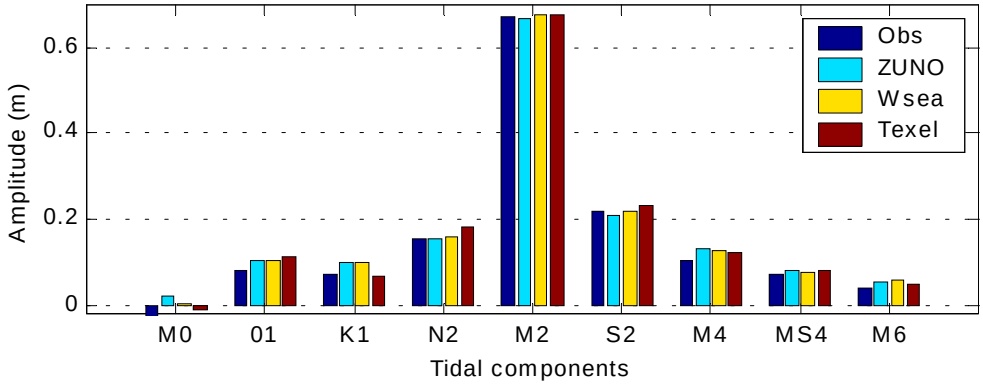

Fig. 5.2 Amplitudes of the water level in Den Helder

The models seem to correspond mutually; this is logical since the ZUNO model is the overall model, in which the other models are nested. However, the Texel model has somewhat larger amplitudes in the semi-diurnal constituents. The modelled amplitudes of the semidiurnal constituents correspond well with the observations. The amplitudes of the higher and compound constituents are fairly similar. The largest deviations are found in the amplitudes of O_1 and K_1. In the Texel model the K_1 amplitude is almost similar to the observations, in contrast to the other models, which have a 55 % larger amplitude. These conclusions are more or less also valid for the analysis of the water level in Texel Noordzee (Figure 5.3).
The deviations of the M_2 constituents of the modelled water level with the amplitude of the measured water level is 6 % in Texel Noordzee, 3 % in Oudeschild and more than 14 % in Den Oever. When comparing the amplitudes in Texel Noordzee with Den Helder, it is clear that the amplitudes of the semi-diurnal components are higher in Texel Noordzee.

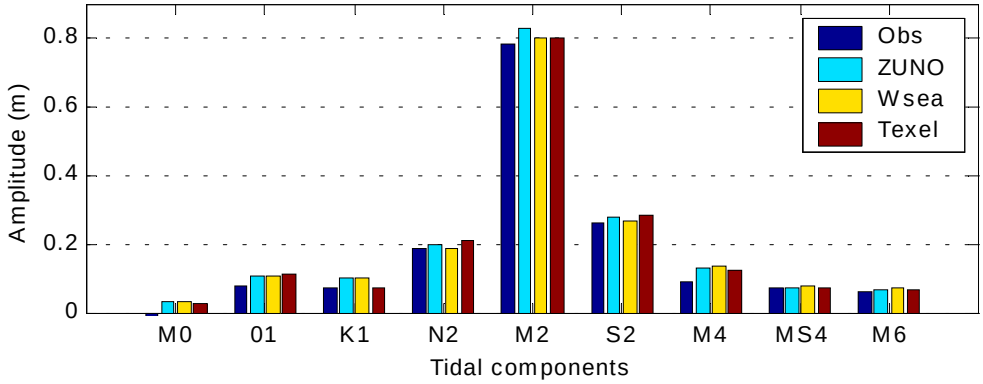

Fig. 5.3 Amplitudes of the water level in Texel Noordzee

Phases

Seven tidal gauges are used for comparing the phases with the results of the Wadden Sea model. The Wadden Sea model is used as it is a detail model of part of the Wadden Sea and it contains enough water level stations for analysing the water levels in that area.

The modelled M_2 phases at the water level stations give a good similarity and differ at most 5 degrees from the tidal gauges.

In contrary to the M_2 phases, the modelled M_4 phases have a rather large deviation with the phases of the observed water levels. The differences in M_4 phases increase from about 14 degrees in Texel Noordzee to 24 degrees in Den Oever. On the other hand in Harlingen the modelled and observed M_4 phase is similar. See figure 5.4. The dashed line on the phase plots represents the 15 degrees line.

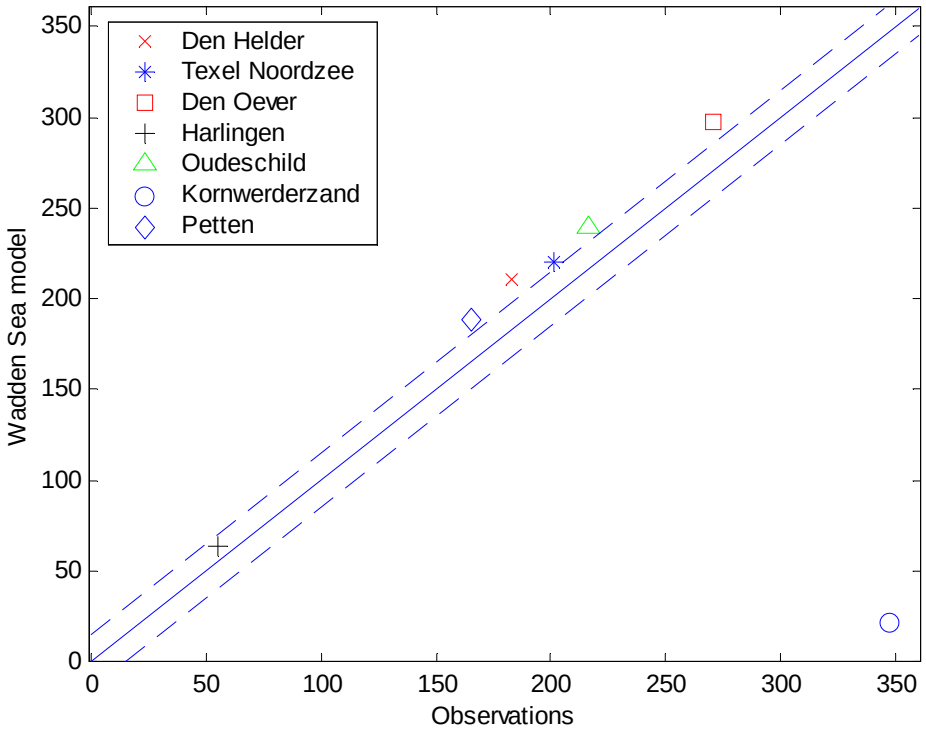

Fig. 5.4 M_4 phases of the water level at several locations

So except for Harlingen, all tidal gauges have about the same deviation in the M_4 phase with the observations.

The phases of eight components analysed from the water level in Den Helder are plotted in figure 5.5. The phases of most of the constituents give good similarity, but the phases of the N_2, M_4 and M_6 constituent differs respectively 16, 16 and 33 degrees. Note that a 16 degrees deviation in the phase of the N_2 constituent means a two times longer time difference than a 16 degrees deviation in the phase of the M_4 constituent.

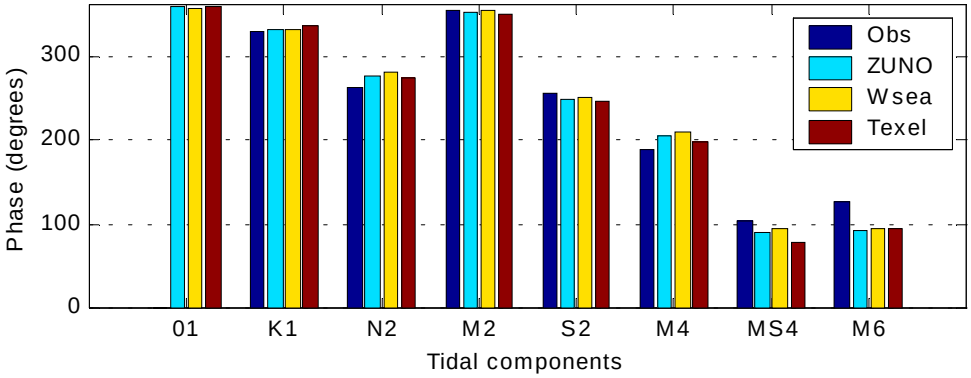

Fig. 5.5 Phases of the water level in Den Helder

Also for the water level in Texel Noordzee most constituents give good resemblance, except for the N_2, M_4 and M_6 constituent. In all analysed tidal gauges the S_2 phase is about 8 to 9 degrees larger than the model results.

Relative phases

As mentioned in paragraph 2.5 the relative phase of M_4 with M_2 plays an important role in de tidal asymmetry. Figure 5.6 shows this relative phase for each of the seven stations. It is obvious that in all stations, except in Harlingen, the relative phase of M_4 with M_2 has a deviation of 20 to 30 degrees. In Harlingen the difference is about 5 degrees.

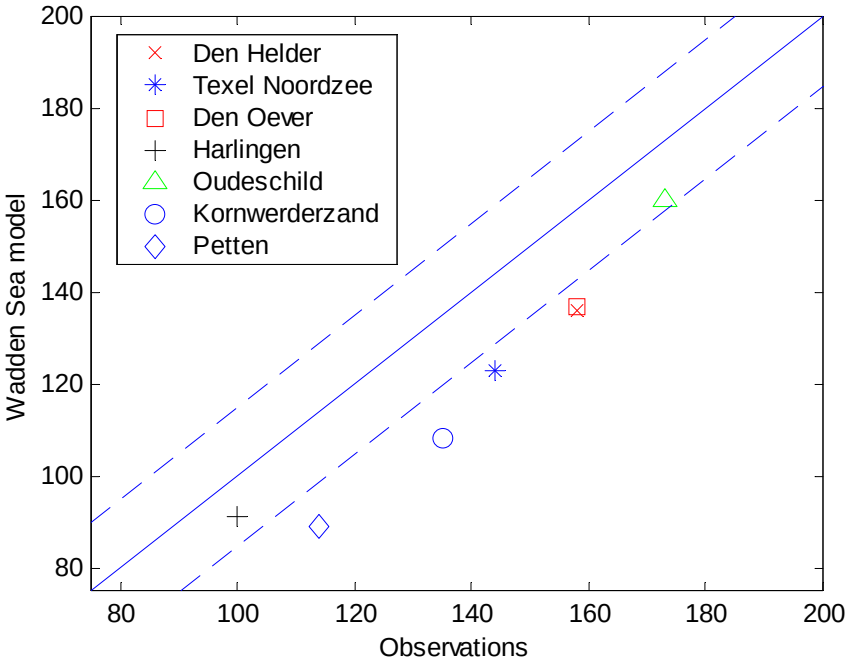

Fig. 5.6 Relative phase of the water level at several locations

Most of the modelled M_4 phases already deviate from the observed phases, which results in the deviations in the relative phases. The M_4 phases in the models are all higher than the observed phases. Since the relative phase is defined as $\Delta\varphi_{M2-M4} = 2*\varphi_{M2} - \varphi_{M4}$ the modelled relative phases will become lower than the observed relative phases, which can be seen in figure 5.7.
In Den Helder the M_4 phase has a deviation of 16 degrees, which leads to a deviation of 22 degrees in the phase difference between M_4 and M_2, which is a time difference of about 23 min.

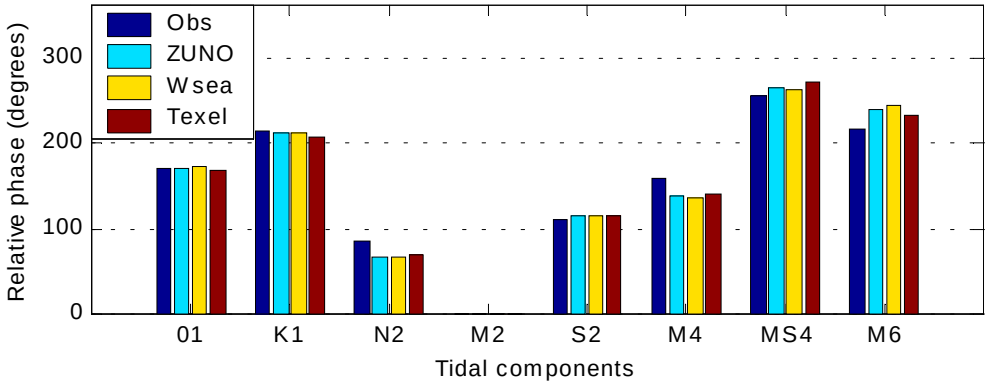

Fig. 5.7 Relative phases of the water level in Den Helder

From the comparisons of the water levels, it can be concluded that generally the amplitudes of the water level elevation and the phases in Den Helder and Texel Noordzee give a good similarity with the measurements. Further into the Wadden Sea the modelled amplitudes get higher compared with the tidal gauges and the deviation in the phases also increases. The phase difference between M_2 and M_4 in Den Helder is rather large.

5.1.3 Propagation of the tidal wave in the Wadden Sea

In figure 5.8 the location of seven water level stations are indicated with a '+'. As can be seen in the legend, the observed and computed amplitudes and phases of a constituent are presented in each station for several runs. The amplitudes are in meters, while the phase in Den Helder is in degrees. At the other stations a period in minutes is presented as the phase lag. This period indicates the time lag between high water at Den Helder and the concerning station. The phase of the water level in Den Helder is thus taking as the reference phase. In this context, high water is the top of the symmetric tidal wave function of a constituent. A negative period at a station means that high water in that station is ahead in time of the high water in Den Helder.

The figure shows that the M_2 amplitude of the water level in Den Oever does not differ much with the M_2 amplitude in Den Helder, but more inwards of the basin, the amplitude starts to increase to 0.84 m in Harlingen.

The M_2 amplitudes at the seaward stations (including Den Helder) are all too large, ranging from 2 % to 10 %. The M_2 amplitudes in the Marsdiep basin are 10 % too high in Den Oever and Harlingen, except for the Wadden Sea model, which is only 2 % too high in Harlingen.

The phase progress along the North Sea coast of the Wadden Islands is reproduced better in the ZUNO model than in the Wadden Sea model. On the other hand, the Wadden Sea model reproduces the progress of the tidal wave in the Wadden Sea itself better. This is clear in the M_2 phase difference between Den Helder and Den Oever in the Texel model, which is 1 hr 35 min. This is close to the actual phase difference of 1 hr 31 min. In the ZUNO model this M_2 phase difference is 1 hr 41 min.

The M_2 tidal wave needs 3 hours to get from Den Helder to Harlingen. The tidal wave in the Wadden Sea needs 2 hr 54 min to reach Harlingen, which thus corresponds well with the observed data. The M_2 tidal wave in the ZUNO model takes 2 hr 29 min.

So, the tidal wave in the model is propagating too fast in this part of the Wadden Sea. This difference is probably caused by the rough schematisation of the geometry of the Wadden Sea in the ZUNO model and the different frictional parameters. A varying Manning coefficient is used in the ZUNO model and a constant Chézy coefficient is used in the Wadden Sea model.

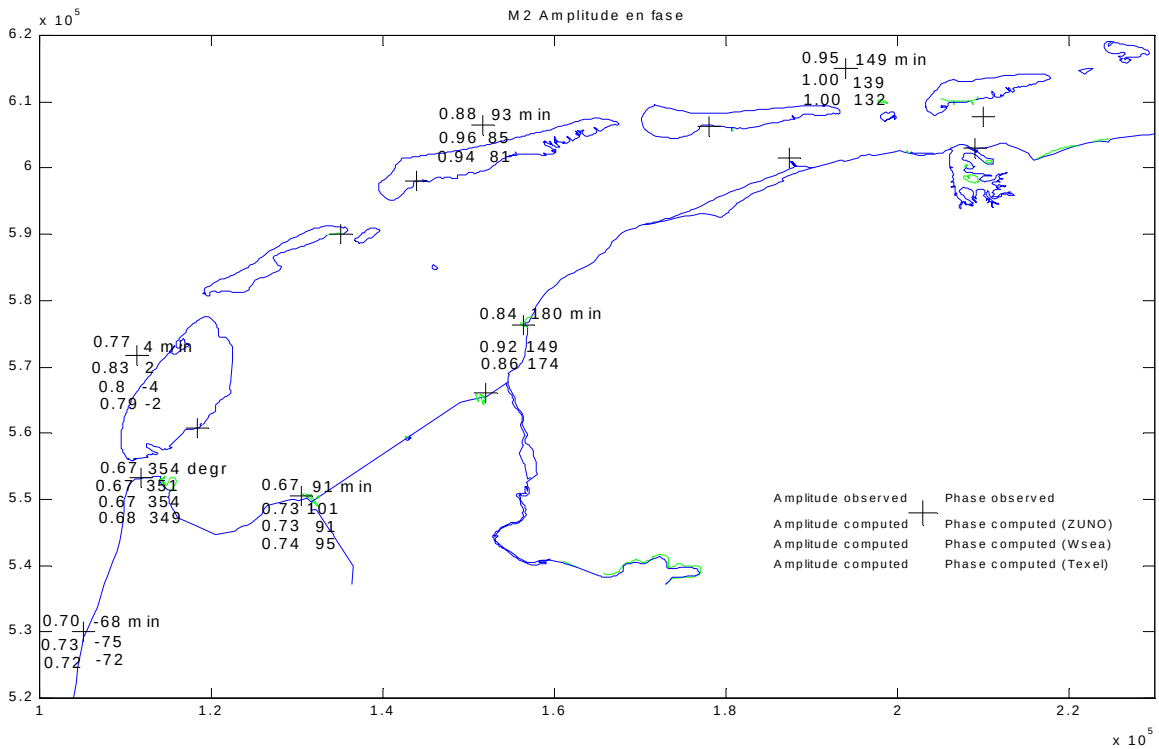

Fig. 5.8 Observed and computed M_2 amplitudes and phases at several locations

5.1.4 Co-tidal charts of the tidal wave propagation

The overall water levels simulated by the ZUNO model agree visually with earlier results by Pingree et al.(1997) and Prandle (1978). The amphidromic systems of M_2 and M_4 as calculated by the model are shown in figures 5.9 and 5.10, showing the well-known patterns. The term amphidrome refers to elevation nodal points where the amplitude tends to zero.
In each amphidromic system, co-tidal lines can be defined, which link all the points where the tide is at the same stage (or phase) of its cycle. The co-tidal lines thus radiate outwards from the amphidromic point. Cutting across co-tidal lines, approximately at right angles to them, are co-range lines, which join places having an equal tidal range. Co-range lines form more or less concentric circles around the amphidromic point, representing larger tidal ranges further away. The tidal waves of amphidromic systems tend to rotate anticlockwise in the Northern Hemisphere and thus also in the North Sea.

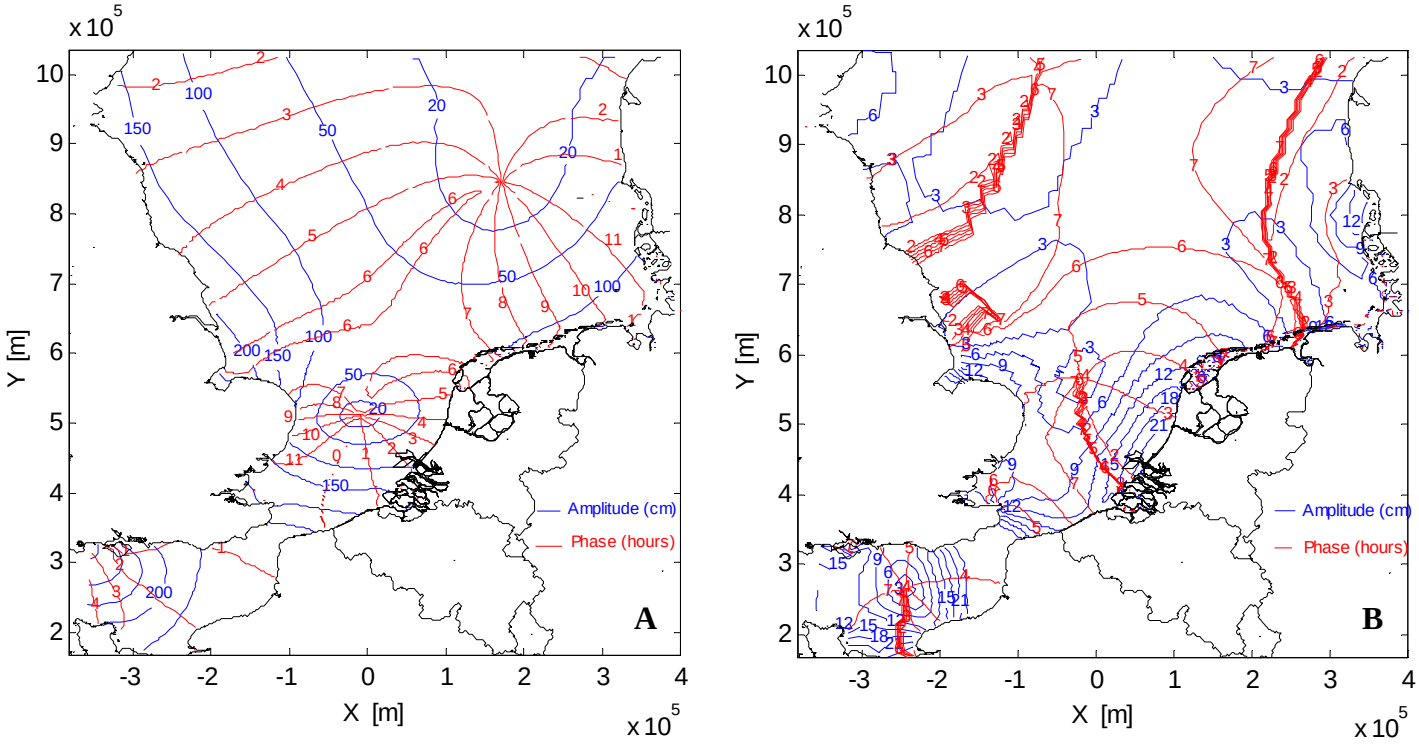

Fig. 5.9 Co-tidal chart of the M_2 (a) and M_4 (b) constituent in the ZUNO model

Figure 5.9 shows the propagation of the M_2 tidal wave along the Dutch coast to the north. The amplitude increases from the amphidromic point towards the Dutch coast. In the co-tidal chart of the M_4 constituent in the ZUNO model it is difficult to gain a clear view of the situation, but along the Dutch coast it does give a clear pattern of the wave propagation. The M_4 tidal wave propagates almost perpendicular to the Dutch coast towards the north, while the M_4 amplitudes, like the M_2 amplitudes, also increase towards the coast. However, the pattern of the M_4 amplitudes near the coast is different than the pattern of the M_2 amplitudes.
Like in previous model studies by others the amphidromic point of the M_2 tidal wave (in the southern North Sea) is situated south of the amphidromic point of the M_4 tidal wave.

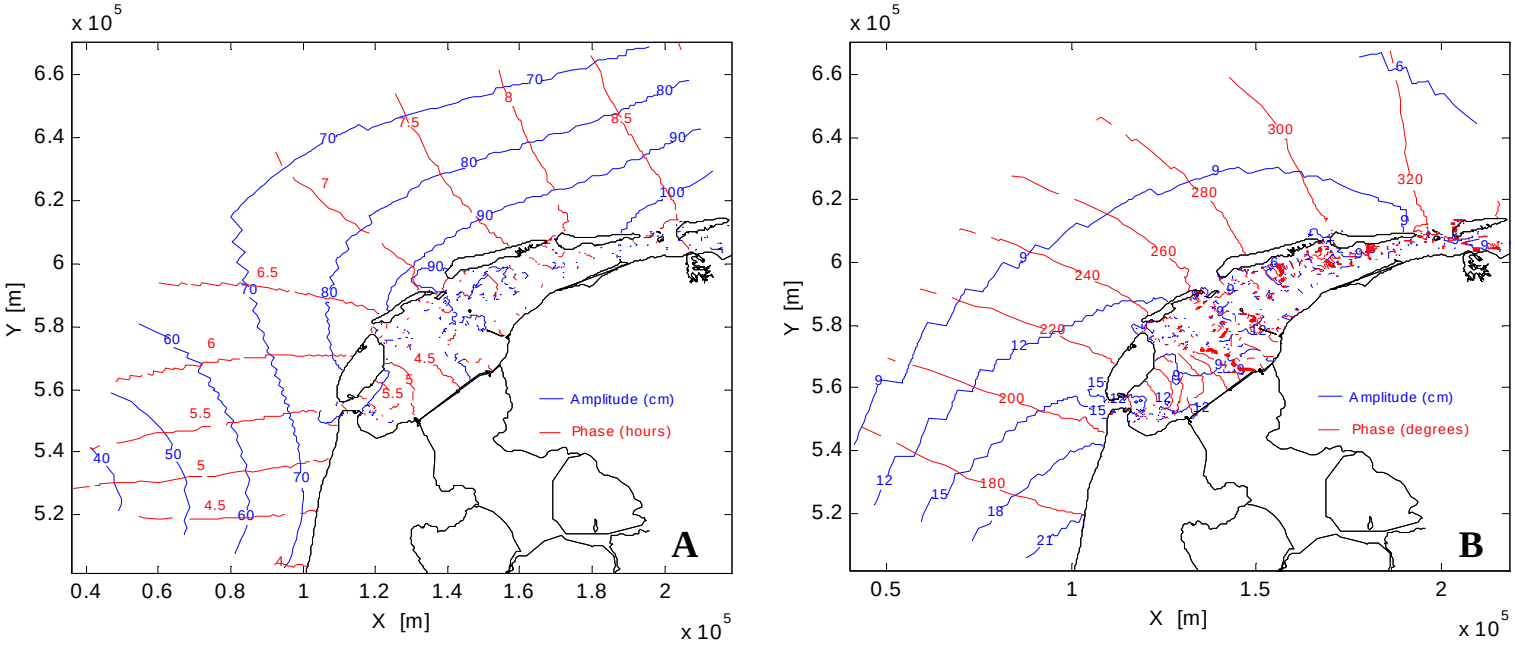

Fig. 5.10 Co-tidal chart of the M_2 (a) and M_4 (b) constituent in the Wadden Sea model

Figure 5.10 shows that the M_2 amplitude (a) also increases in north-western direction along the Wadden Islands, in contrary to the M_4 amplitude (b) which decreases in this direction.
Due to the complicated geometry of the Wadden Sea the tidal waves are not propagating uniformly in the basins. The tidal wave propagates fast in the channels, but slows down on the shoals and flats. So, the contour plot of the amplitudes and also of the phases in the Wadden Sea is rather messy.
In figure 5.10a the M_2 phase lines have a plotting interval of 20 degrees, which is a period of 41 minutes. In figure 5.10b this interval period is about 20 min. The M_4 phase lines are more or less perpendicular to the coast of the Wadden Islands, but further away from the coast they tend to deviate to the west.
In the M_2 contour plot, the crossings of the co-tidal lines with the co-range lines are approximately at right angles. However, in the M_4 contour plot, this is often not the case. Since the M_4 constituent is a higher harmonics, generated by non-linear phenomenon, it is more dependable of and mainly influenced by the local geometry and bathymetry.

5.2 Discharge

5.2.1 Observations

First analysis of the time series for the discharge by Ridderinkhof (2000) is done by applying harmonic analysis (least squares fit) using 65 tidal components. The results are presented below. The amplitude of the 14 most important components, here defined as tidal components with an amplitude larger than 5% of the M_2 tidal amplitude, are presented in table 5.1. This table also includes the results if the harmonic analysis is performed separately for the year 1999 and the year 2000. The Rayleigh criterion requires that the length of the time series is at least 366 days in order to be able to distinguish all 65 frequencies and to get reasonable values for every constituent, which do not include a neighbouring constituent.

Tidal component	Period (hours)	Amplitude volume transport (m3/s) period		
		1998-2000	*1999*	*2000*
O_1	25.8193	5139	4113	4310
K_1	23.9345	3915	4732	3962
Mu_2	12.8718	9367	9218	8785
N_2	12.6583	10580	10490	10239
Nu_2	12.6260	4076	3181	4587
M_2	12.4206	68564	68908	67278
Lab_2	12.2218	3528	3518	3429
L_2	12.1916	7205	7380	6849
S_2	12.0000	17837	16661	17687
K_2	11.9672	3503	3973	4489
M_4	6.2103	7410	7121	7672
MN_6	4.1662	3592	3492	3491
M_6	4.1402	6596	6614	6403
$2MS_6$	4.0924	6534	6641	6463
Net flow	-	-2587	-2029	-2589

Table 5.1 Amplitude of tidal components of the volume transport through the Marsdiep tidal inlet for different periods of analysis, Ridderinkhof (2000).

Table 5.1 shows that there are only small differences in amplitudes of the tidal components for the periods analysed. The most dominant basic components are M_2, S_2 and N_2. The amplitude of the 'internally generated' overtides with periods of about 6 (M_4) and 4 hours (MN_6, M_6 and $2MS_6$) are about equal and contribute significantly in that their amplitude is larger than the amplitude of the basic diurnal components (K_1 and O_1).
The net flow is in the seaward direction (negative values indicate an ebb surplus), which confirms previous modelling studies (Ridderinkhof, 1988). However, its magnitude is larger than these models suggested. This difference might be caused by wind forcing and the supply of fresh water from the IJsselmeer which were neglected in the previous modelling studies.
Due to the propagating character of the tidal wave in the Texel inlet, a phase lag exists between the water level and the currents. Although the tidal wave passes the tidal gauge of Den Helder in the south-west of the Texel inlet earlier than the ferry track, this does not explain the phase lag.

Analysis showed that the phase lag of the M_2 amplitude is 50 degrees, which is a period of 1 hr 44 min. Figure 5.11 shows the measured water level in Den Helder (solid line) and the measured discharge, marked with red stars, which illustrates the phase lag between the currents and the water level. The discharge reaches his maximum relative short period. Note that the time between the slack moment and the moment of maximum flood discharge is evidently shorter than the time needed from the maximum flood discharge to reach the slack moment. So, in the inlet the flood currents are generally higher than the ebb currents.

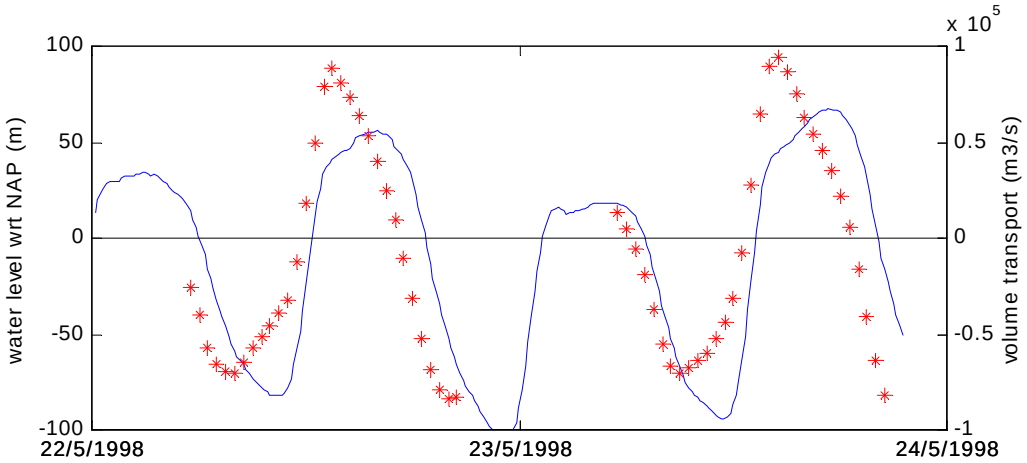

Fig. 5.11 Measured water level and discharge for two days. Note that the discharges are only measured during the day time.

5.2.2 Models

In each of the three models, a cross-section was placed along the gridline with the highest geographical resemblance with the mean ferry track. The resulting time series of the discharge through these cross-sections are, just like the measured time series from the ADCP, harmonically analysed. The period, which is harmonic analysed, is equal for the models and the measurements. The models hardly differ from each other, except for the M_2 amplitude. The ratio of the modelled M_2 amplitude to the measured M_2 amplitude is 1.08 in the ZUNO model, 1.10 in the Wadden Sea model and 1.06 in the Texel model. As can be found in the previous paragraph, the M_2 amplitude calculated in the analysis over a year is about 2 % higher than the value, which is calculated in the analysis over a period of 32 days. In the case of comparing the model results with the one year analysis, the deviations in the M_2 amplitude decrease.
The residual discharge in the ZUNO and Wadden Sea models has a deviation of more than 100 % with the measurements. The residual discharge in the Texel model differs even more. However, when taking the residual discharge from the year analysis by Ridderinkhof, the deviations are much smaller: about 10-15 %.

The other constituents correspond reasonable well with the observations from the TESO data as can be seen in figure 5.12.

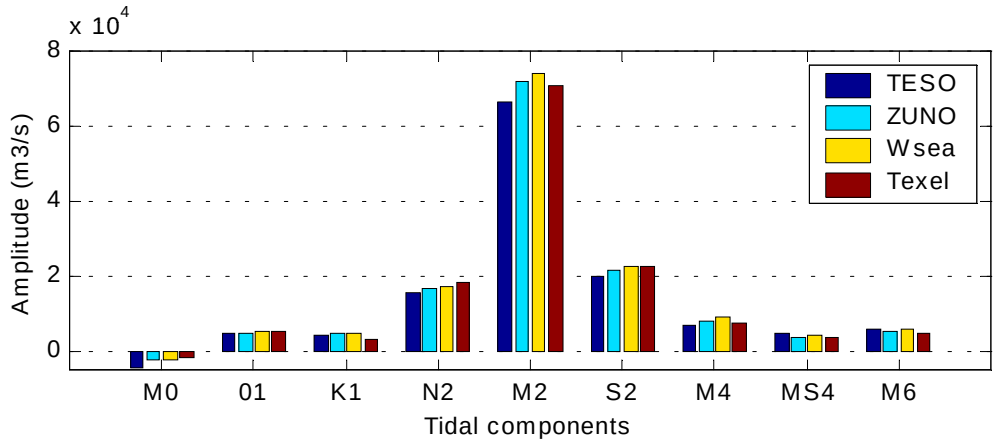

Fig. 5.12 Amplitudes of the volume transport through the Texel inlet

The modelled M_2 phase differs at most 5 degrees (in the Texel model), which is a period of 10 minutes, with the measured M_2 phase (see figure 5.13). The M_2 phases in the other models are equal to the observed M_2 phase. However, the modelled M_4 phase deviates 58 degrees (60 min) and the MS_4 phase in the ZUNO model 19 degrees (20 min) with the measurements. The observed O_1 phase is 20 degrees (1 hr 23 min) and the observed K_1 phase is 12 degrees (50 min) ahead of each of the models. The Wadden Sea model produces the best corresponding M_6 phase with respect to the other two models.

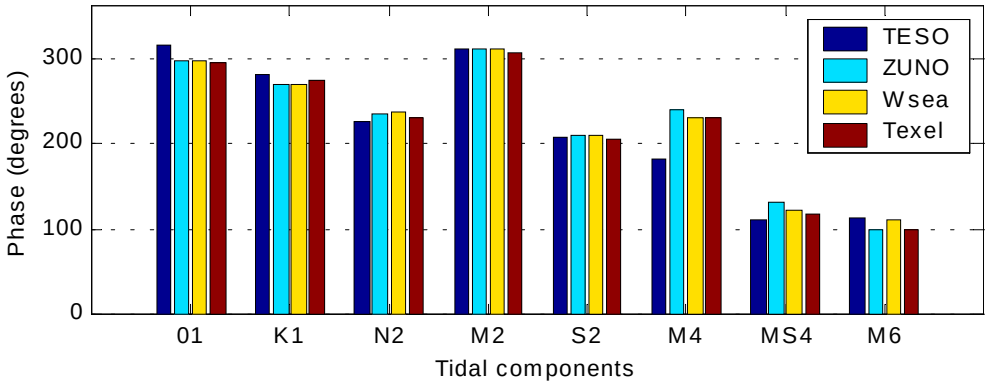

Fig. 5.13 Phases of the volume transport through the Texel inlet

In figure 5.14 the relative phases between the M_2 phase and the other phases are plotted.
The previous mentioned deviations in the phases of the M_4 and MS_4 constituent (and to a lesser degree, O_1 and K_1), logically result in deviations in the relative phases of these constituents. The other relative phases give good similarities with the measurements.

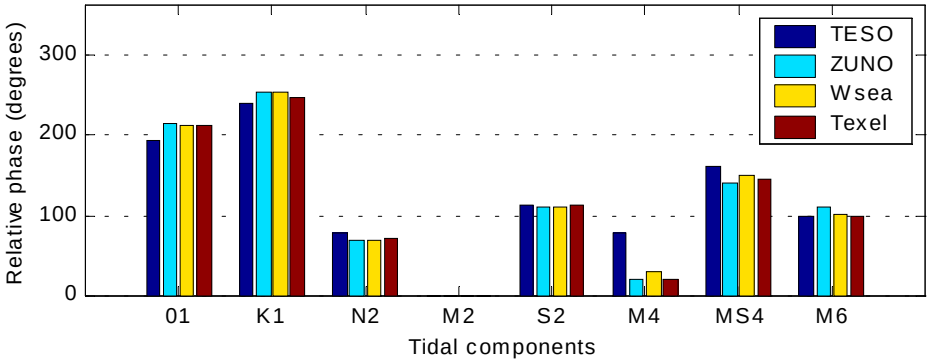

Fig. 5.14 Relative phases of the volume transport in the Texel inlet

The relative phases of M_4 and MS_4 in the Wadden Sea model are about 14 degrees higher compared to the two other models. Since M_4 and MS_4 are higher and compound harmonics, generated by non-linear phenomenon, a reason for this could be the different friction parameters used in the models.

5.3 Currents

5.3.1 Observations

The currents which are analysed, are composed from measured currents in the east and north direction and then rotated to the main axes, which is determined in each point (see chapter 3). The locations of the 17 points are equidistant in the south direction, while all the points are at the same longitude. See figure 5.15. The red marks represent the measured data.

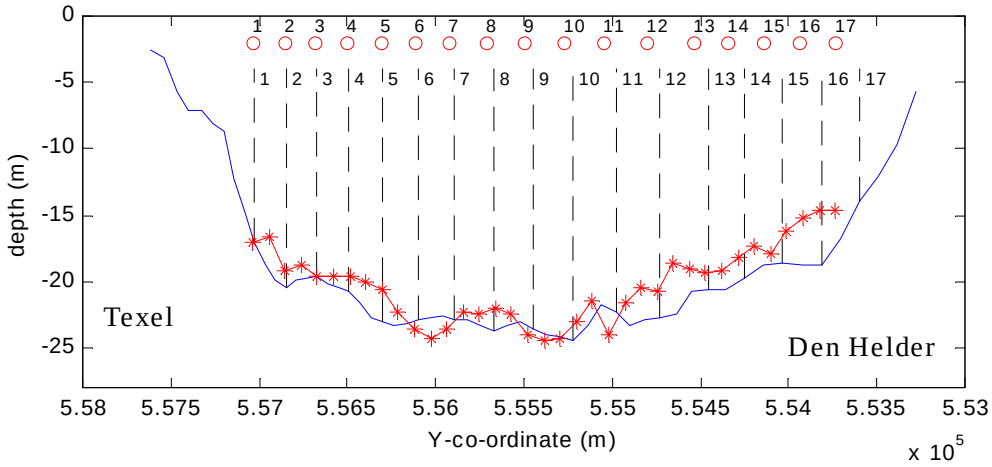

Fig. 5.15 Bottom profile of the Texel inlet with the data points. The red marks and circles represent the measured data and the blue solid line the Texel model.

In figure 5.16 time series of the currents at 4 points, located in the Texel inlet, are plotted. Point 2 is located in the north of the inlet and point 16 in the south of the inlet.

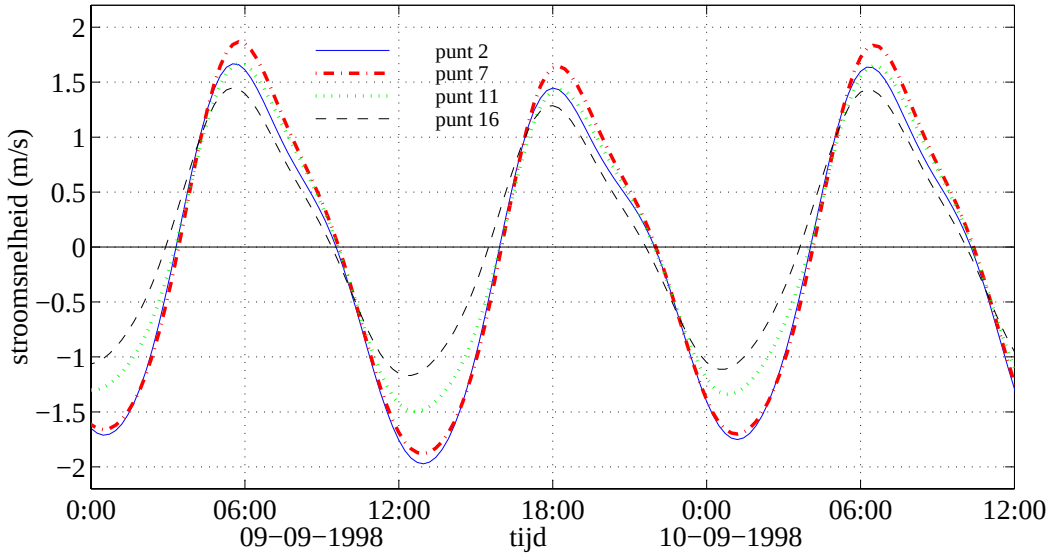

Fig. 5.16 Time series of currents at 4 points in the Texel inlet (de Leeuw, 1999)

The figure shows that the mean depth currents in the Texel inlet differ not only in phase but also in amplitude. The phase of the M_2 component is increasing from south to north, as a consequence of the southern origin of the tidal wave. The southern part of the tidal inlet is ahead of the northern part by approximately 10 degrees (about 20 minutes).
The M_2 constituent is the largest semi-diurnal component and dominates the tidal signal through the Marsdiep tidal inlet. The maximum currents occur somewhat northerly of the centre of the inlet, where the flood channel enters the Marsdiep basin.
When analysing the current time series in figure 5.16, it is found that the variation of the maximum currents across the inlet is larger during ebb than during flood. During flood the maximal difference is found between point 7 and point 16. On the other hand during ebb this maximal difference is found between point 2 and point 16.

5.3.2 Models

Amplitudes

The main currents in each of the 17 points (measurements and models) are harmonically analysed. The M_2 and M_4 amplitudes of the points in the models and observations are plotted in figure 5.17. Note that the scale on the horizontal axis does not always start with the value of 0 m/s.

The ZUNO model is too rough for an analysis of the currents since there are only 6 grid cells across the inlet and the results are therefore not plotted. To be sure a simple analysis of the overall model results, showed that the model agrees fairly with the Texel model.

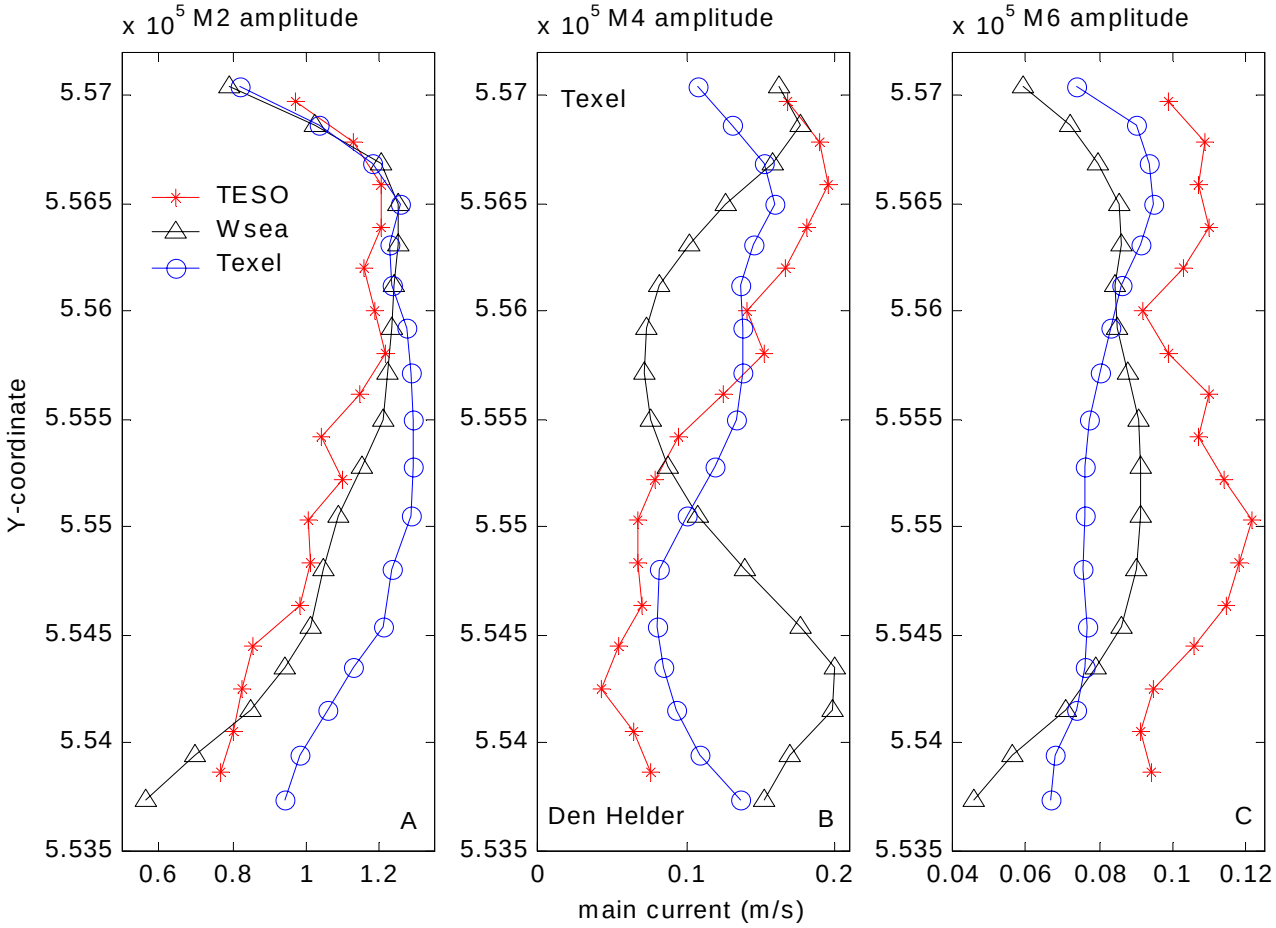

Fig. 5.17 M_2 (a), M_4 (b) and M_6 (c) amplitudes of the main current across the inlet

The figure shows that the amplitude of the observed ('*') M_2 component is as high as 1.2 m/s in the main direction. Directly inward of the inlet, the channel bifurcates, with the main (ebb and flood) channel to the north (Texelstroom) and a much smaller channel to the south (Malzwin; see appendix A). This causes the M_2 amplitudes in the northern part of the inlet to be clearly higher than the amplitudes in the southern part. The difference is about 0.3-0.4 m/s for the M_2 component. The maximum M_4 amplitude reaches a value of 0.18 m/s in the northern part, and 0.07 m/s in the southern part. Towards the southern shore of the inlet the M_4 amplitude decreases, while towards the northern shore the amplitude increases.

The Wadden Sea model produces more similar M_2 amplitudes across the inlet than the Texel model. On the other hand, the Texel model gives much better amplitudes for the M_4 constituent. During sensitivity runs it became clear, that the time step used in the models was a rather sensitive parameter for M_4 results.
The M_6 component is mainly generated by friction of the M_2 tidal wave. This is illustrated by the similar distribution of the M_2 and M_6 constituent across the Texel inlet, with a maximum north of the centre of the inlet. The M_6 amplitude is fairly high (0.08-0.12 m/s), causing the M_6 constituent to be even stronger than the M_4 constituent in the southern part.
The O_1 component is the largest diurnal component with amplitudes up to 0.10 m/s, while the K_1 component is the second largest component with a somewhat smaller amplitude of 0.06 m/s.
The S_2 component reaches values up to 0.3 m/s in the main channel, whereas the N_2 component gets as large as 0.2 m/s. These two components principally show the same pattern or distribution as the M_2 component. These rather large semi-diurnal components cause a significant difference in current speeds between neap and spring tide, varying from 1.0 to 2.0 m/s.
The MS_4 component is almost monotonically decreasing from north to south, with a slight increase in the utter southern part.

Phases

Figure 5.18 shows that the M_2 phase increases from south to north, due to the southern origin of the tidal wave. The southern part of the inlet is about 10 degrees (20 min) ahead of the northern part of the inlet. The influence of the friction is the smallest in the main channel and so the relative importance of the inertia effects the largest. The period that is needed for the water to change from direction (slack water) is therefore the longest in the main channel. The phase difference in the measurements between points close to the channel and points in the channel is rather small, but consistent in the water column.

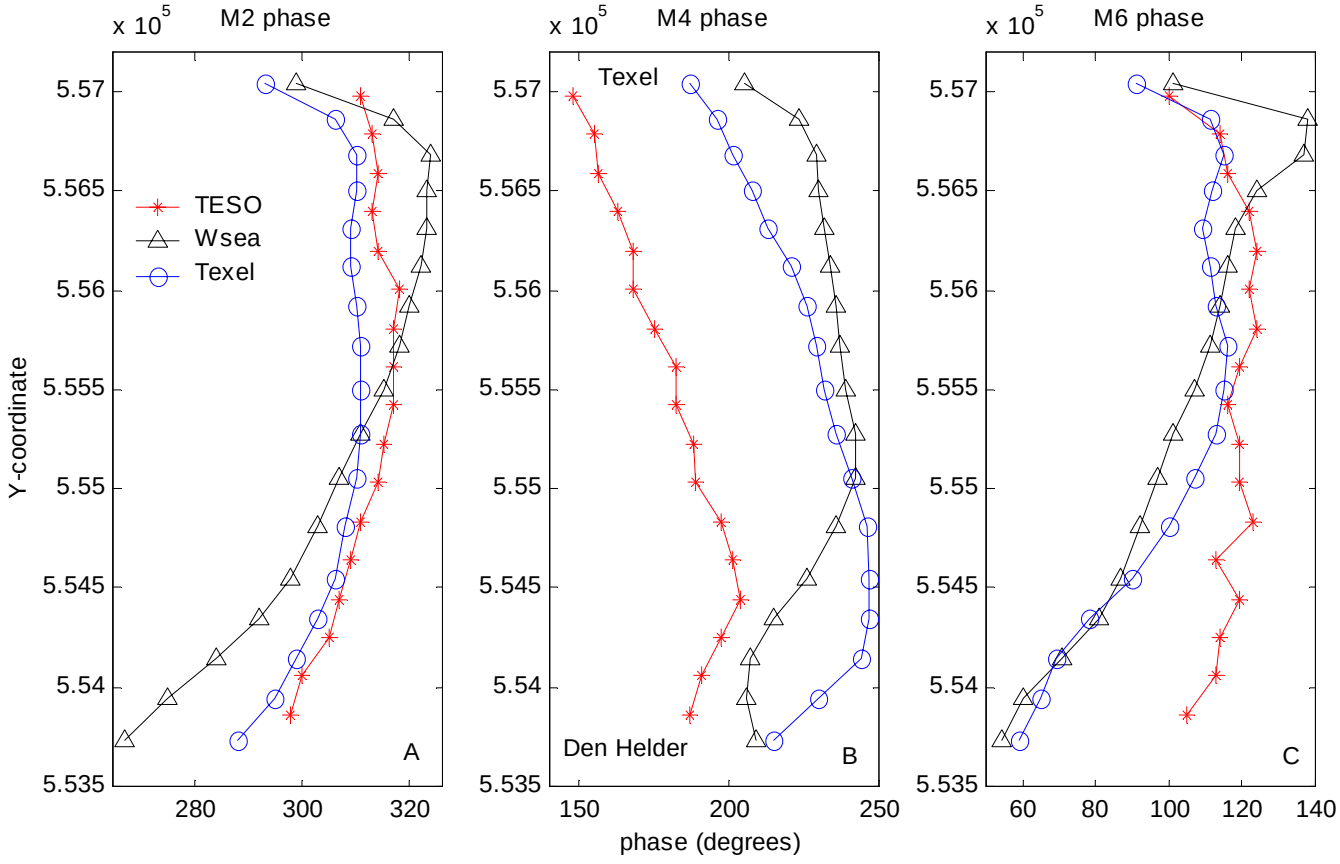

Fig. 5.18 M_2 (a), M_4 (b) and M_6 (c) phases of the main current across the inlet

The Texel model gives the best M_2 phases, but there is a deviation of 5 to 10 degrees with the measurements. In the case of M_4 phases the models do not produce similar phases. In the Texel model deviations in the M_4 phases range from about 30 degrees to more than 50 degrees. This was already concluded in the analysis of the water levels and discharges. The Texel model gives a fairly similar distribution of the phases, but still with a deviation of 40 to 60 degrees with respect to the measurements. The M_6 phases are somewhat higher in the main channel of the inlet, with slightly decreasing phases away from it. More closer to the shores the M_6 phase decreases stronger, probably due to the friction of the shores.
The S_2 phases of the Texel model have a deviation of 10 to 20 degrees with the measurements, while the phases of the N_2 constituent are similar. Both semi-diurnal constituents slightly decrease from north to south. The Texel model gives again better phases than the Wadden Sea, which is also the case in the O_1 and K_1 constituent. The MS_4 phases seem to have about the same distribution as the M_4 phases.

Relative phases
In the particular case of the Marsdiep tidal inlet, the interaction of the M_2 component and its quarter-diurnal higher harmonic M_4 is first considered. The deviations in the modelled phases result in deviations in the relative phase difference between M_4 and M_2. This mean difference between the two components lies around 85° across the inlet, which varies from 50° to 120°. Apart from the overall deviation, the general distribution of the relative phase difference between M_4 and M_2 is rather similar between the models and the measurements. This can be seen in figure 5.19.

The relative phase difference between the M_2 and M_4 component is generally used to characterise the tidal asymmetry caused by the interaction of these two components. See paragraph 2.5.
Maximum enhancement of flood currents with respect to ebb currents occurs at a relative phase difference of 0° and the reverse at a difference of 180°. Differences of 90° and 270° cause changes in the slack water periods preceding flood and ebb, but do not result in a difference of the maximum velocities. However, in these last two cases, the presence of the M_6-component can result in such a difference.
In the ferry measurements, a mean phase difference of 85º causes the flood velocities to exceed the ebb velocities by approximately 0.1 m/s in the centre of the inlet. In the model results however, the mean phase difference is about 25º, which is closer to maximum

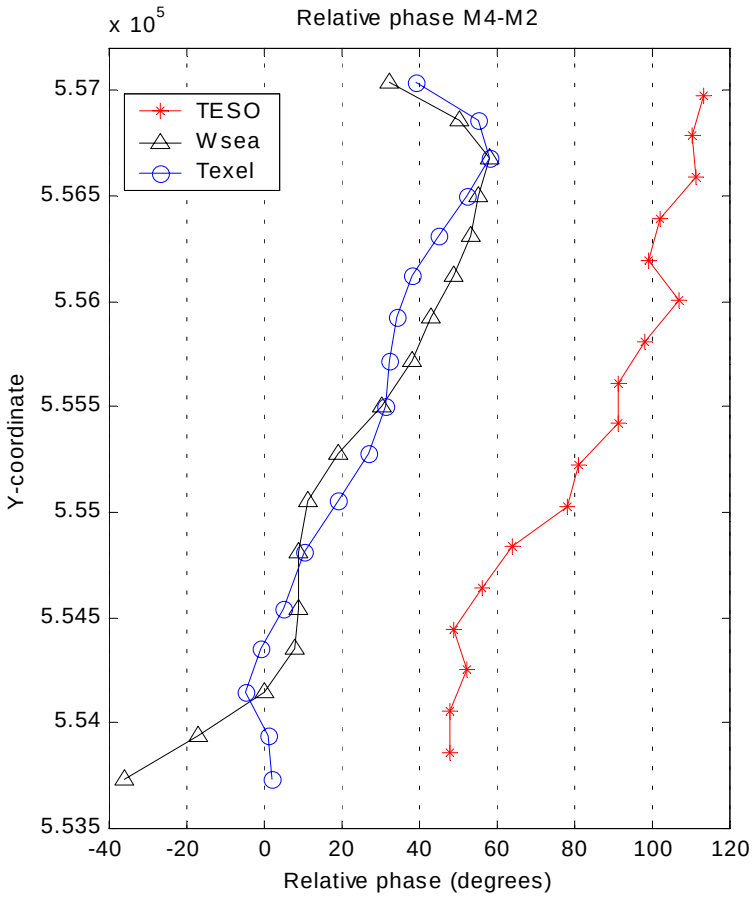

Fig. 5.19 Relative phases of the main current across the inlet

enhancement of flood currents with respect to ebb currents. So, in the models this results in an enhancement of the flood currents with respect to the ebb currents.

5.3.3 Residual currents

The residual currents in the Texel inlet consist of three distinct features. The first one is a consequence of the throughflow that exists from the Vlie basin as discussed in Ridderinkhof (1990). The main cause of this throughflow is the larger amplitude of the tidal wave in the Vlie basin in comparison with the Marsdiep basin. The second cause is the supply of fresh water from the IJsselmeer, which originates from the river Rhine and is being sluiced into the Wadden Sea. So, the amount of supplied fresh water depends on the discharge of the Rhine, which is larger in fall and winter than in spring and summer. The third feature is the existence of residual eddies, caused by tide-topography interactions.
Although this residual current can be made visible by averaging over the tidal motion, this flow is not constant due to the varying discharge of the Rhine in time. Since this water is fresh, a density driven secondary circulation will exist. The strength of this estuarine circulation depends on the magnitude of the salinity gradient, which varies in time. This density driven flow also appears in the mean flow as calculated with the harmonic analysis (Ridderinkhof, 2000).
All these features make the mean flow calculation hard to interpret, since it contains a contribution of the tidal residual eddy, the throughflow and the estuarine circulation. By using a large time scale in the mean flow calculation, the estuarine circulation will not contribute to the mean flow, as the fresh water drainage is very irregular in time.

The presence of the earlier mentioned tidal residual eddy in combination with the throughflow component add a M_0 component (mean flow) to the tidal signal, which also influence the tidal current asymmetry.
In the northern part M_0 is about 0.18 m/s in the outward direction, leading to a reversal of the asymmetry by increasing the ebb-velocities with this amount, while decreasing the flood velocities. In the southern part, the direction of the mean flow due to the residual eddy is inward but the through flow is still directed outward, resulting in an inward flow of approximately 0.07 m/s. In figure 5.20 the residual current of the Texel model and the measurements are plotted as vectors.

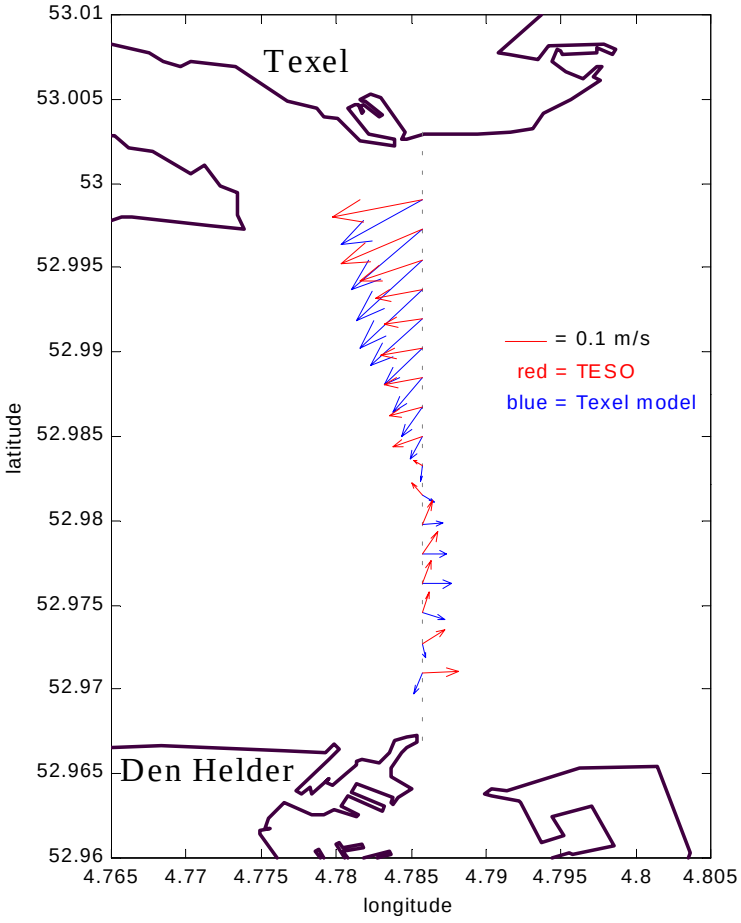

Fig. 5.20 The residual currents as vectors

6 Sensitivity Analysis

To determine the model's performance and how the model responds to several parameter settings a sensitivity analysis is performed. The sensitivity analysis consists of several stages. First several runs with the default parameter settings were made and the output is evaluated to check the general performance of the model. This validation is described in the previous chapter.
After these initial computations, several computations were made with different parameter settings, to see how these parameters influence the results. Parameter settings include:

- bottom roughness
- boundary conditions
- time step
- bathymetry
- grid
- 3D

The sensitivity analysis is only done for the Texel model. The ZUNO model has been validated and well calibrated and documented.
By analysing the results of the computations the model can be evaluated and checked on overall performance. All runs start at April 19, 1999 and end at May 23, 1999. The period, which is selected from the model results to analyse, is 32 days, starting from April 21, 1999 and ending at May 23, 1999.

6.1 Bottom roughness

In the Texel model the Manning parameter is varied to investigate the sensitivity of this parameter on the discharge through the inlet. Two additional runs are made with a Manning parameter of 0.022 and 0.030. The default run had a Manning parameter of 0.026.
It is clear from figure 6.1 that the Manning parameter (n) has rather large influence on the semi-diurnal constituents. When increasing the Manning parameter the bottom roughness increases and the semi-diurnal constituents are influenced the most. The values of n=0.022 and n=0.030 are not reasonable values for modelling estuaries. The common values in these areas range between 0.024 to 0.027.

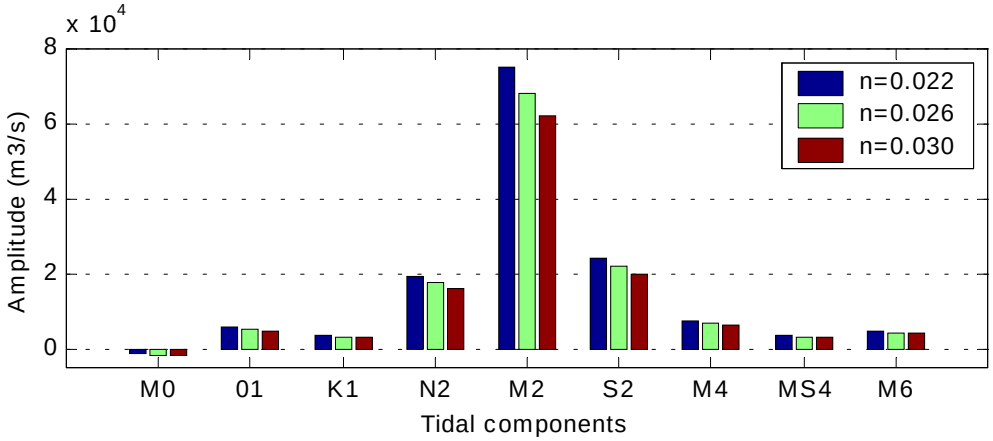

Fig. 6.1 Influence Manning parameter on amplitudes of discharge through inlet

The influence of the Manning parameter on the phases of the discharge through the Texel inlet is also noticeable. See figure 6.2. The phases of the diurnal and semi-diurnal constituents of the run with n=0.022 all differ 2 or 3 degrees with the run with n=0.026 and 4 or 5 degrees with the other run. The quarter-diurnal constituents have almost similar phases in the three models and therefore the run with n=0.022 has the largest relative phase difference of M_4 and MS_4 with M_2. The M_6 phase differs even 12 degrees between the run with n=0.022 and the run with n=0.030, so the Manning parameter has a distinct influence on the M_6 constituent, which is logical as the M_6 constituent is chiefly generated by bottom friction. The Manning parameter also influences the M_6 amplitude. The amplitude decreases 5 % with a 0.004 higher Manning parameter.

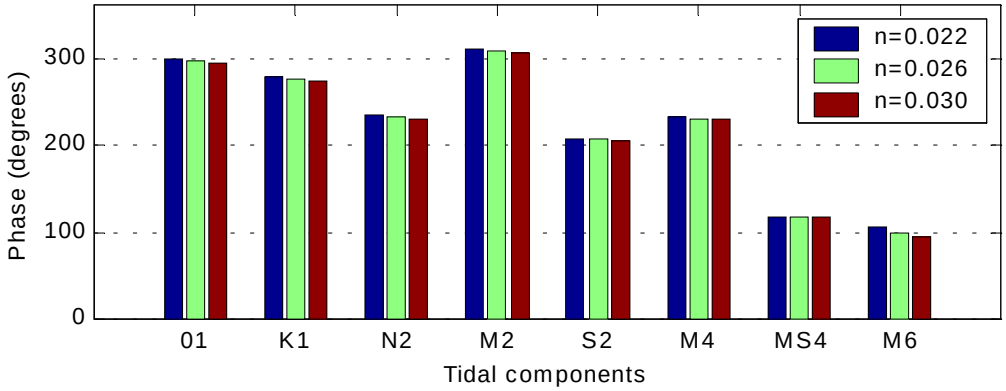

Fig 6.2 Influence Manning parameter on phases of discharge through inlet

The sensitivity analysis makes clear that tuning the model via bottom roughness the difference of the phase of M_4 in the model and the measurements can not be changed. Thus the difference in relative phase of M_4 to M_2 stays about 60 degrees. By changing the Manning parameter to n=0.022 the relative phase difference between M_4 and M_2 increases with just 8 degrees. For solving this problem three possibilities are taking into account:

- modify the bathymetry with a more accurate data set
- nesting in the Wadden Sea model (more accurate in the Wadden Sea)
- modify the boundary phase values in de Wadden Sea.

These possibilities will be discussed in the next paragraphs.

6.2 Boundary conditions

First the boundaries for the Texel model are chosen as time series. With an additional program a time series boundary can be transformed in a harmonic boundary. By doing this, it is easy to modify phases and amplitudes of harmonic components on boundaries of a nested model. The time series created with the nesting of the Wadden Sea model in the ZUNO model is transformed in a harmonic boundary. This created the possibility to modify the M_4 phase on the boundaries of the Wadden Sea model. First the boundary conditions of the ZUNO model were modified.

6.2.1 Tuning ZUNO

After analysing more tidal gauges in the southern part of the North Sea, it became clear that the M_4 phase in several water level stations was not similar to the phase resulted from the ZUNO model. Two tidal gauges, located at about 100 km south of the northern open boundary of the ZUNO model, Ekofisk and Auk Alpha, were also analysed. These two tidal gauges already had a difference between the computed and observed M_4 phase of about 50 degrees. As stated earlier, this deviation in M_4 phase is decreased to 16 degrees in Den Helder. The computed M_4 phase is only similar to the observed M_4 phase in two areas, viz. near the Maasvlakte and close to the southern open boundary.

Several runs are made to investigate the sensitivity of the forced M_4 phase at the northern boundary of the ZUNO model to the water level elevation in Den Helder (see figure 6.2). The extra phase added to the M_4 constituent on the northern boundary is plotted along the x-axis. The M_4 phase of the water level in Den Helder is plotted along the y-axis and varies roughly from 199 to 204 degrees, which remains 11 degrees too high. The M_4 amplitude of the water level remains rather constant.

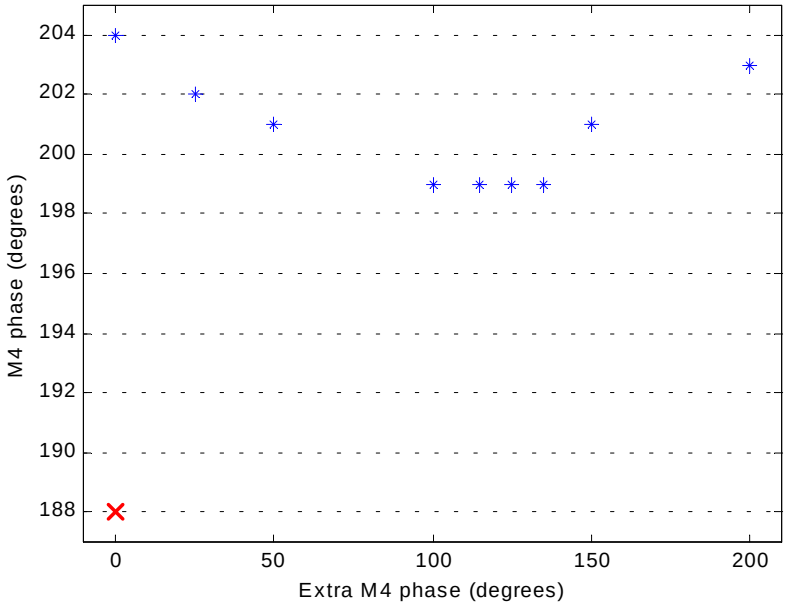

Fig 6.2 Sensitivity of M_4 phase in water level Den Helder. The red cross represents the observed phase and the blue stars represent the phases in the ZUNO models.

Forcing the boundary with all 50 constituents the relative phase difference M_4-M_2 deviates 22 degrees with the measurements. When omitting the M_4 constituent on both boundaries of the ZUNO model, the relative phase difference of M_4 with M_2 deviates only 12 degrees. Besides this, the deviation of the M_4 amplitude of the water level in Den Helder also decreases from 28 % to 12 %. This can be seen in figure 6.3. So, the adding the M_4 constituent on the boundaries of the ZUNO model gives less similar results of the M_4 phase and amplitude of the water level at Den Helder. Even in the case of forcing the boundaries in the ZUNO model with only the M_2 constituent, the relative phase difference between M_4 and M_2 is remarkably similar to the observations. However, this forcing is not realistic.

Varying the boundary forcing in the ZUNO model does not result in a similar relative phase difference between M_4 and M_2 of the water level in Den Helder.

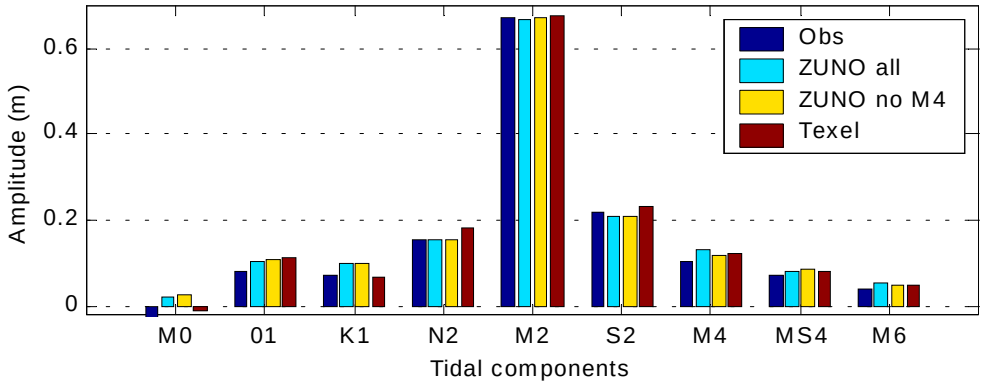

Fig. 6.3 Amplitudes of the water level in Den Helder for different boundary conditions

For the amplitudes and phases of the discharge the omitting of the M_4 constituent also has influence. But in this case the deviation of the M_4 amplitude increases from 12 % larger to 22 % smaller than the observed M_4 amplitude. Although the lack of the M_4 constituent in the boundary forcing, M_4 amplitudes in the discharge (and water levels) are generated in the model and are most dominant in shallow areas. The M_4 phase decreases with just 7 degrees.
Thus the omitting of the M_4 constituent in the model forcing gives better results for the water level in Den Helder, but on the other hand the M_4 amplitude of the discharge deviates more.

6.2.2 Type of boundary condition

In the first default run of the Texel model, two current and two water level boundaries were applied: west-current, south-water level, north-current and east-water level. Sensitivity runs with a current time series at the east boundary influenced the M_2 amplitude of the discharge hardly (2 % decrease), but if influenced the M_4 amplitude with an increase of 17 %. This was independent from the boundary types at the North Sea. Variations in these types of boundary hardly affect the phases. The relative phase differences varied at most 4 degrees.
The comparison of mean discharges in the default run with a run which has all water level boundaries and with a run in which the (sluiced) discharge in Den Oever is zero, is shown in table 6.1. The run with no discharge in Den Oever has the same boundary types as the default run.

Boundary type	East	Den Oever discharge	Texel Inlet	South	West	North
Default	1535	250	-1770	-5078	-3869	-2982
All water levels	1484	250	-1719	-6975	-8815	140
Discharge = 0	1726	0	-1710	-5126	-3859	-3048

Table 6.1 Mean discharge through boundaries and inlet in m^3/s

In the run with no sluice discharge in Den Oever, the discharge through the Texel inlet is more or less similar to the default run. The discharge through the east boundary increases with 242 m3/s and the discharge through the inlet decreases about 9 m3/s. So apparently the Marsdiep basin imports more water from the Vlie basin, to keep the discharge through the inlet more or less stable. When using all water level boundaries, the distribution of the water in the North Sea is remarkable different, than the default boundary conditions. The mean discharge through the northern boundary is very low and rather high through the south and west boundary.

6.3 Time step

Several runs were made with different time steps to study the influence of the time step on the results. Runs were made with time steps of 120s, 60s and 30s. As can be seen in figure 6.4 the time step has an influence, which should not be underestimated. The semi-diurnal amplitudes increase with a decreasing time step. This is also the case for the higher and compound constituents. The diurnal constituents remain more or less the same. The influence on the phases is at most a change of 3 degrees, which is rather low.

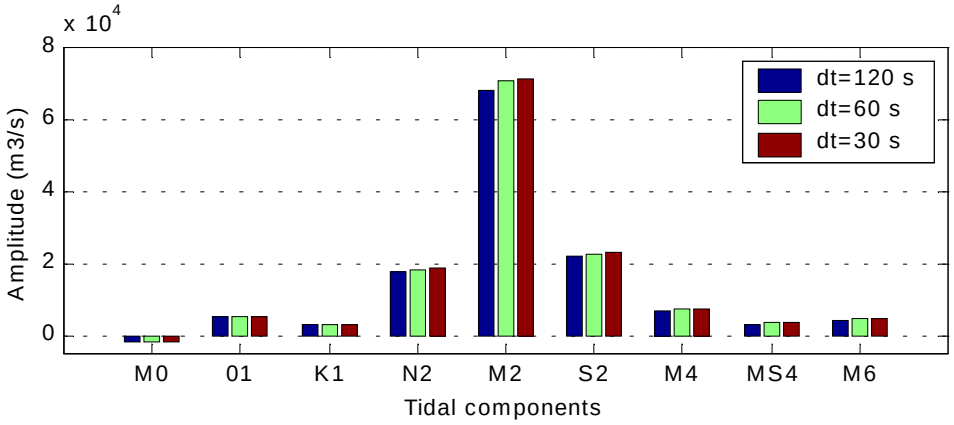

Fig 6.4 Influence of the time step on the discharge through the inlet

To investigate the sensitivity of the currents, the main currents in the observation points across the tidal inlet are plotted for three runs with different time steps. As can be seen from figure 6.5 the time step also influences the distribution of the currents in the Texel inlet. In the case of the M_2 amplitudes the run with time step of 30 s is closest to the measurements. In the case of the M_4 amplitudes the run with the time step of 60 s produces the most similar amplitudes.

The run with time step of 120 s gives unlikely phases for M_2 and M_4. The runs with 60 s and 30 s give mutual similar phases. In the further runs a time step of 60 s is chosen to keep a reasonable computational period.

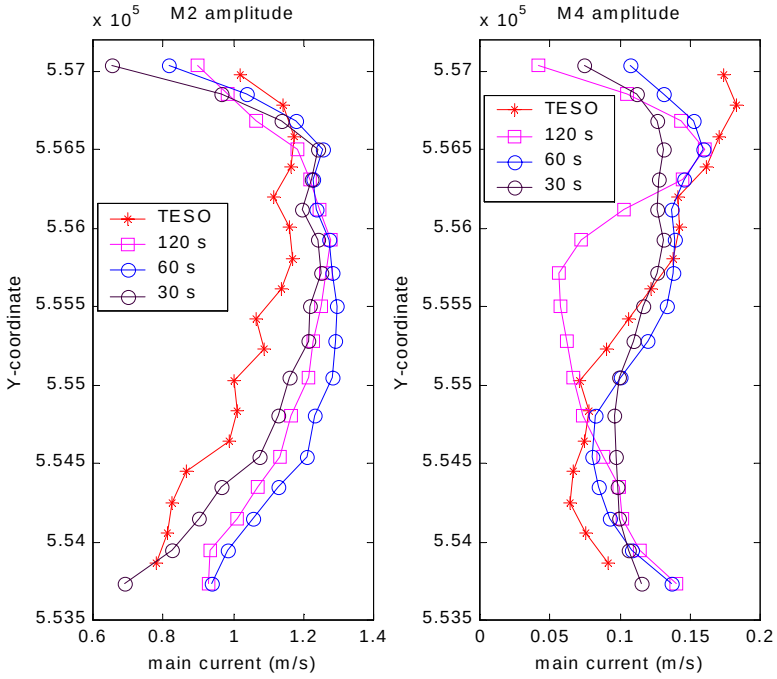

Fig. 6.5 Influence of time step on current amplitudes

6.4 Bathymetry

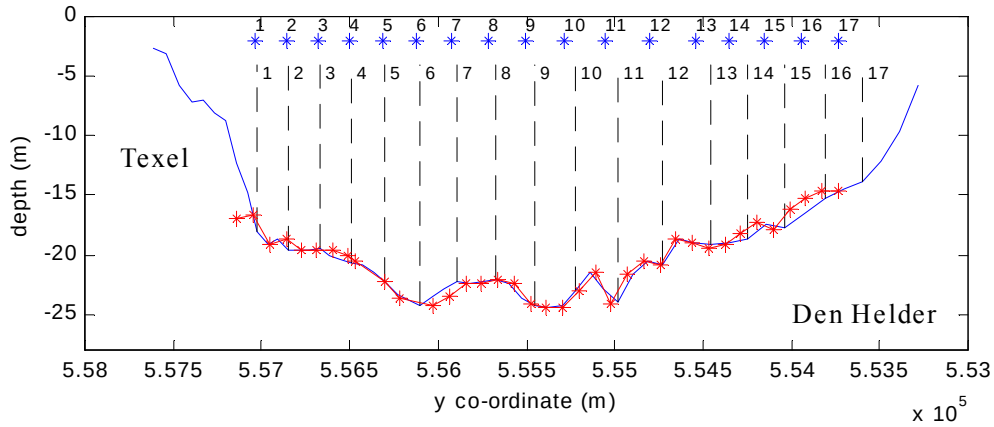

Fig. 6.6 Cross-sections of the ferry track. The blue solid line represents the model and the red stars represent the measurements. The 17 observation points are also plotted for model (black dashed line) and ferry measurements (blue stars).

The modelled amplitudes of the main current discussed in previous paragraphs differ from the amplitudes of the measured currents. Due to the fact that the discharge amplitudes fairly agree with the measured amplitudes, the deviations in the currents are caused by differences in the bathymetry. E.g. a larger cross-sectional area in the models can result in lower currents. Since the width of the Texel inlet in the models agrees more or less with the measured width, the only adjustable parameter is the bathymetry. The ferry data only gives information about the local bathymetry that is covered by the tracks. Therefore, only the bathymetry for the gridline (with the observation points) is adjusted. The adjusted depth profile along this gridline is presented in figure 6.6 and the adjustments are made on the basis of the ferry data. The grid cells, which are adjusted, have a mean size of 150 by 200 m.

The current results of the run with the adjusted depth are plotted in figure 6.7.
The run with the new depth gives amplitudes that are closer to the measured amplitudes than the default run. There still is some deviation in the amplitudes, but this can be explained since there is still a small difference in modelled M_2 amplitude and the measurements of 3 %. The M_4 amplitudes are produced very well.

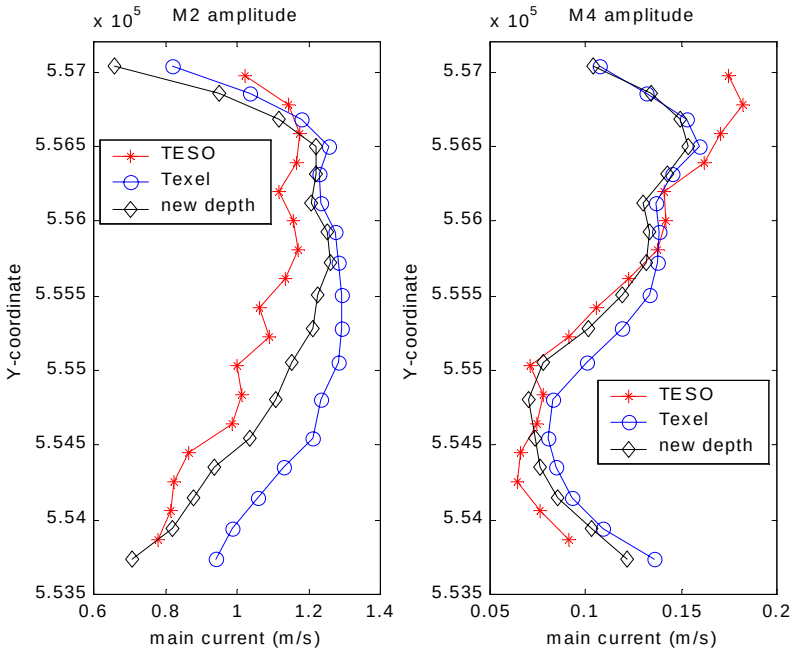

Fig. 6.7 Amplitudes of the main current for new depth

6.5 Grid

The eastern boundary of the Texel model in the Wadden Sea was partially placed on a water shoal. To investigate the influence of the location of the eastern boundary, a new model was build, whereby the grid extended further into the Wadden Sea. See figure 6.8. The new eastern boundary was placed near the water shed from Texel to Harlingen. The other three boundaries also changed. The location of these boundaries was determined on the basis of new depth observations, which became available during this study. The depth observations came from RIKZ Haren and had a high resolution of 20 metres.

The 'Noorderhaaks' (a sandbar; see fig 1.1) west of the Texel inlet, was modelled as dry points. First all boundaries were time series of water levels, generated from the Wadden Sea model. The time step was 60 s. The Manning parameter was kept 0.026.

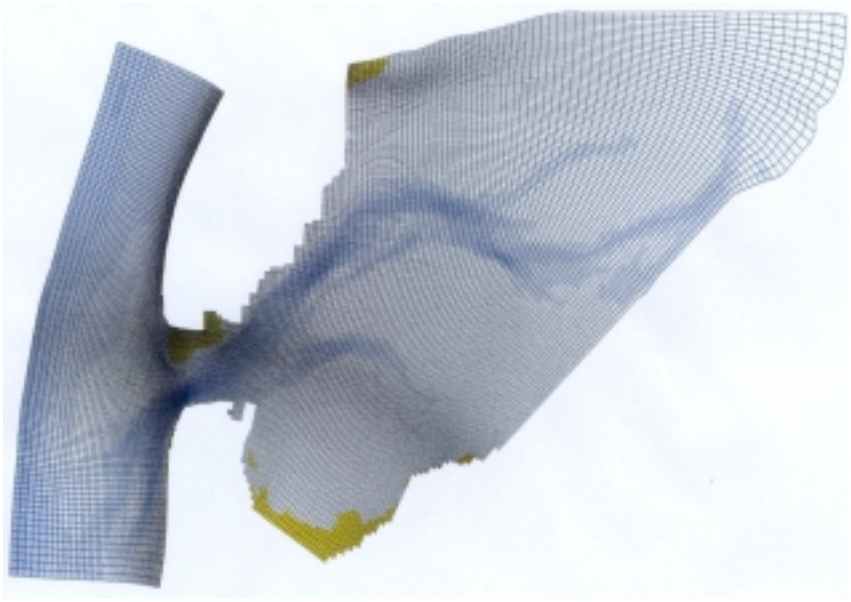

Fig. 6.8 Grid and bathymetry of the Basin model

An extra discharge location was added in Kornwerderzand, which is a sluice in the Afsluitdijk. The eastern boundary reaches up to Harlingen. So besides the tidal gauge of Kornwerderzand also the tidal gauge at Harlingen can be used for validation. The situation in the Texel inlet remained the same; the same observation points and the cross-section were used.

The amplitudes of the discharge simulated by the default run of the Basin model are shown in figure 6.9.

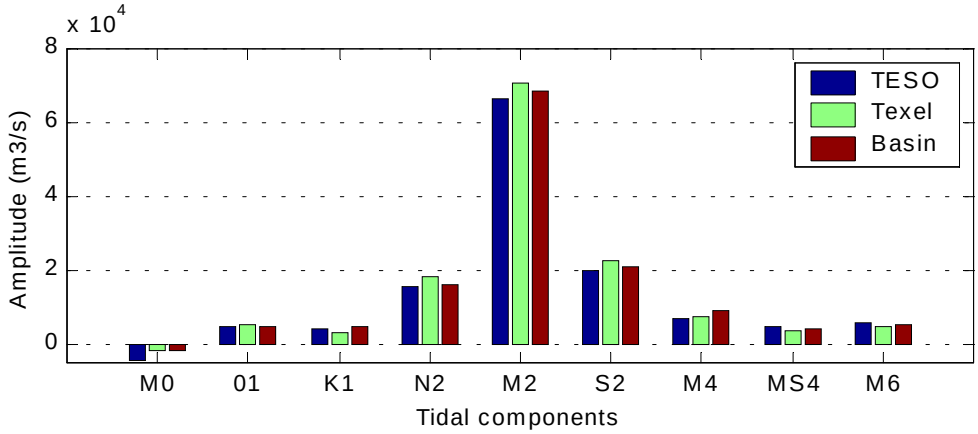

Fig. 6.9 Amplitudes of discharge in the Basin model

The amplitudes of the semi-diurnal constituents are closer to the measured amplitudes than the Texel model. The difference of the M_2 amplitude in the Basin model and the measurements is about 3 %. However, if the measurements are analysed for a year (see paragraph 5.2.1) the modelled M_2 amplitude is even similar (difference of 0.5 %) with the measured M_2 amplitude. The higher and compound constituents are slightly higher than in the Texel model.

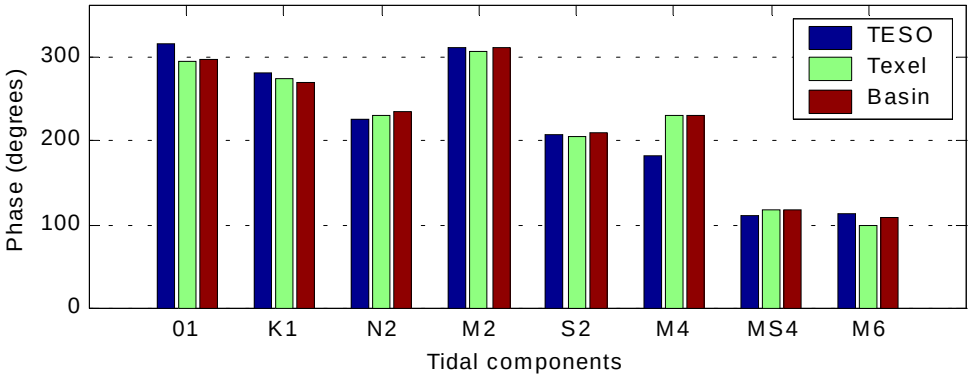

Fig. 6.10 Phases of the discharge of the Basin model

Just like in the amplitudes, the phases of the semi-diurnal constituents are slightly higher. See figure 6.10. The modelled M_2 phase is even similar with the measured M_2 phase. The fact that the basin model has all water level boundaries, is not the reason for the differences in the amplitudes and phases of the discharge. This is checked with a run of the Texel model with all water level boundaries.

Although this basin model produces better amplitudes and phases for most of the constituents, the relative phase difference between M_4 and M_2 still exists.

Deepening the Wadden Sea in basin model
To investigate the sensitivity of the M_4 phase additional runs are made with the basin model. In the first run the bathymetry in the Wadden Sea is adjusted. Starting from a gridline just eastward of the ferry track the bathymetry is deepened with 2 meter. By deepening the depth in the basin, the tidal wave propagation will probably be influenced, because the frictional effects are less due to a greater water depth.

In another run only the deeper channels are deepened to study if the tidal wave propagates faster when only the main channels are deepened. The channels which are deeper than 10 meters are deepened with another 5 meters.

The deepening of the Wadden Sea in the basin model did not give any satisfying results. This is probably due to the fact that the basin model is nested in the Wadden Sea model. The Wadden Sea model prescribes mainly tidal propagation for the basin model via the forcing on the open boundaries. Therefore, the bathymetry in the Wadden Sea model is also adjusted in order to investigate the tidal wave propagation. Again the channels which are deeper than 10 meters are deepened with 5 meters.

The amplitudes of all analysed constituents of the discharge have increased. However, the phases remain the same. The amplitudes of the semidiurnal constituents increased with about 5 %. The amplitudes of the quarter-diurnal constituents increased with more then 11 %. The diurnal constituents just slightly increased with about 2 %.
Since the phases remained the same, the relative phases do not change either.

6.6 3-Dimensional

Since the measurements from the ferry also contain currents in every 0.5 m vertical water column, a 3D model was set up to compare the current profiles in the vertical. This model consists of 8 layers. Each layer represents a user-defined percentage of the water column. As the largest changes in current speeds are in the lower part of the water column, the lowest 4 layers represent only 30 % of the water column.
In the model the κ-ε model is used as the turbulence model. The κ-ε model is a second order turbulence closure model. In this model both the turbulence energy κ and dissipation rate of turbulent kinetic energy ε are calculated by a transport equation. From κ and ε the mixing length L and viscosity are determined. The mixing length is now a property of the flow and in the case of stratification no damping functions are needed, which is one of the main advantages of the k-e turbulence model. The κ-ε model is about the most elaborate model that has been used so far and even so there is no common opinion on the relative merits of the various models.
The default value for the vertical eddy viscosity is 1*10-6 m^2/s. Since this run is made to get a first idea of the similarities and differences with the 2D run, the partial slip conditions and z_0 are not taken into account.

When comparing the 3D amplitudes of the discharge with the 2D amplitudes in the Texel model, it is clear from figure 6.11 that the amplitudes of the semi-diurnal constituents all decreased. The decreasing factor was exactly the same for the three constituents, namely 0.957. The amplitudes of the other constituents all slightly decreased in the 3D run compared with the 2D run. The phases remained the same, except for the M_6 constituent that changed 2 degrees or 1 minute.

During the final stage of this study, modellers found an error in the modelling program with respect to 3D modelling. In a run with varying layer thickness, the model produced higher shear stresses than the 2D run, which resulted in lower current speeds. This explains the already discussed deviations in amplitudes of the discharge through the inlet. The bug had no influence in a 3D run with equidistant layers.

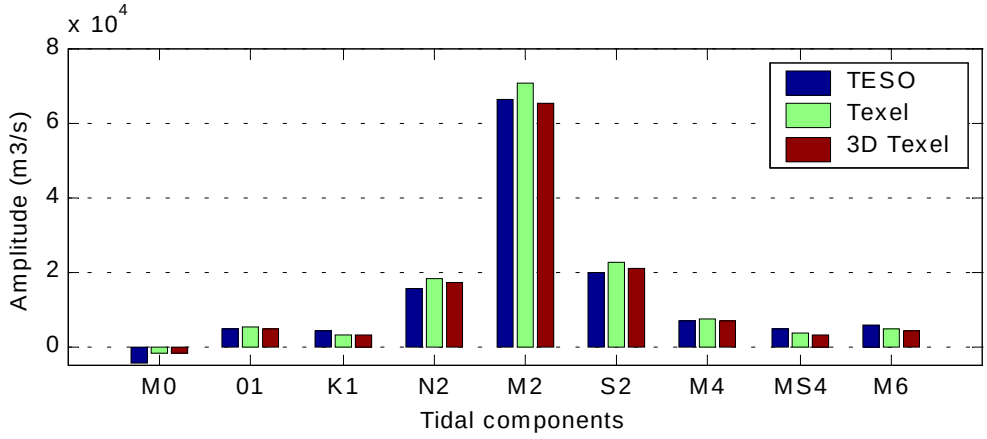

Fig. 6.11 Amplitudes of the discharge for a 3D run

When analysing the main current amplitudes of the 3D run, the pattern of the M_2 amplitudes corresponds with the measured M_2 amplitudes. However, due to the lower M_2 amplitude of the discharge, all amplitudes are 0.04 m/s smaller than the measured amplitudes. In the M_4 amplitudes and the phases no changes are perceived.

With the 3D run it is possible to create vertical current profiles in the observation points along the ferry track. These points correspond with the points in the measured data. The modelled and measured amplitudes can now be presented as a current profile, as plotted in figure 6.12 for point 5. Point 5 is chosen because the modelled and measured M_4 amplitude of the (depth-averaged) main current is similar in this point. There are still some deviations in the M_2 and M_4 amplitudes of the main current in most of the points. Therefore the magnitude of the modelled amplitudes does not agree with the measured amplitudes. However, both patterns of the current profiles are interesting to plot.

The water column in the model is divided in 8 layers but the amount of layers in the water column in the measurements varies. Each layer or bin has a size of 0.5 m in the vertical. Since the ADCP start measuring about 5 meters beneath the water surface, the upper part of the water column can not be presented. Besides this, the bottom in one of the 17 points also varies due to the spatial variability of the ferry track, as is described in paragraph 3.3. In order to get a good comparison, the lower 36 bins of the measured data are used for creating the current profile; so starting at the bottom.

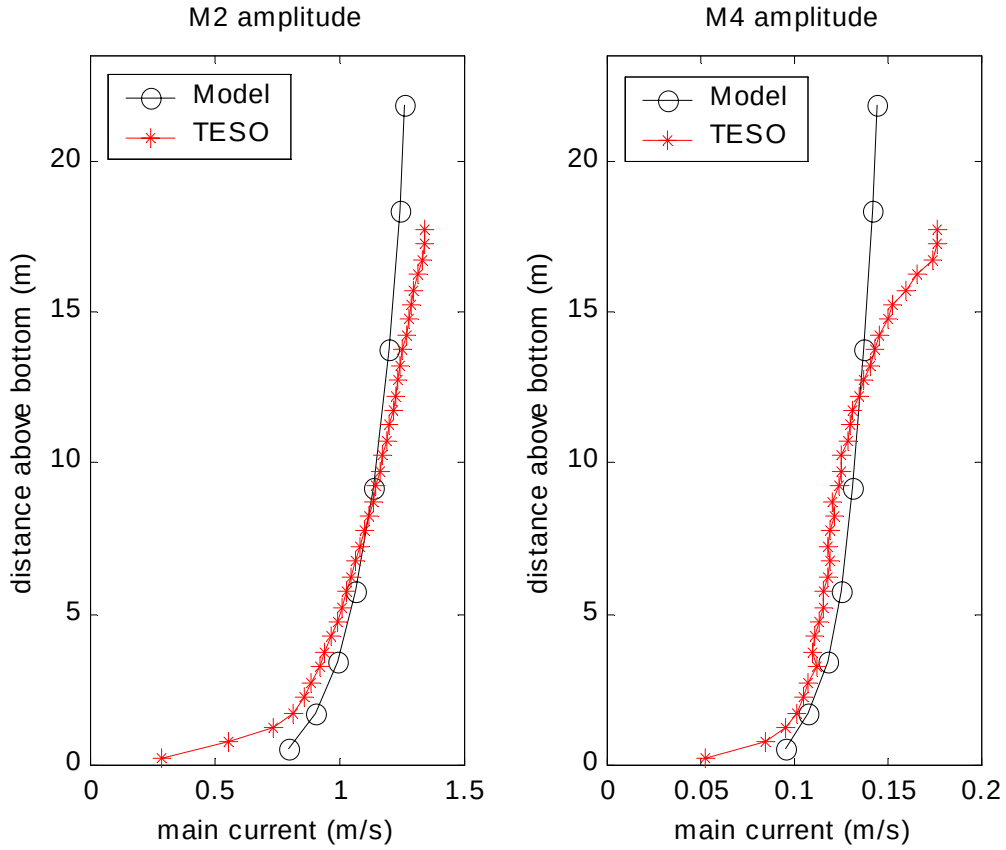

Fig 6.12 Vertical profile of amplitudes of the main current in point 5; 8 non-equidistant layers

The distribution of the M_2 amplitudes in the vertical is fairly similar between the model and the measurements. However, considering figure 6.12 it is evident that the model does not accurately reproduce the decrease in the currents close to the seabed, although the model does show a reduction in magnitude in the near-bed region. The two patterns of the M_4 amplitudes correspond mutually in the lower half of the water column, but towards the surface the measured M_4 amplitudes increase.

An additional run with ten equidistant layers does give the exact same amplitudes and phases of the discharge as the 2D run. The difference with the first 3D run (with the higher shear stress) is that the near-bottom M_2 amplitudes are slightly larger in the new run. In the M_4 amplitudes the difference is even smaller. The overall profiles of the M_2 and M_4 amplitudes are similar in both runs. Compared to the measurements the model produces a smoother current profile for the M_2 amplitudes and also for the M_4 amplitudes in the upper half of the water column.

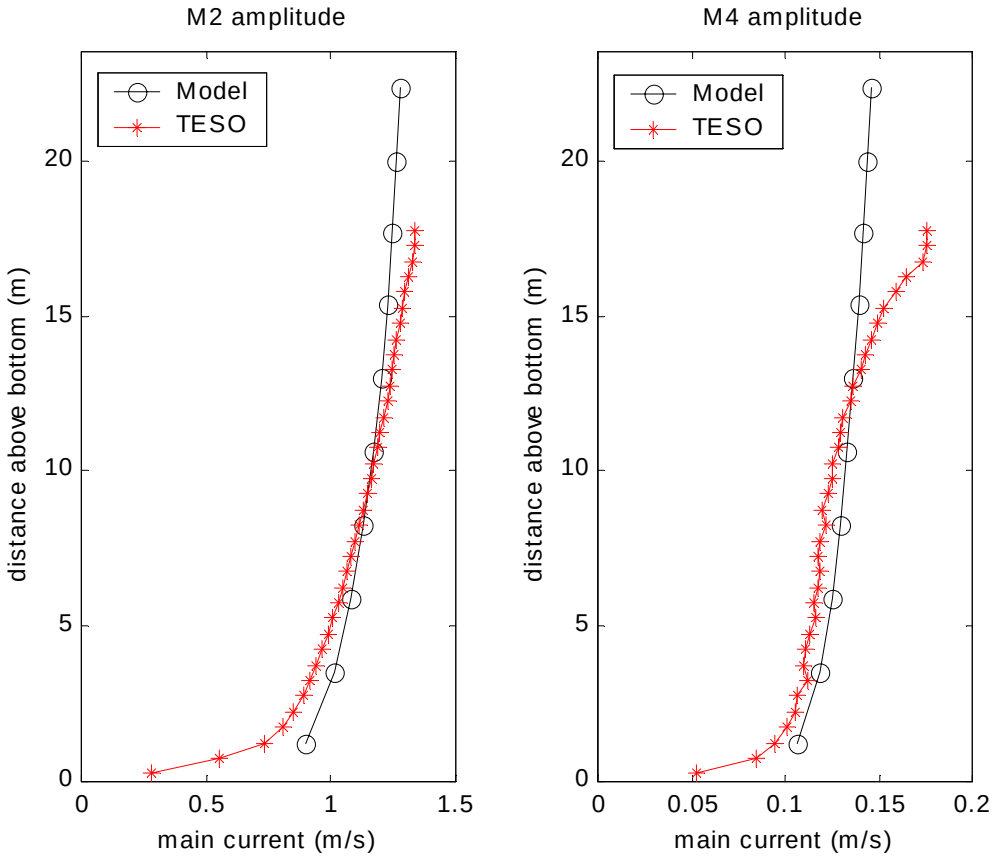

Fig. 6.13 Vertical profile of amplitudes of the main current in point 5; 10 equidistant layers

An explanation for the increased M_4 amplitude (and also a slight increase of the M_2 amplitude) of the main current near the surface can not be found. Perhaps this is a result of density gradients caused by the fresh water discharges from the sluices in the Marsdiep basin. In this study, the effects of density gradients are not taken into account. So, this is just a recommendation for future work.

A study of Davies and Lawrence about the M_4 tide in the Irish Sea showed that by adding meteorological effects to a model run, the near-surface M_4 component of the currents significantly increased. In the case of a model with a time-varying eddy viscosity, the M_2 and M_4 tidal currents are influenced by wind effects, with M_4 near-surface tidal currents being increased significantly by wind effects in the model. So including wind effects in the models could generate higher M_4 currents near the surface, which is found in the measurements.

7 Evaluation of the model runs

By analysing and comparing the model results of the several runs of the different models in this study with the measurements, experience and knowledge on the effects of different parameters are acquired. Especially the sensitivity analyses resulted in useful knowledge. Using this knowledge, improvements in the parameter settings and boundary conditions in the models can be made. These improvements are applied on the detailed model. Since the Basin model gives better results than the Texel model in both amplitudes and phases (see paragraph 6.5), the basin model is taken as the detailed model on which the improvements are applied.

The Wadden Sea model is used as the overall model for nesting the Basin model. All boundaries in the Basin model are forced with water level elevations, which are thus generated in the Wadden Sea model. A result of the analyses in chapter 5 is the difference in the discharge of the M_4 phase between the models and the measurements. Each model produces a higher M_4 phase in the discharge through the Texel inlet than the M_4 phase in the observed discharge. In the analysis of the water level in Den Helder also a deviation in the modelled M_4 phase with the measurements is found. In the water level this deviation is about 16 degrees and in the discharge through the Texel inlet the deviation is around 55 degrees.

Modifying the M_4 phases in the boundary conditions of the ZUNO model does not result in improved M_4 phases in water levels and discharge. It became clear that the M_4 constituent is mainly generated in the model by the non-linear aspects of tidal propagation. Thus the influence of the M_4 constituent on the boundary forcing is rather small. The co-tidal charts in paragraph 5.1.4, showing the amphidromic points in the North Sea also illustrate this.
With an additional program the time series boundaries are transformed into harmonic boundaries. This offers the opportunity to modify phases and amplitudes of boundary conditions in a detail model. Modifying the M_4 phases in the boundary conditions of the Wadden Sea model proved to be a nice tool for minimising the differences in the M_4 phases in the models.

7.1 Modifying boundary conditions

7.1.1 Minimising difference M_4 phase water level Den Helder

By uniformly adding a phase in degrees to the boundary conditions, it is possible to minimise the difference between the modelled M_4 phase and the measured water level at Den Helder. An additional run was made for this. The forcing consists initially of the eight most important constituents: the constituents, which are used in the analyses. As can be seen in figure 7.1 the modified boundary conditions also influence the amplitudes of the water level in Den Helder.

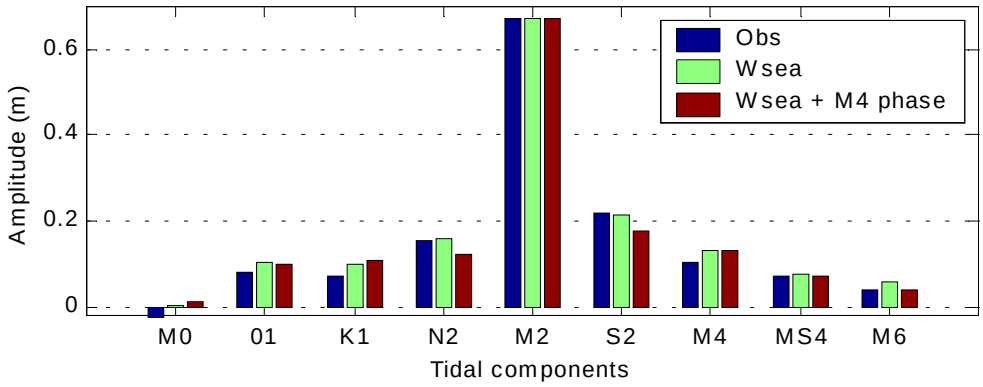

Fig 7.1 Amplitudes of the water level at Den Helder

Especially the N_2 and S_2 amplitudes decrease together with the M_6 amplitude, which even improved with respect to the measurements. The analysis of the model results of this run showed that when the modelled M_4 phase was equal to the measured M_4 phase of the water level at Den Helder, phases of other constituents are also influenced. This is showed in figure 7.2. Remarkable is the K_1 phase, which deviates about 35 degrees with the default Wadden Sea model run.

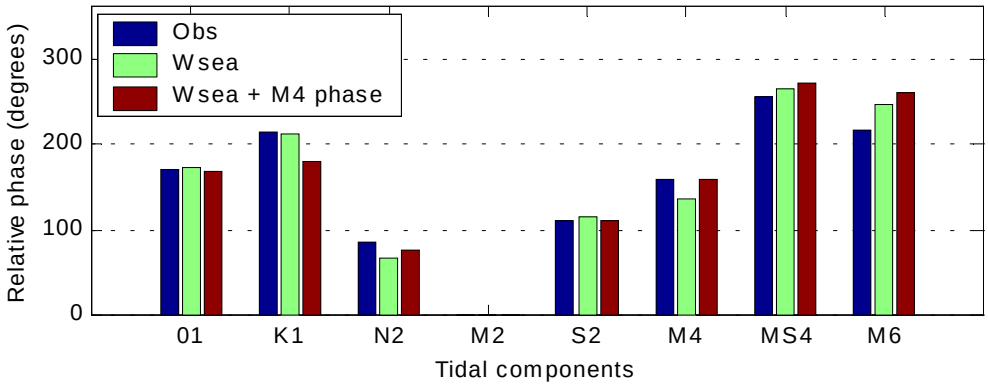

Fig 7.2. Relative phases of the water level at Den Helder

Water level in Texel Noordzee

The deviations, which are found in the amplitudes of the water level at Den Helder, are also more or less valid for the water level in Texel Noordzee. But in this case also the amplitudes of M_2 and M_4 in the new run decrease in comparison with the default run.

The phases of the water level in Texel Noordzee of the new run give very good similarities with the phases of the observed water level. See figure 7.3. Exception is the K_1 phase, which again deviates 35 degrees.

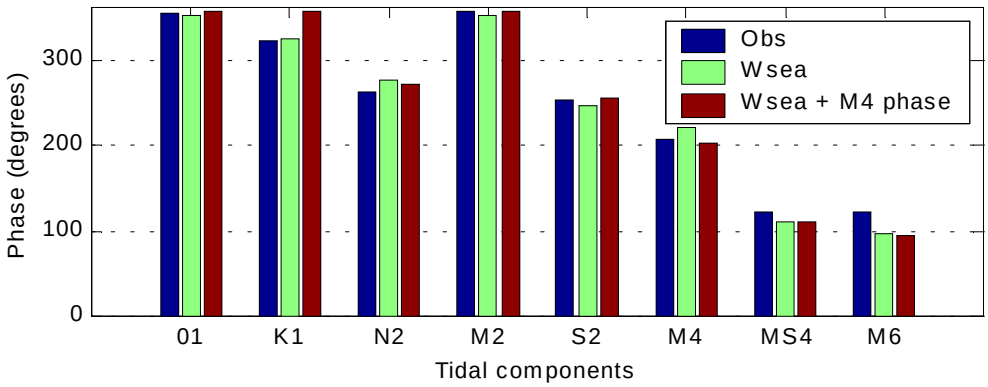

Fig 7.3 Phases of the water level at Texel Noordzee

Discharge through the Texel inlet

Like in the analysis of the water levels in Den Helder and Texel Noordzee, the N_2 and S_2 amplitudes in the new run decrease in comparison with the default run. The other amplitudes correspond with the amplitudes of the default run.

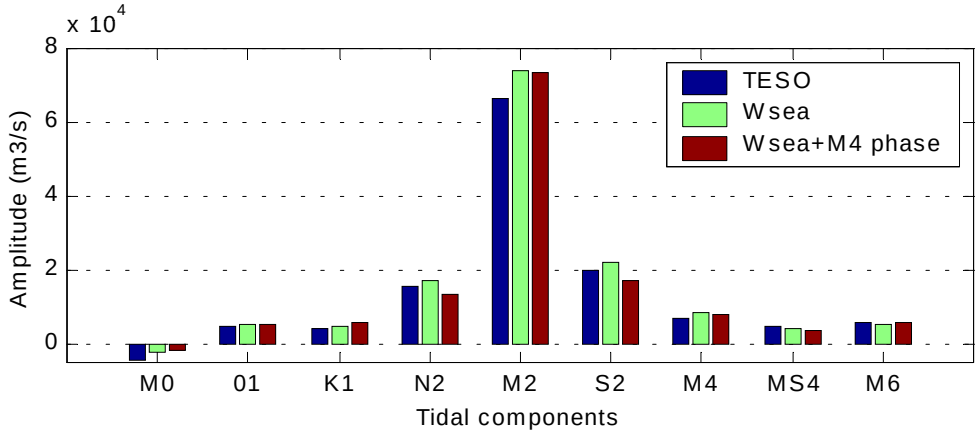

Fig 7.4 Amplitudes of the discharge through the inlet

Remarkable is that when the modelled M_4 phase in the water level at Den Helder is equal to the M_4 phase of the observations, the difference of the modelled M_4 phase with the M_4 phase of the observed discharge only partially decreases. The difference becomes about 25 degrees, with is about half of the original difference of 55 degrees. The other phases do not change a lot by modifying the M_4 phase in the boundary forcing. Except for the K_1 phase, which is now 18 degrees higher than the K_1 phase of the default run.

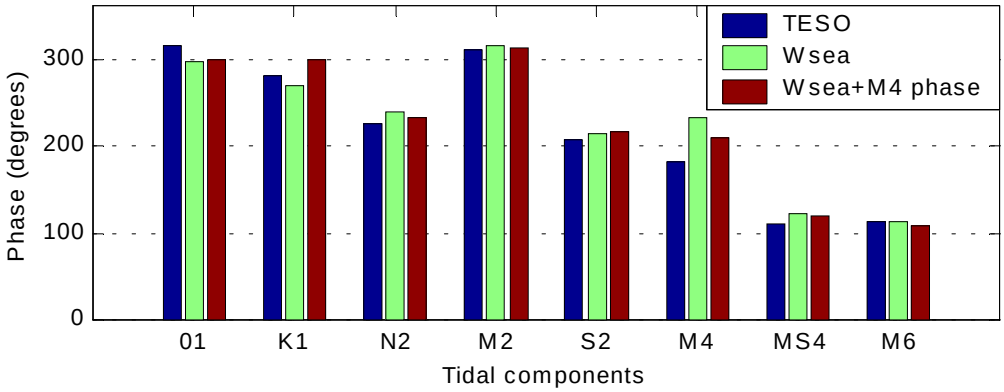

Fig 7.5 Phases of the discharge through the inlet

7.1.2 Minimising difference M_4 phase of discharge

Water levels

Another additional run was executed to minimise the difference in the M_4 phase in the discharge even more. In this case, the analysis showed that when the modelled M_4 phase of the discharge is equal to the M_4 phase of the observed discharge, the M_4 phase of the modelled water level at Den Helder deviates again with the measurements. This can be seen in figure 7.6. The difference of the K_1 phase is again present in the new run. The M_6 phase decreases even more compared to the M_6 phase in the default run.

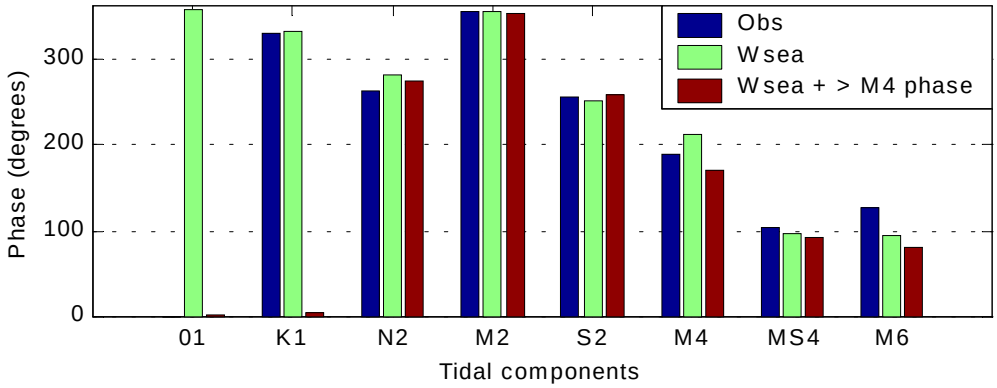

Fig 7.6 Phases of the water level in Den Helder

In the water level elevation at Texel Noordzee the M_6 phase in the new run does not decreases as much as in the water level in Den Helder. The changes in the phases of the other constituents mainly correspond with the changes in the water level at Den Helder. The decreases of the M_4 phase in Texel Noordzee and Den Helder between the new run and the default run are similar.

Discharge through the inlet

In the analysis of the discharge of the new run compared with the default Wadden Sea model run, some previous mentioned conclusions can be applied. The new model run produces lower amplitudes of the semidiurnal constituents. The other amplitudes are not influenced a lot and thus remain about the same.

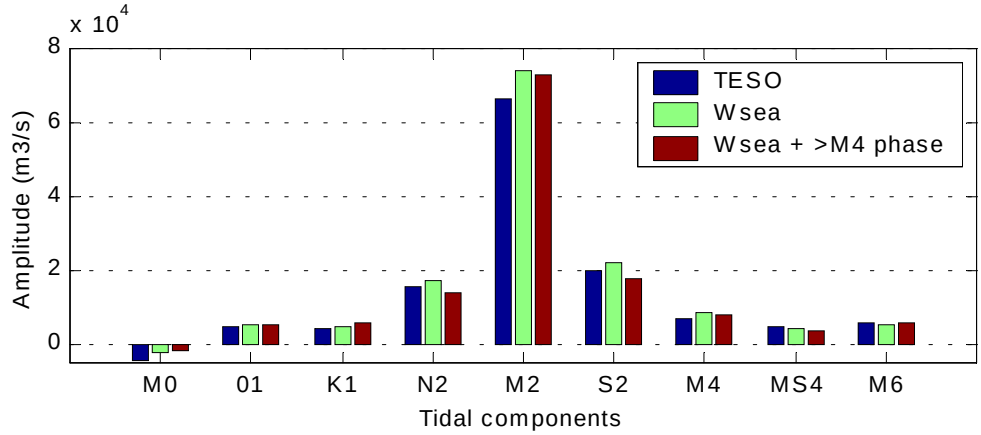

Fig 7.7 Amplitudes of the discharge through the inlet

The goal of this new model run was to diminish the difference between the modelled M_4 phase in the discharge through the Texel inlet with the observed M_4 phase. As can be seen in figure 7.8 the modelled M_4 phase is equal to the observed M_4 phase. So the relative phase difference of M_4 with M_2 in the new run has become equal to the relative phase difference from the measurements. The K_1 phase produced in the new model run, is 18 degrees to high.

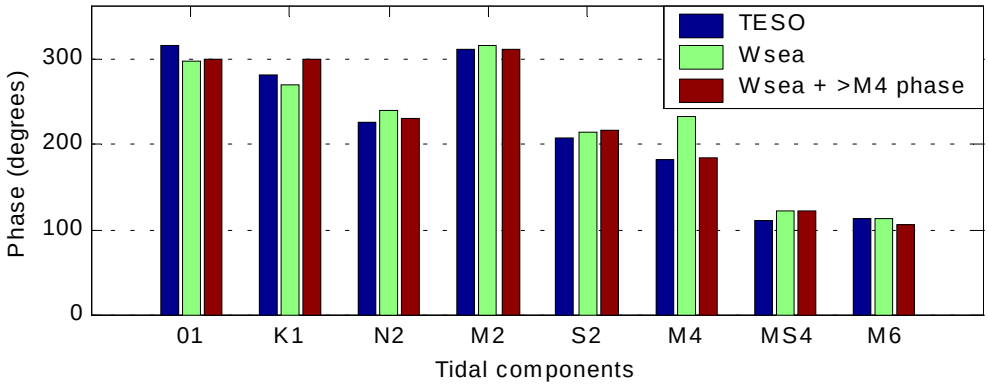

Fig 7.8 Phases of the discharge through the inlet

Due to the importance of the currents in the sediment transport, the boundary conditions, which are used in the run discussed in this paragraph, are chosen as the boundary forcing in future runs for the area around the Texel inlet.

7.2 Basin model

As mentioned in previous paragraphs, the Basin model is nested in the Wadden Sea model, which is forced by eight harmonic components. In this Wadden Sea model run the difference in the M_4 phase of the discharge is minimised. This is discussed in paragraph 7.1.2.
This Basin model includes the most updated bathymetry, which was available during this study. The bathymetry of one gridline, which resembles the ferry track, is adjusted to the measured depth. Besides the watershed between the Vlie basin and the Marsdiep basin, the model area also includes the entire ebb-delta. See appendix D for the parameter settings that are chosen.

Performing a harmonic analysis of 32 days on the basin model results gives amplitudes and phases for the eight constituents. The amplitude of e.g. the N_2 constituent consists of only the N_2 constituent, which is forced on the model boundary. When performing a harmonic analysis of 32 days on the observations, the amplitude of e.g. the N_2 constituent also consists of some neighbouring constituents of the N_2 constituent. Due to the record length of 32 days, nu_2 and K_2 can not be distinguished from the N_2 constituent. In order to distinguish these constituents from the N_2 constituents, record lengths of respectively 206 and 183 days are needed.
So, for an equivalent comparison, the record length of the observations that is harmonically analysed must be longer than 206 days. In the following analyses the observations are harmonically analysed over a period of one year. However, the model results are still harmonically analysed over a period of 32 days.

To give an idea of the performance of the model, the model results of the final run are analysed and compared with the observations. These comparisons are discussed in the following paragraphs.

7.2.1 Water levels

Since the Basin model is nested in the Wadden Sea model, the water levels of the Basin model generally correspond with the water levels in the Wadden Sea model. In previous analyses of the water levels, it was already concluded that the modelled water levels generally correspond with the water levels from the tidal gauges.
The modelled amplitudes of the water level in Den Helder (see figure 7.9) correspond with the observed amplitudes for most of the components. The M_6 amplitude of the observations has increased by changing the record length to one year.

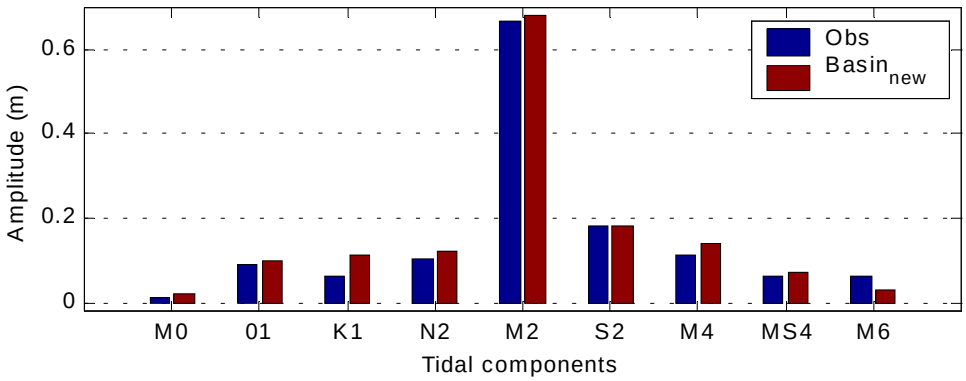

Figure 7.9 Amplitudes of the water level at Den Helder

The Basin model also produces similar phases. Exception is the M_6 phase, which deviates 34 degrees with the observations.

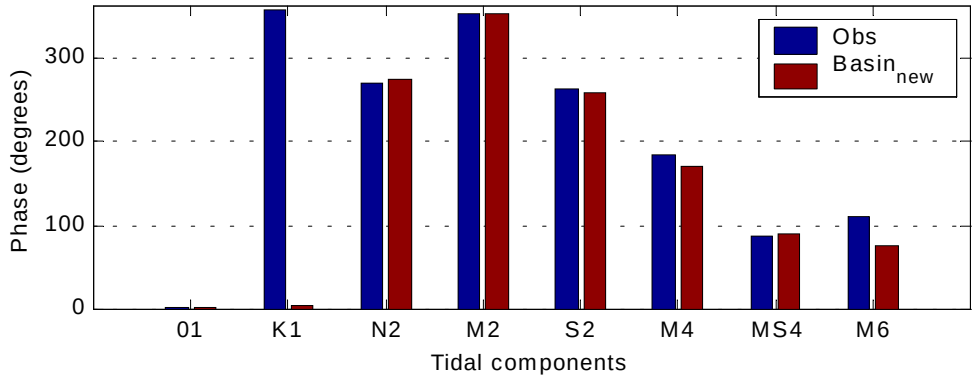

Figure 7.10 Phases of the water level at Den Helder

7.2.2 Discharge

Analysing the time series of the discharge through the Texel inlet shows that the modelled amplitudes correspond well with the ferry measurements. Note that the M_4 constituent is well produced by the model. This is the result of adjusting the boundary conditions in the Wadden Sea model. The only considerable deviation is found in the phase of the MS_4 constituent. This deviation is almost 40 degrees.

The time series of the discharges are plotted in appendix G. The new boundary conditions give a more similar time series of the discharge with the observations, especially for the period just after maximum discharge.

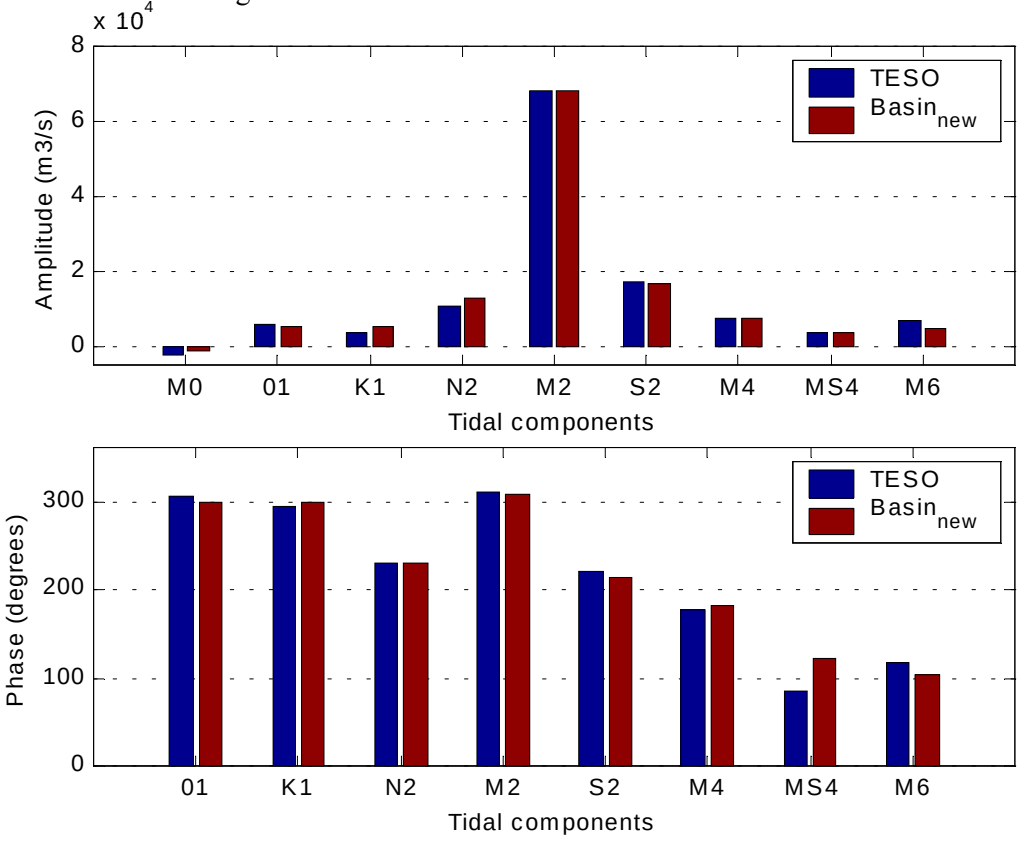

Figure 7.11 Amplitudes (top) and phases (bottom) of the discharge through the Texel inlet

7.2.3 Currents

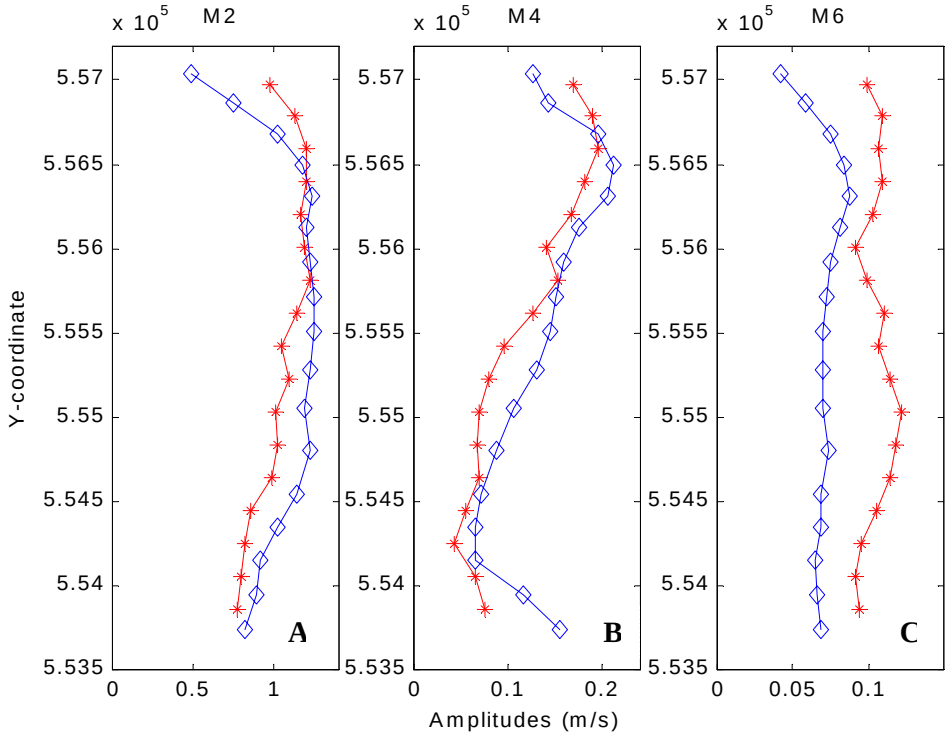

Figure 7.12 The M_2(a), M_4(b) and M_6(c) amplitudes of the main current across the inlet. The red line represent the measurement while the blue line represents the basin model.

In figure 7.12 the amplitudes of the current in the main direction are showed. The general distribution of the modelled M_2, M_4 and M_6 amplitudes corresponds with the measurements. The modelled M_2 and M_4 amplitudes are close to the measured amplitudes. The modelled M_6 amplitude however, is somewhat lower than the measured M_6 amplitudes. This is also found in the discharge through the inlet. The magnitude of the M_6 amplitude appeared to be sensitive to the time step.
When comparing the distributions of the M_2 and M_6 amplitudes some similarity is found. The M_6 constituent is generated and dissipated by bottom friction. Bottom friction is strongly influenced by the magnitude of the current. Since the M_2 amplitudes of the currents are by far the largest currents across the inlet, the distribution of the M_6 amplitudes more or less agrees with the distribution of the M_2 amplitudes.

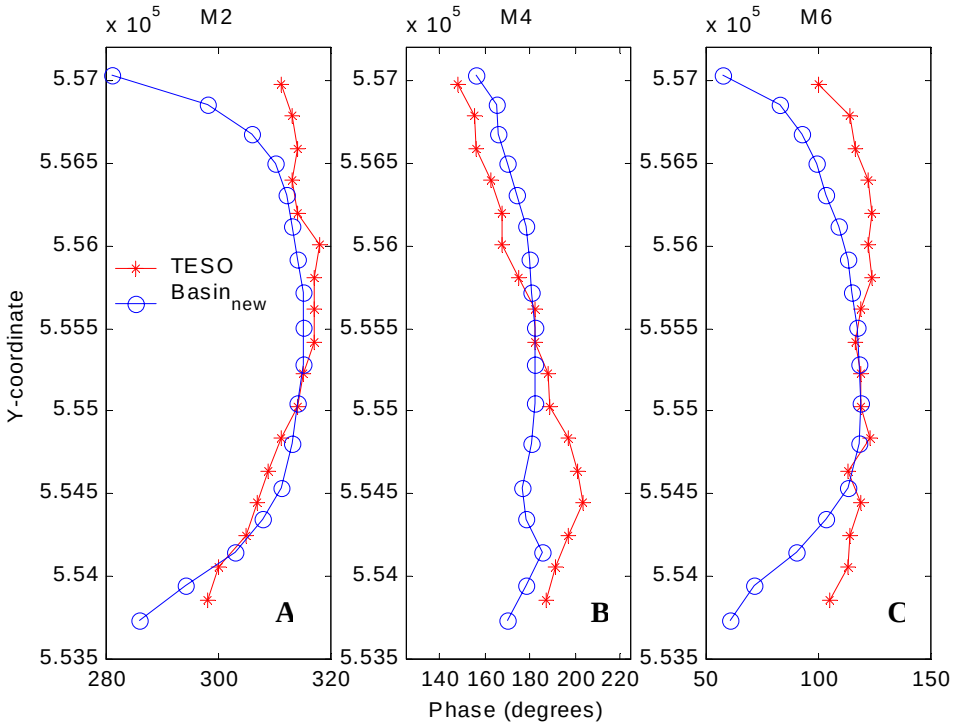

Figure 7.13 The M_2(a), M_4(b) and M_6(c) phases of the main current

The M_2, M_4 and M_6 phases of the main current in the measurements and in the basin model are showed in figure 7.13. The distributions of all three modelled phases show good similarity with the phase distributions of the measurements. As in the case of the amplitudes, the distribution of the M_6 phases also agrees more or less with the distribution of the M_2 phases.
In all previous runs in this study, a difference of about 50 degrees between the modelled and measured M_4 phases existed. Since the boundary forcing in the Wadden Sea model has been adjusted, this difference has decreased. The result is that the modelled M_4 phases are now close to the measured M_4 phases.

7.2.4 Residual currents

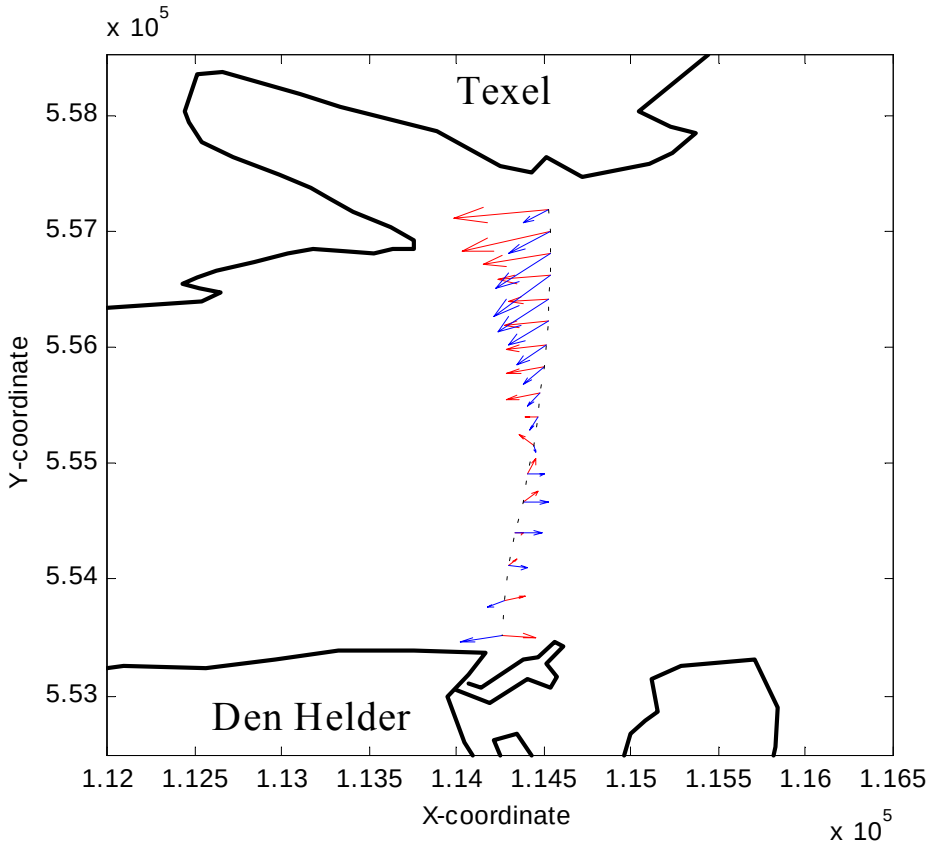

Figure 7.14 Residual currents as vectors. Red vectors represent the measurements and the blue vectors represent the model

Figure 7.14 shows the measured and modelled residual currents as vectors. Differences in direction of the residual current vectors are noticeable across the entire inlet. Differences in magnitude of the residual currents are also noticeable, mainly in the northern part of the inlet near the Mokbaai. The Mokbaai is the bay west of the ferry harbour of Texel. In paragraph 5.3.3 the residual currents of the Texel model are discussed. Figure 5.20 shows that in the northern part of the inlet the Texel model does simulate residual current vectors of the same magnitude as the measurements. These differences in the residual current vectors between the two models can be explained by differences in the local bathymetry around the Mokbaai. The bathymetry in the Texel model shows a gully in the inlet of the Mokbaai, which is not the case in the (more recent) bathymetry of the Basin model. The latter model does not simulate considerable flow currents into or in the bay. See appendix C for a detail map of the grid and bathymetry in the inlet.
The directions of the upper blue vectors, which represent the residual currents of the model, coincide with the local bathymetry in that part of the inlet. It also agrees with the direction of the main currents in that part of the inlet. In the most southern part of the inlet, the modelled residual current direction differs about 180 degrees with the measurements. The upper red vectors, which represent the measured residual currents, all appear to have a deviation in the direction compared with the modelled vectors.

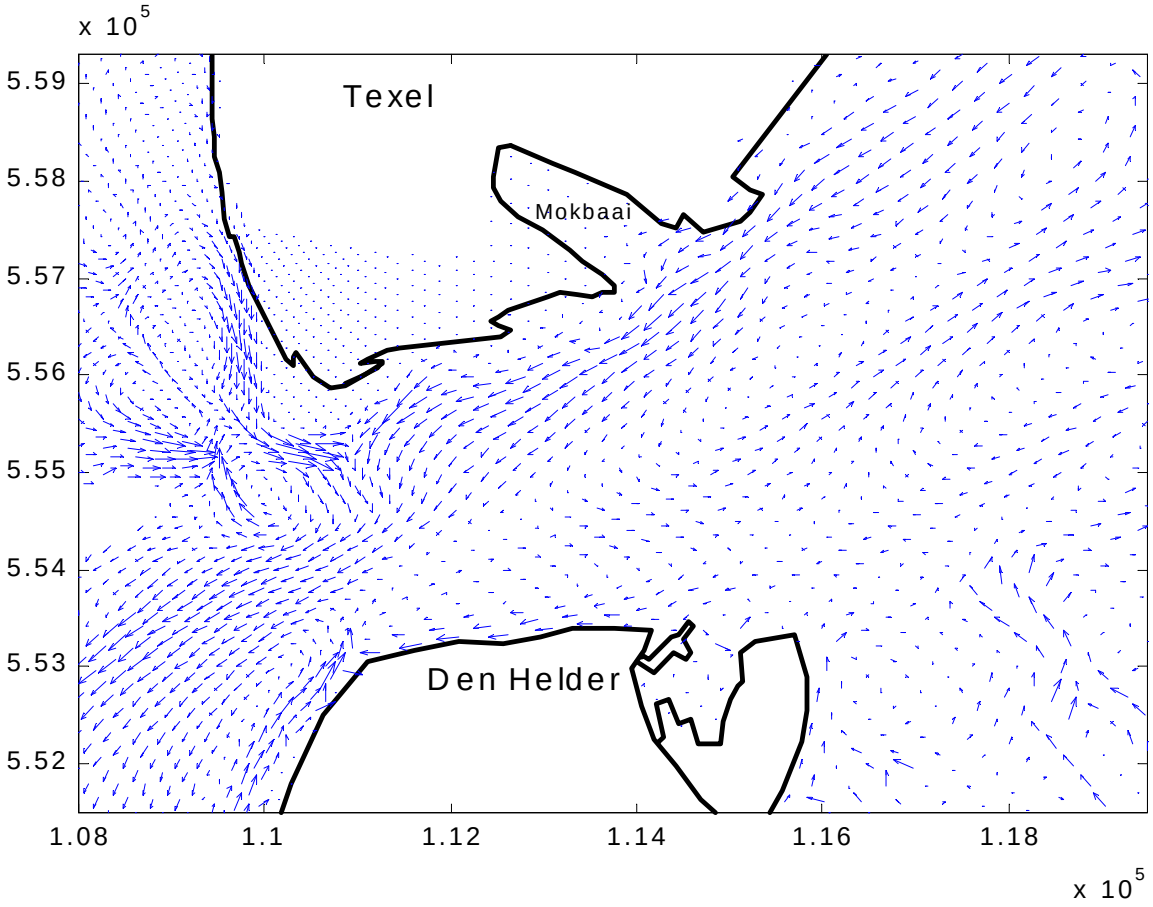

Fig 7.15 Residual currents in the Texel inlet

To get an idea of the spatial variation of the residual currents, the residual circulation pattern of the Texel inlet is presented in figure 7.15. In the northern part of the inlet the residual currents are directed seawards. These residual ebb currents mainly flow into the ebb channels south of the Noorderhaaks (see appendix A). Residual flood currents are present in the Molengat. Along the coast of North Holland a residual flood current is simulated. The main flood current enters the Texel inlet in the south-west and is directed to the north-east. Due to this current the model simulates a residual eddy in the southern part of the inlet. This eddy causes the seaward residual current in the most southern part of the inlet. The figure shows that the residual currents have a fairly high spatial variability in the inlet.

7.2.5 Tidal asymmetry

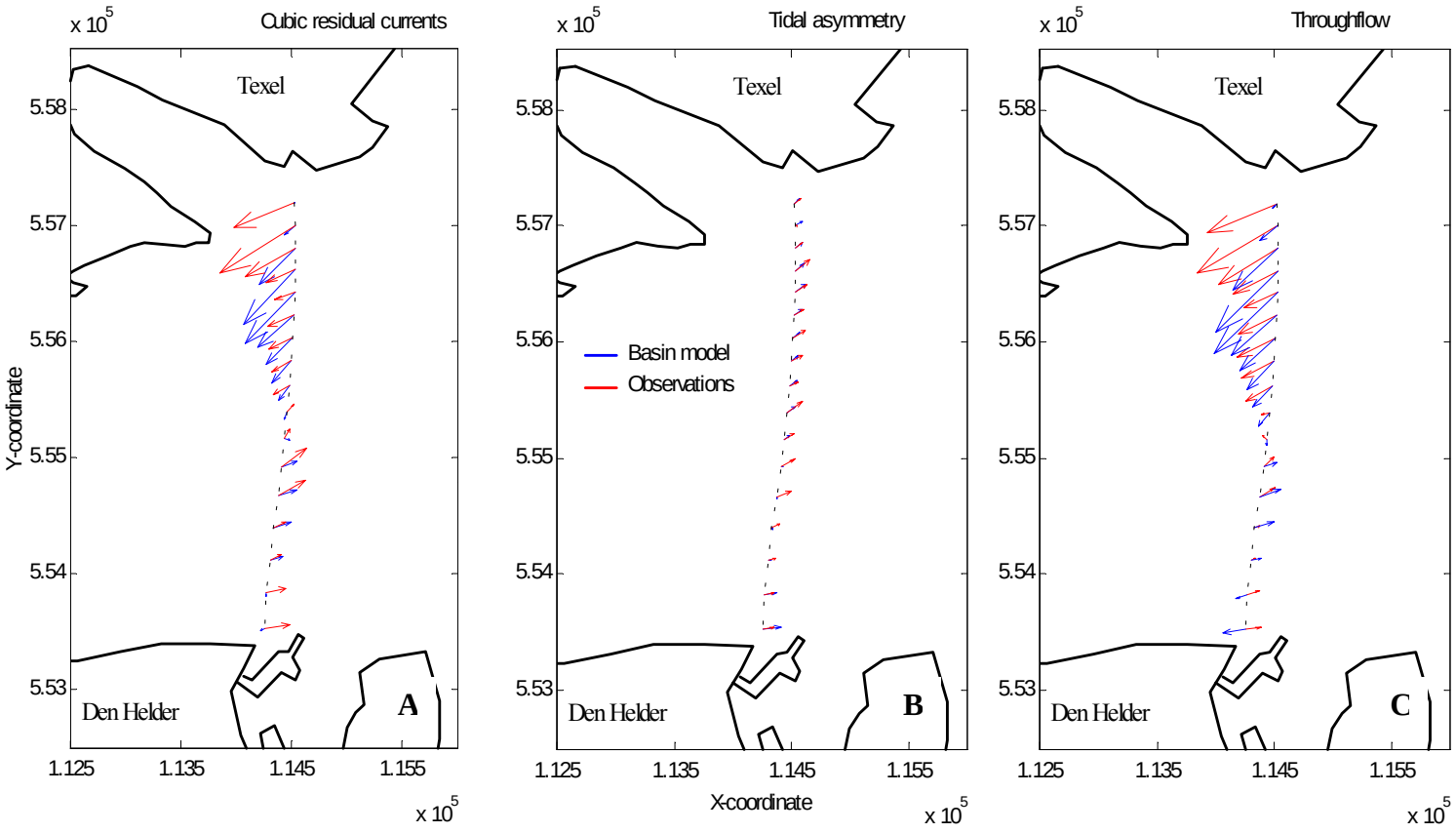

Figure 7.16 A: Cubic residual currents across the inlet. B: Cubic residual currents by tidal asymmetry. C: Cubic residual currents by throughflow. The red vectors represent the observations and the blue vectors represent the basin model.

To get a first idea of the direction of the sediment transport, a simplification of a sediment transport formula is made. A bed load transport formula has the following structure:

$$S = \rho_{sed}\,\beta|u|^{b-1}u$$

Assuming that b=3 gives the relation of the current in the bed load transport:

$$S \approx u^3$$

By averaging u to the third power over 29 tidal periods another vector is created, which gives a first idea of the direction of the bed load transport. This is done for the measurements and model results along the ferry track. See figure 7.16a. Vectors at the northern half of the inlet show a distinct transport seaward. This is the case for the measurements and also for the model. In the southern half of the inlet both blue and red vectors show an inward transport. An exception is the most southern part of the inlet, where the model simulates a relative small seawards bed load transport.

Integrating the transport vectors across the inlet gives a seaward bed load transport for the model as well as for the measurements. This is also valid for the integration of the residual currents across the inlet. In appendix F the residual currents and the mean cubic currents for the whole model area are plotted.

The simplified formula for the bed load transport can also be written in a component caused by tidal current asymmetry and a component caused by the throughflow. The rewriting of the formula is described in appendix E. The throughflow consists of the flow of the Vlie basin into the Marsdiep basin and discharges of the sluices in Den Oever and Kornwerderzand. The Basin model simulates a mean throughflow of about 650 m^3/s from the Vlie basin into the Marsdiep basin. The forced discharge in each of the two sluices is 250 m^3/s.

The component of the mean cubic tidal current, which is caused by the tidal current asymmetry, is plotted as vectors in figure 7.16b. It is clear that tidal current asymmetry causes a bed load transport into the Marsdiep basin. This transport is more or less uniform across the inlet for the measurements as well as for the basin model.

The transport vectors caused by the throughflow are plotted in figure 7.16c. Due to the fact that the component caused by tidal current asymmetry is rather small, the general pattern of the throughflow component corresponds with the pattern of the total mean cubic currents. Considerable deviation of the model results with the measurements is found in the southern part of the inlet. Here, the measurements give a transport vector directed into the basin while the Basin model gives a transport vector of about the same magnitude directed seawards. In appendix D the residual currents in the total model area are plotted.

The role of the relative phase between the M_4 phase and the M_2 phase in the tidal current asymmetry is already discussed in paragraph 2.5. The Basin model is nested in the Wadden Sea model, which was forced with new boundary conditions. Adding a M_4 phase created this new boundary forcing. Comparing the old and the new boundary forcing, a distinct difference is found in the mean cubic currents caused by the tidal current asymmetries. These are stronger in runs with the old boundary forcing. The run with the new boundary forcing produces more or less similar transport vectors as the measurements. See figure 7.17a. Exception is the northern part of the inlet, which is already discussed. The stronger tidal current asymmetries in the old runs cause a larger inward bed load transport. This can be seen in figure 7.17b.

The integration of the residual currents of old runs across the inlet shows a seaward residual flow, which is in agreement with the new runs and the measurements. However, integrating the mean cubic currents across the inlet in the old runs gives an inward bed load transport. This is in contrast with the new boundary forcing and the measurements. The influence of the component caused by tidal asymmetry is larger in the runs with the old boundary conditions than in the runs with the adjusted boundary conditions.

So, by adjusting the M_4 phase in the boundary conditions the bed load transport vectors become more or less similar with the observations. In the runs forced with the old boundary conditions the tidal current asymmetry is simulated too strong compared to the measurements. This results in other transport fields.
Paragraph 2.5.2 shows that when the phase difference between M_4 and M_2 (β) is close to 0˚ the flood currents are larger than the ebb currents due to tidal current asymmetries. When β is around 90˚ the tidal current curve is symmetric. In the old boundary conditions β was about 25˚. Figure 7.17a shows that the flood currents in the old run are indeed larger than the flood currents in the run with the new boundary conditions (β=75˚).

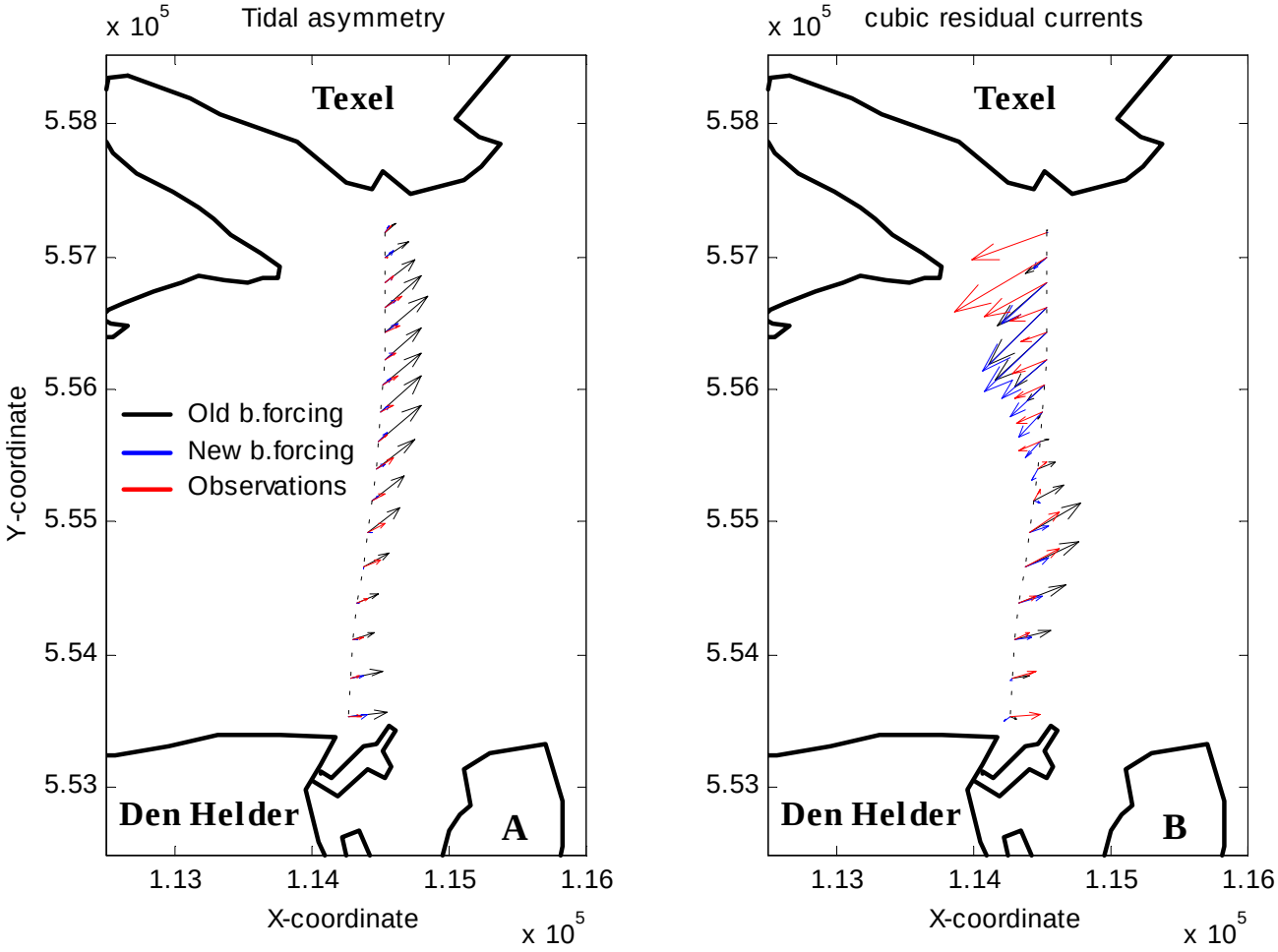

Figure 7.17 A: Cubic residual currents caused by tidal asymmetry. B: Total residual transport vectors for the two model runs and the observations.

7.2.6 3-Dimensional run

Since the effects of wind and density gradients are present in the current measurements with the ADCP, these effects will probably be taken into account in future modelling of the Texel inlet. The density gradients and wind will induce a 3D-flow structure. To get a first idea of the currents in a 3-dimensional run, a run is set up with five equidistant layers.

In this paragraph a first analysis of the tidal currents in this 3-dimensional run is given. The 3D run produces similar water levels and discharges through the Texel inlet compared to the 2D run.

After determining the depth-averaged main current for the 3D run, a comparison can be made with the 2D run and the measurements. As can be seen in figure 7.18, the transport vectors in the 3D run have some deviations with the 2D run. The 3D run produces slightly larger transport vectors than the 2D run. However, the directions of the vectors of both runs are similar.

The transport vectors caused by tidal current asymmetries are similar in both models. The transport vectors caused by the throughflow show the same deviations as in the total transport vectors.

In the 2D run the mean throughflow at the watershed between the Marsdiep basin and the Vlie basin was about 650 m^3/s. In the 3D run this throughflow was slightly higher namely 700 m^3/s. This difference causes the larger total transport vectors in the 3D run.

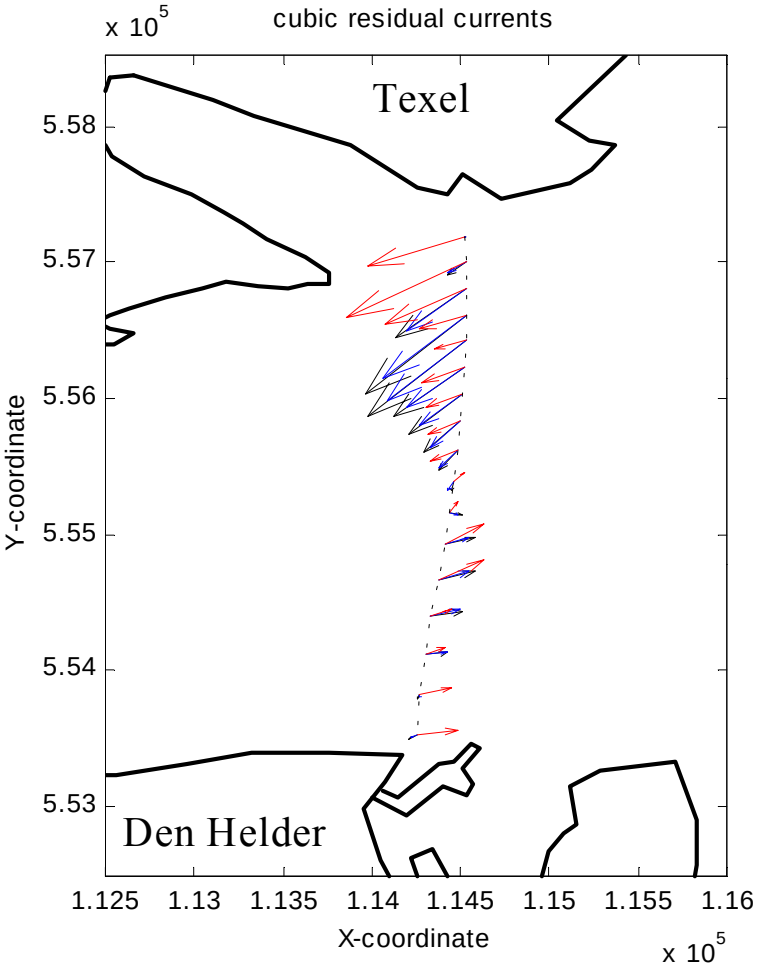

Figure 7.18 Total cubic residual currents. The red vectors represent the measurements, the blue vectors the 2D basin model and the black vectors represent the 3D basin model.

For more reliable 3D runs, more experience and knowledge about 3D effects in the model runs are required.

8 Conclusions and recommendations

The ADCP, mounted on the ferry between Den Helder and Texel, provides a detailed data set of measurements of current velocities and discharges through the Texel inlet. This data set forms a useful set for validation and calibration of numerical models for the area around the Texel inlet. Besides these measurements, also water levels measured at several locations are used for validating the models. For a relative accurate comparison the measurements and model results are harmonically analysed. This harmonic analysis approach yields the required amplitudes and phases of harmonic tidal components. The advantage of using this approach is that deviations in amplitude and phase of different components can be precisely quantified.

Analyses of the ferry measurements show that the M_2 component is the dominating tidal signal in the discharge through the Texel inlet. The net flow has a seaward direction, which confirms previous modelling studies. The ferry measurements also include depth data of the area covered by the ferry tracks. This data shows a detailed bathymetry consisting of sand waves of several meters high. This detailed bed formation is not used in the bathymetry of the model.

During the validation it became clear that by nesting the detailed 'model' in the existing Wadden Sea model, much better amplitudes and phases are simulated than in the case of nesting the detailed model in the larger ZUNO model. The main improvement is that the tidal wave propagation in the Wadden Sea is better simulated. Validation of the models with the discharges shows a large deviation of 50 degrees in the M_4 phase between the measurements and the model results. This is important since the relative phase difference between M_4 and M_2 plays a large role in the tidal current asymmetry. This asymmetry can cause a net transport of sediments even when there is no net transport of water.

By performing several sensitivity studies, experience and knowledge on the effects of different parameters are acquired. The knowledge is used to adjust the existing detailed model. The new 'model' (called the Basin model) contains the most recent bathymetry and a grid, which is extended to the watershed. The Basin model was nested in the Wadden Sea model. Astronomical boundary conditions were applied on the open boundaries of the Wadden Sea model. During the calibration these boundary conditions are adjusted to minimise the difference in the M_4 phase between the modelled and the measured discharge. Besides this, the local bathymetry in the model is adjusted to the depth measurements from the ferry data.

Comparisons of the model results with the measured water levels and discharge show that the Basin model is capable of reproducing similar amplitudes and phases for almost all analysed components in the measurements. After the calibration, the modelled currents across the Texel inlet fairly correspond with the measured currents in amplitudes as well as in phases.
However, the modelled residual currents show some deviations with the measured residual currents. The model does not simulate considerable flow into or in the Mok bay. This results in deviations in the residual currents with the measurements in that area. In the most southern part of the inlet the modelled residual current vectors are in the opposite direction of the measured vectors. The model simulates a residual eddy in the southern part of the inlet that causes this deviation. This is contrary to previous modelling studies by Ridderinkhof (1988).

To get a first idea of the bed load transport, which is simplified by u^3, the cubic tidal currents are time averaged. The throughflow from the Vlie basin and the discharges from the sluices mainly influence these cubic residual currents. By adjusting the M_4 phase in the boundary conditions, the influence of the tidal current asymmetry is decreased, which corresponds more to the measurements. Integrating the mean cubic currents across the inlet gives an export for the measurements and also for the run with the new boundary conditions. However, the runs with the old boundary conditions give an import of bed load transport into the Marsdiep basin.
This shows that the phase difference between M_4 and M_2 plays indeed an important role in the tidal current asymmetries and bed load transport through the Texel inlet.

A 3D run with equidistant layers produces similar amplitudes and phases as the 2D run. On the other hand, a 3D run with varying layer distances produces lower amplitudes for all constituents. The reason is that the bed shear stress in the 3D run (non-equidistant layers) differs from the 2D run and the 3D run with equidistant layers.

On the basis of the analyses in this model study no distinct explanation can be given for the large-scale import into the Marsdiep basin. Since this study is focused on the tidal current flows, addition of other processes can lead to more insight in the mechanisms that cause this import. Some recommendations are suggested to consider in further studies.

- Wind-effects can strongly influence the tidal flow and transport through the inlet. Wind can cause currents and waves, which can stir up sediments from the bottom. The wind can also set-up the water level in the basin during a severe storm, which might increase the flood currents drastically. It sometimes occurs that the ebb current is entirely suppressed. So, an improvement of the model is the addition of the wind and wave processes.

- A possible mechanism for net import of course sediment is estuarine circulation. The strength of the estuarine circulation depends on the magnitude of the salinity gradient. To model this circulation, the sluice discharges must be modelled as fresh water flows. Besides this, more accurate data about the discharges from the two sluices in the Marsdiep basin is needed. Also the discharge from a smaller sluice in the harbour of Den Helder might influence the results.

- Extension of the model using the Bottom and Transport module of Delft3D-MOR to make morphodynamical computations possible.

- Verifying the bathymetry, which is used in the overall models like the ZUNO model, with depth measurements. Large deviations of the bathymetry used in the overall models with the measurements, can be a possible cause of the deviation in the M_4 phase in the discharge through the Texel inlet.

References

General

Bowden, K.F., 1983, **Physical Oceanography of coastal waters**, *Marine Science*

Brown, J., Colling, A., Park, D., Philip, J., Rothery, D., Wright, J., 1989, **Waves, tides and shallow-water processes**, *The Open University/ Pergamon*

Cheng, R.T., 1990, **Residual currents and long-term transport**, *Coastal and estuarine studies, Springer-Verlag*

Doodson, A.T., Warburg, H.D., 1969, **Admiralty manual of tides**, *Hydrographic Department, Admiralty, London*

Dronkers, J., Scheffers, M.B.A.M, 1996, **Physics of Estuaries and Coastal Seas**, *Balkema*

Eisma, D., 1997, **Intertidal deposits**, *CRC Press*

Elias, E., 1999, **The Egmond model**, *WL | Delft Hydraulics Report*

Emery, J.W., Thomson, R.E., 1997, **Data analysis methods in physical oceanography**, *Pergamon*

Hibma, A., 1999, **Process-based modelling of tidal inlet dynamics**, *WL | Delft Hydraulics Report*

Holthuijsen, L.H., 1998, **Toegepaste Fysische Oceanografie**, *Lecture Notes ctwa5317, Delft University of Technology, Department of Civil Engineering*

Kalkwijk, J.P. Th., 1976. **De analyse van getijden.** *Lecture notes b75, Delft University of Technology*

Kjerfve, B., 1988, **Hydrodynamics of Estuaries**, *Estuarine Physics, Vol. I & II, CRC Press*

Lynch, D.R., Davies, A.M., 1995, **Coastal and Estuarine Studies**, *American Geophysical Union*

Math Work Inc., 1996, **Matlab User Manual**, *The language of Technical Computing*

Molen, van der, J., 2000, **A 2DH Numerical Model of Tidally Induced Sand Transport in the Southern North Sea**, *Interactions between Estuaries, Coastal Seas and Shelf Seas, pp. 265-285*

Partridge, P.W., 1992, **Computer modelling of seas and coastal regions**, *Computational Mechanics Publications Elsevier Applied Science*

Stelling, G.S., Booij, N., 1997**, Computational modelling in open channel hydraulics,** *Lecture notes, Ctwa4340, Delft University of Technology*

Uncles, R.J., 1987, **Dynamics of Turbid Coastal Environments**, *Continental Shelf Research, Vol. 7*

Vreugdenhil, C.B., 1994, **Numerical methods for shallow-water flow**, *Water Science and Technology Library*

Vriend, H.J., de, Dronkers, J., Stive, M.J.F., Van Dongeren, A. & Wang, J.H.,1998**. Coastal inlets and tidal basins. Part one.** *Lecture notes, Ctwa5303, Delft University of Technology*

Wang, Z.B., 1989, **Mathematical modelling of morphological processes in estuaries**, *Thesis Delft University of Technology*

WL | Delft Hydraulics, **Delft3D-FLOW, User manual**, release 3.10

Zimmerman, J.T.F., 1976, **Mixing and flushing of tidal embayments in the western Dutch Wadden Sea**, *E.J. Brill*

Cited

Davies, A.M., Lawrence, J., 1994, **A three-dimensional model of the M4 tide in the Irish Sea: The importance of open boundary conditions and influence of wind**, *Journal of Geophysical Research, Vol 99: pp. 16.197-16.227*

Dronkers, J., 1986, **Tidal asymmetry and estuarine morphology**, *Netherlands Journal of Sea Research 20 (2/3), 117-131*

Friedrichs, C.T., Aubrey, D.G., 1988, **Non-linear tidal distortion in shallow well-mixed estuaries: a synthesis,** *Estuarine, Coastal and Shelf Science 27, 521-545*

Godin, G., 1972, **The analysis of tides**, *Liverpool University Press*

Kreeke, van de, J., Robaczewska, K., 1993, **Tide-induced residual transport of coarse sediment; application to the Ems estuary**, *Netherlands Journal of Sea Research 31*

Leeuw, R., de, 1999, **Getij-asymmetrie en sedimenttransport in het zeegat van Texel**, *Report*

Louters, T., Gerritsen, F., 1994**, Het mysterie van de Wadden. Hoe een getijdesysteem inspeelt op zeespiegelstijging**, *Ministerie van Verkeer en Waterstaat, Directoraat-Generaal Rijkswaterstaat, Rijksinstituut voor Kust en Zee/RIKZ*

Parker, B.B. (ed.), 1991, **Tidal Hydrodynamics**, *John Wiley, New York, pp. 237-268*

Pingree, R.D., Maddock, L., 1978, **The M4 tide in the English Channel derived from a non-linear numerical model of the M2 tide**, *Deep-sea Research, Vol 25: pp. 53-63*

Pingree, R.D., Sinha, B., 1997, **The principal lunar semidiurnal tide and its harmonics**, C*ontinental Shelf Research, Vol. 17, Pergamon*

Postma, H. (ed.), 1982, **Hydrography of the Wadden Sea: movements and properties of water and particulate matter,** *Stichting Veth tot steun aan Waddenonderzoek, Leiden*

Prandle, D., 1980, **Co-tidal charts for the southern North Sea**, *Deutsches Hydr.Inst. Hamburg, Vol. 2, pp 69-81*

Ridderinkhof, H., 1988, **Tidal and residual flows in the Western Dutch Wadden Sea, I: Numerical model results**, *Netherlands Journal of Sea Research, Vol. 22: pp. 1-22*

Ridderinkhof, H., 1988**, Tidal and residual flows in the Western Dutch Wadden Sea, III: Vorticity balances**, *Netherlands Journal of Sea Research, Vol. 24: pp. 9-26*

Ridderinkhof, H., 2000, **Continuous current measurements in the Marsdiep tidal inlet using a ferry-mounted ADCP,** *preliminary abstract*

Sha, L.P., 1989, **Sand transport patterns in the ebb-tidal delte of Texel inlet, Wadden Sea, The Netherlands**, *Marine Geology 86, pp. 137-154*

Steijn, R.C., van Banning, G.K.F.M., Roelvink, J.A., 1998**, Gevoeligheidsberekeningen Eijerland en ZW-Texel. Fase 2: ZW-Texel**, *Alkyon and WL Delft Hydraulics, Report A266/Z2430*

Stelling, G.S., 1984, **On the construction of computational methods of shallow water flow problems**, *Rijkswaterstaat communications, No. 35*

Swart, de, H.E., 1996, **Lange golven**, *collegedictaat Instituut voor Marien en Atmosferisch onderzoek, Utrecht*

Tomczak, M., 1996, **The Shelf and Coastal zone**, *lecture notes, Flinders University of South Australia*

Appendices

A Texel inlet and its outer delta

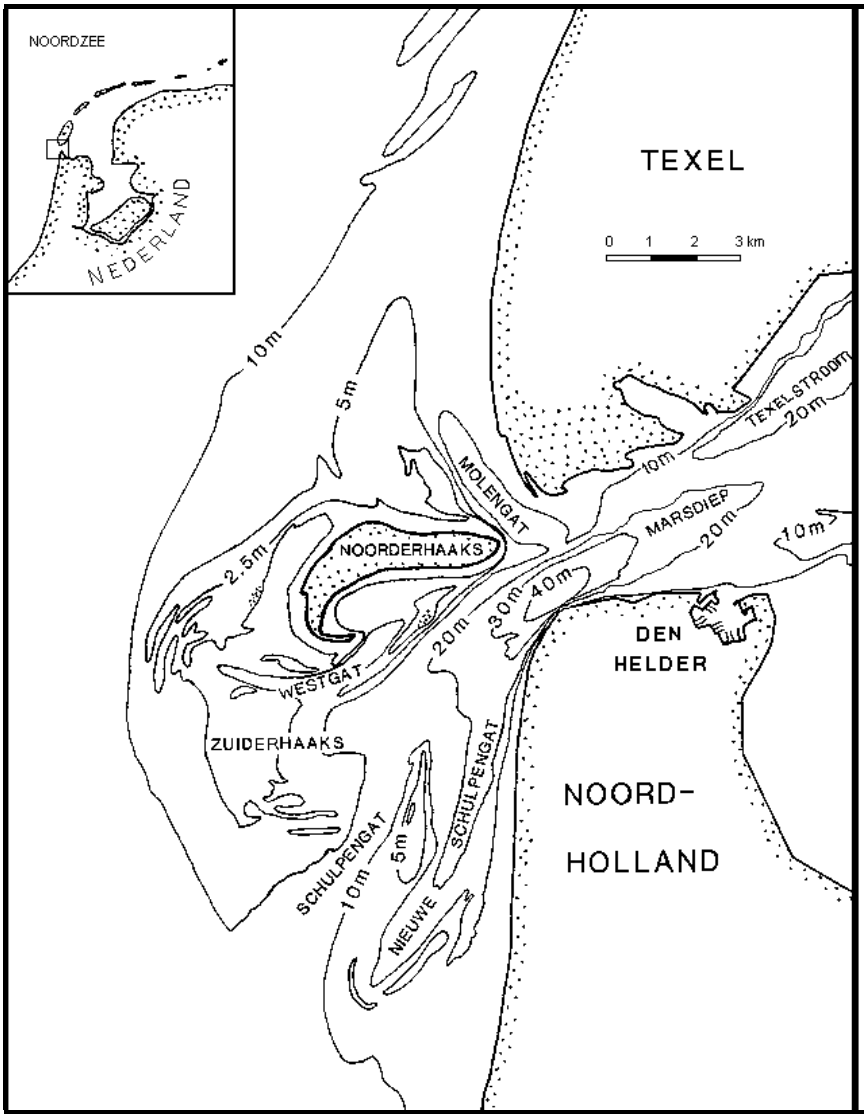

Fig A.1 The Texel inlet and its outer delta (Sha, 1989)

B Pre-processing programs

RGFGRID
The RGFGRID program is used to create, manipulate and visualise orthogonal, curvilinear model grids for the Delft3D-FLOW water motion program. A Delft3D-FLOW grid is an ordered set of horizontal co-ordinates, at the locations of the depth points. The depth values are created with the program QUICKIN (see action Quickin). A curvilinear grid provides optimum grid resolution at minimum computational expense.

RGFGRID is designed in such a way, that grids can be created with minimum effort, without specifying grid spacing at all grid boundaries. A rough sketch of the grid can be drawn by splines, which are transformed into a rough grid, that can be smoothly refined and orthogonalised by the program.

When constructing a grid, several restrictions of numerical nature have to be taken into account:
- Grid lines must intersect perpendicularly
- Grid spacing must vary smoothly (M- and N smoothness) over the computational region.

The orthogonality is the extent to which a cell resembles a square. It should be kept low (< 0.04) as the error in the Delft3D-flow cross advection term is proportional to this value. The M and N smoothness give the ratio between adjacent grid cell lengths. A maximum factor of 1.3 to 1.4 is advised to minimise inaccuracy errors in finite difference operators.

QUICKIN
The main purpose of the QUICKIN program is to create, manipulate and visualise model bathymetries for the Delft3D-FLOW water motion program. A Delft3D-FLOW bathymetry is an ordered set of depth values that are assigned to an ordered set of (curvilinear) grid points. Curvilinear grids are created with the program RGFGRID. A Delft3D-FlOW bathymetry is created by interpolation of raw depth data onto the (curvilinear) grid.

> The raw depth data, consisting of a set of scattered x,y,z co-ordinates, are called ‘samples’. The interpolated depth values and their corresponding x,y co-ordinate positions in the grid will simply be called ‘depths’.

One of the problems of depth interpolation is that the samples may originate from various sources, each of different date, quality and resolution. If these samples are all copied into one large file, the ‘high’ quality data would be contaminated with ‘low’ quality data, leading to non optimal interpolation results.

C Grid and bathymetry in the Texel inlet

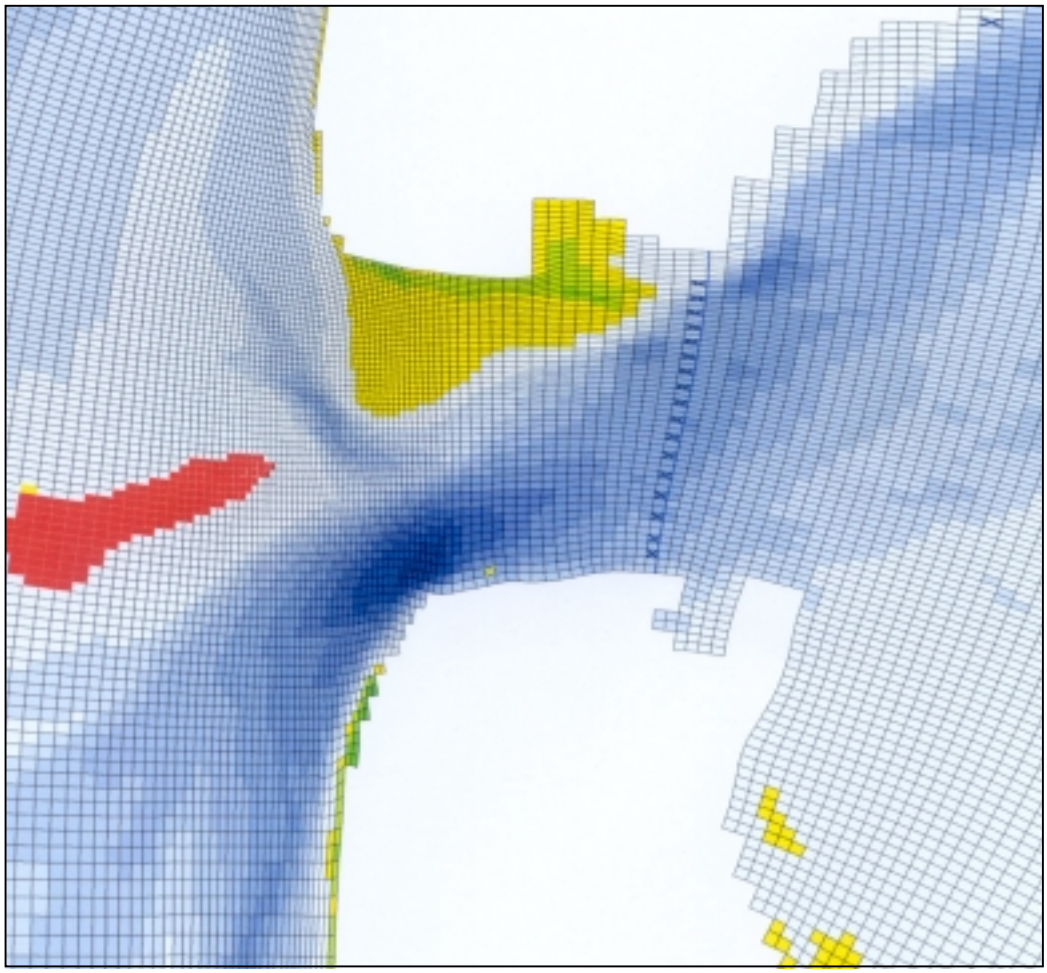

Figure A1. Detailed picture of the grid and bathymetry of the Texel inlet in the Basin model. The yellow cross is the water level station at Den Helder. The blue crosses represent the observation points in the model.

D Parameter settings of the Basin model run

The parameter settings of the final 2D run of the Basin model are:

Parameter	Value
Latitude	52.5 ˚
Time step	60 sec
Gravity	9.81 m/s^2
Water density	1023 kg/m^3
Air density	1.000 kg/m^3
Temperature	15 ˚C
Salinity	31 ppm
Bottom roughness Manning (uniform)	0.026
Horizontal eddy viscosity	1.00 m^2/s
Extra drying/flooding procedure	max
Threshold depth	0.10 m
Smoothing time	60 minutes

E Cubic residual current formula

For a calculation of the bed load transport the following empirical formula can be used:

$$S = \rho_{sed}\,\beta |u|^{b-1} u \tag{1}$$

Considering b=3 and leaving out the quasi-constant parameters, the formula can be written as the square absolute value of the velocity multiplied by the velocity vector, which results in:

$$S = |u|^2 \begin{pmatrix} u \\ v \end{pmatrix} \tag{2}$$

The velocity vector in a grid point is composed from the u-velocity in the x-direction and the v-velocity in the y-direction. These two velocities can be defined as the sum of a mean component and a periodic component:

$$v = \hat{v} + \tilde{v} \tag{3a}$$

$$u = \hat{u} + \tilde{u} \tag{3b}$$

When substituting (3b) in the square absolute value of the velocity vector (2), the scalar is defined as:

$$\begin{aligned} |u|^2 &= ((u^2 + v^2)^{1/2})^2 = (\hat{u} + \tilde{u})^2 + (\hat{v} + \tilde{v})^2 \\ &= \hat{u}^2 + \tilde{u}^2 + 2\hat{u}\tilde{u} + \hat{v}^2 + \tilde{v}^2 + 2\hat{v}\tilde{v} \end{aligned} \tag{4}$$

Substituting (4) and (3a & 3b) in (2) gives:

$$S = (\hat{u}^2 + \tilde{u}^2 + 2\hat{u}\tilde{u} + \hat{v}^2 + \tilde{v}^2 + 2\hat{v}\tilde{v}) \begin{pmatrix} \hat{u} + \tilde{u} \\ \hat{v} + \tilde{v} \end{pmatrix} \tag{5}$$

Multiplying the scalar with the vector, a new vector is created of which the numerator and the denominator have to be averaged over a tidal cycle. The new vector (6) is:

$$S = \begin{pmatrix} \overline{\hat{u}^3 + \hat{u}\tilde{u}^2 + 2\hat{u}^2\tilde{u} + \hat{u}\hat{v}^2 + \hat{u}\tilde{v}^2 + 2\hat{u}\hat{v}\tilde{v} + \tilde{u}\hat{u}^2 + \tilde{u}^3 + 2\hat{u}\tilde{u}^2 + \hat{v}^2\tilde{u} + \tilde{v}^2\tilde{u} + 2\hat{v}\tilde{v}\tilde{u}} \\ \overline{\hat{v}\hat{u}^2 + \hat{v}\tilde{u}^2 + 2\hat{u}\tilde{u}\hat{v} + \hat{v}^3 + \hat{v}\tilde{v}^2 + 2\hat{v}^2\tilde{v} + \tilde{v}\hat{u}^2 + \tilde{v}\tilde{u}^2 + 2\hat{u}\tilde{u}\tilde{v} + \hat{v}^2\tilde{v} + \tilde{v}^3 + 2\hat{v}\tilde{v}^2} \end{pmatrix}$$

The cubic mean component of the velocities is of a lower magnitude than the rest. When averaging over a tidal cycle, the periodic components (which are not square or cubic) become zero. By omitting these parts the vector can be simplified into:

$$S = \begin{pmatrix} \overline{\tilde{u}^3 + \tilde{u}\tilde{v}^2 + \hat{u}\tilde{v}^2 + 3\hat{u}\tilde{u}^2 + 2\hat{v}\tilde{v}\tilde{u}} \\ \overline{\tilde{v}^3 + \tilde{v}\tilde{u}^2 + \hat{v}\tilde{u}^2 + 3\hat{v}\tilde{v}^2 + 2\hat{u}\tilde{u}\tilde{v}} \end{pmatrix} \tag{7}$$

The components containing only the periodic time series represent the bed load transport caused by tidal asymmetry. The other components represent the bed load transport caused by the throughflow.

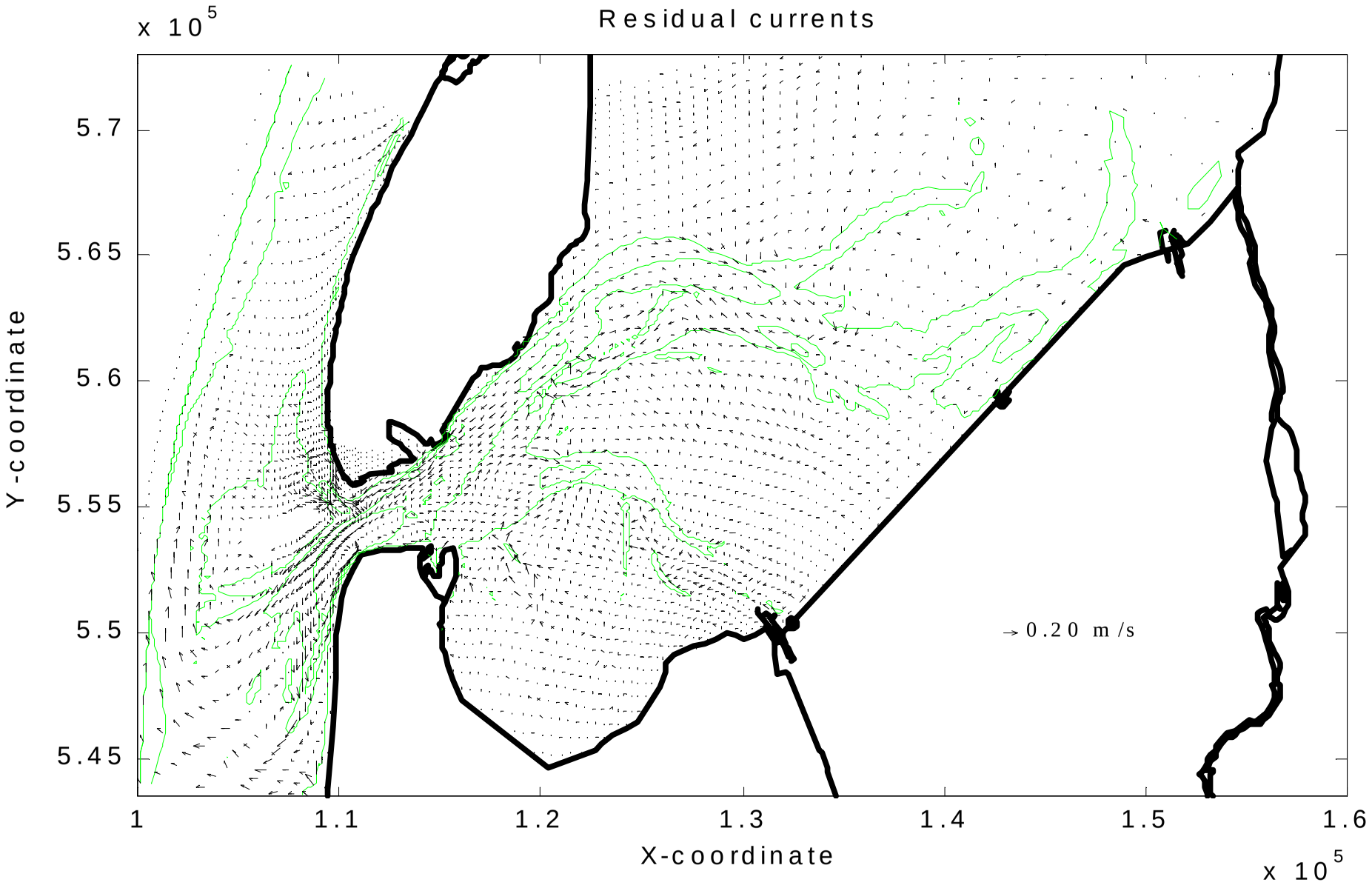
Residual currents
x 10^5
5.7
5.65
5.6
5.55
5.5
5.45
Y-coordinate
1
1.1
1.2
1.3
1.4
1.5
1.6
X-coordinate
x 10^5
→ 0.20 m/s

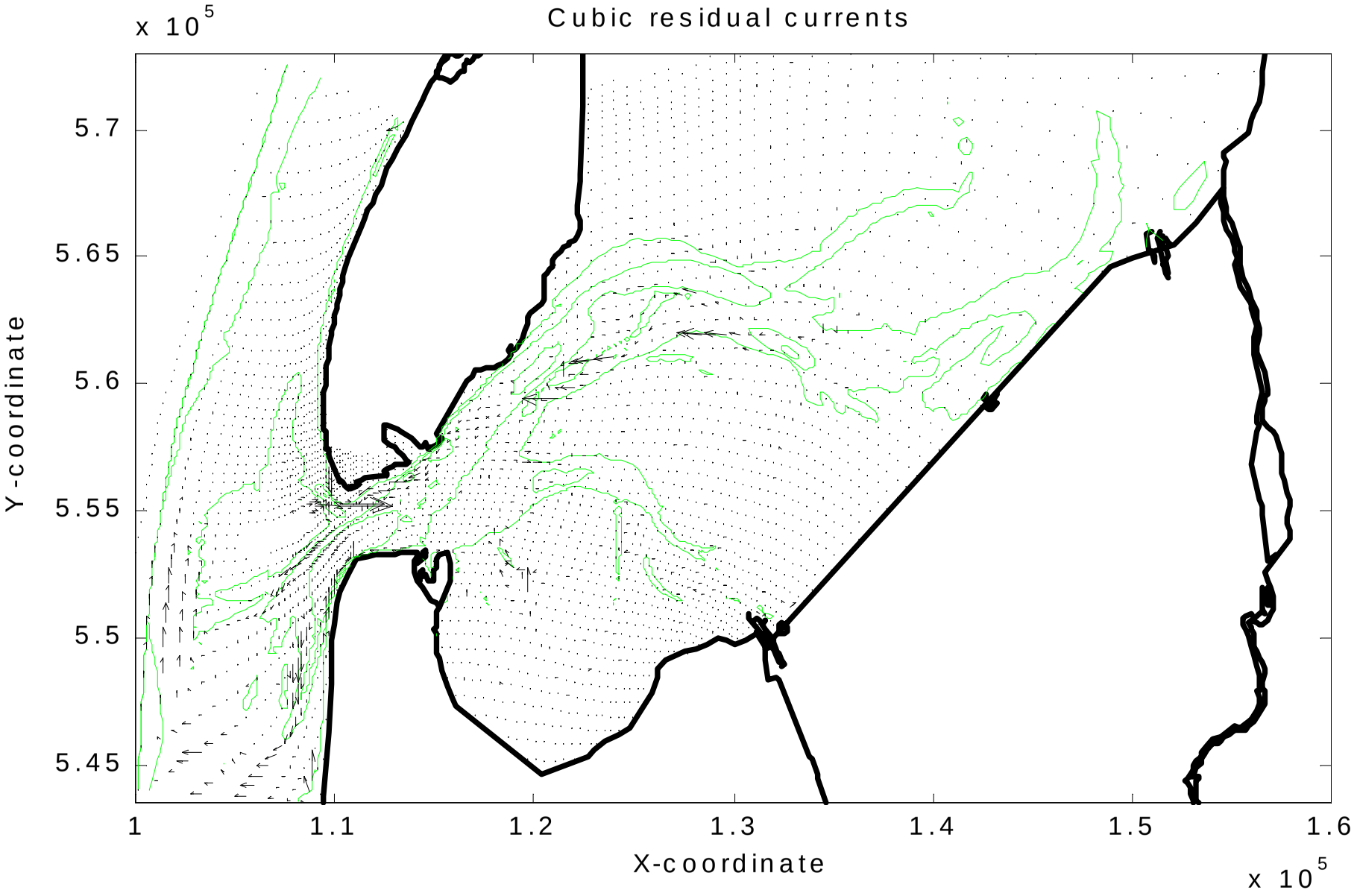
Cubic residual currents
x 10^5
5.7
5.65
5.6
5.55
5.5
5.45
Y-coordinate
1
1.1
1.2
1.3
1.4
1.5
1.6
X-coordinate
x 10^5

G Time series of discharge through the inlet